

PhD Thesis

Per Jensen

Translocator Protein Imaging with ^{123}I -CLINDE SPECT

- Method Development and Clinical Research

Principal Supervisor: Lars H Pinborg MD DMSc

Submitted on 28 February 2017

This thesis has been submitted to the Graduate School of Health and Medical Sciences,
University of Copenhagen on 28 February 2007

Title: Translocator Protein Imaging with ^{123}I -CLINDE SPECT – Method Development and
Clinical Research

Author: Per Jensen

Department: Neurobiology Research Unit, Department of Neurology, Rigshospitalet, Denmark

Institution: Faculty of Health and Medical Sciences, University of Copenhagen

Principal Supervisor: Associate Professor Lars H Pinborg MD DMSc

Co- supervisors: Associate Professor Per Meden MD PhD and Prof. Derk Krieger MD PhD

Evaluation Committee:

Professor Olaf B. Paulson MD DMSc (Chair), Neurobiology Research Unit, Department of
Neurology, Rigshospitalet, Denmark

Dr Alexander Gerhard MD, Division of Neuroscience & Experimental Psychology, University of
Manchester, United Kingdom

Professor Leif Østergaard MD PhD DMSc, Center of Functionally Integrative Neuroscience,
Institute for Clinical Medicine, Aarhus University, Denmark

Introduction

Molecular imaging of the translocator protein (TSPO) in the brain provides a unique window into diseases of the brain. It visualises reactive microglia, astrocytes as well as macrophages crossing the blood brain barrier from the blood into the brain parenchyma, which together constitute an immune response.

Since the discovery of TSPO in the late 1970's, it has been linked to a broad range of neurological, psychiatric and oncological diseases. However, TSPO imaging has yet to be implemented clinically. There are several reasons: methodological issues, the cost of molecular imaging, and the clinical relevance for TSPO imaging has not been demonstrated in diagnostics, disease progression or treatment response.

Since 2010, at the Neurobiology Research Unit, TSPO imaging has been conducted using ^{123}I -CLINDE, a second-generation single photon emission computed tomography (SPECT) TSPO radiotracer.

The major aim of the current work is to advance ^{123}I -CLINDE SPECT imaging into clinical research of neurological diseases. To reach this aim this thesis presents four studies, arranged like a classical three-stage rocket.

The first part consists of two 'proof of concept' studies demonstrating the feasibility of ^{123}I -CLINDE SPECT in diverse and challenging clinical settings: the fatal cancer disease glioblastoma and the recently discovered autoimmune disease anti-NMDA receptor encephalitis. Each study points forward to future larger clinical studies.

The middle part focuses on further development and validation of the ^{123}I -CLINDE SPECT scanning method. This study was performed in collaboration with postdoc Ling Feng. New and important discoveries about TSPO tracer stability were made and implemented in the final study. The tip of the rocket is a clinical investigative study describing the longitudinal development of the TSPO expression in recovering patients 2-18 weeks after stroke. Here I also had the opportunity to develop experience as a neurologist in training.

I think that the rocket has reached orbit, although much work is still to be done.

Per Jensen, Copenhagen, February 2017

Table of contents

INTRODUCTION.....	4
ACKNOWLEDGEMENTS.....	9
LIST OF PUBLICATIONS	10
Study 1.....	10
Study 2.....	10
Study 3.....	10
Study 4.....	10
ABBREVIATIONS	11
SUMMARY IN ENGLISH	12
DANSK RESUMÉ	14
1. BACKGROUND.....	16
The Translocator Protein – History, localization, structure and function	16
TSPO and neuroinflammation.....	17
Microglia	17
Astrocytes.....	18
Macrophages	18
TSPO radiotracers	19
The rs6971 polymorphism.....	19
TSPO imaging studies in diseases of the human brain.....	20
2. OBJECTIVES	21
3. DESCRIPTION OF THE RESEARCH PROJECTS.....	22
Study 1 – Proof of concept: ¹²³I-CLINDE-SPECT in anti-NMDAr encephalitis	22
Background	22
Case description	23
Study design and materials.....	23
Study 2 – Proof of concept: ¹²³I-CLINDE SPECT in Glioma	23
Background	23
Study design and demographics.....	24
Study 3- Advances in protocol and test-retest variability of ¹²³I-CLINDE SPECT.....	25
Background	25
Study design and demographics.....	25

Study 4 - Clinical study: ¹²³I-CLINDE SPECT in stroke	27
Background	28
Study design and demographics	31
4. METHODS	34
Molecular imaging with SPECT	34
2-tissue compartment modelling	35
The ¹²³I-CLINDE SPECT scanning protocol	37
SPECT scanning.....	37
Post processing of ¹²³ I-CLINDE SPECT images and blood measures.	38
Magnetic resonance imaging	39
Methods used in study 1	39
Methods used in study 2	39
Acquisition and reconstruction of ¹⁸ F-FET PET:.....	39
Regions of interest.....	39
The Sørensen-Dice index	40
Methods used in study 3	41
Regions.....	41
Brain uptake	41
Blood uptake	41
Percentage difference	41
Intraclass correlation coefficient	42
Coefficient of variation	42
General least squares model.....	43
Methods used in study 4	44
Structural MRI sequences	44
Delineation of ROIs	44
Rehabilitation measures	44
Statistical analysis	45
5. RESULTS	46
Results – study 1	48
Results - study 2	48
Baseline	48
Follow-up	48
Results - study 3	51
Test-retest variability of brain uptake and distribution volumes and the effect of genotype on variability measures ..	51
Effect of centrifugation on plasma to whole-blood ratio	52
Effect of genotype on the parent fraction, brain uptake and distribution volumes	52
Results - study 4	53
TSPO expression in lesion-related ROIs.....	54
Correlations between TSPO expression, clinical outcome measures and necrosis.....	54
TSPO expression in ROIs unrelated to the lesion	55

6. DISCUSSION AND PERSPECTIVES	60
Study 1.....	60
Study 2.....	60
Study 3.....	61
The test-retest variance of V_T in ^{123}I -CLINDE SPECT	61
Estimating brain uptake with mSUV and mSUV ₆₀₋₉₀	61
Effect of blood centrifugation	62
Study 4.....	63
TSPO expression and stroke recovery	63
TSPO expression and lesion necrosis.....	63
TSPO expression in stroke compared to healthy volunteers.....	64
Future analyses for the current study	64
7. CONCLUSIONS.....	66
Conclusions on the studies.....	66
Study 1.....	66
Study 2.....	66
Study 3.....	66
Study 4.....	67
Conclusions on the thesis objective.....	67
8. REFERENCES.....	68
APPENDIX.....	74
Study 1.....	74
Study 2.....	76
Study 3.....	82
Study 4.....	109
DECLARATIONS OF CO-AUTHORSHIP	132

Acknowledgements

Special thanks to my principal supervisor Lars H. Pinborg for providing guidance and opportunity to conduct the presented research. And thank you to my co-supervisor Per Meden for delivering the clinical background for the stroke project and never giving up with stroke patient recruitment. Thank you to Ling Feng for developing the ¹²³I-CLINDE SPECT scanning protocol and kindly teaching it to me.

Thank you to Gerda Thomsen, Svitlana Olsen and Glenna Skouboe at the SPECT lab. You are both professional and also very fun and pleasant to work with. The majority of the data from the current work exist because of your experience, flexibility and commitment to research. And thank you to Agnete Dyssegaard for performing the blood sample analysis very skilfully and carefully.

Thank you to all who have helped to realise the studies in this thesis: Lars V Knudsen, Stine Andersen, Josephine Torp, Claus Svarer, Henrik Steghlich-Arnholm, Carsten Thomsen, Anders Ohlhues, Vincent Beliveau, Melanie Ganz, Jens D Mikkelsen, Henrik B Hansen, Sebastian Ebert, Hanne D Hansen, Louise Nielsen and Gitte M Knudsen.

Thank you for all the laughs and ‘real talk’ in the cosy small office: Louise Jørgensen, Mette T Foged and Minna Littman. It has been a blessing to get to know you.

I would like to thank everybody at the NRU, from professors to cleaning personnel for providing an incredibly inspiring workplace environment.

Final thanks go to my two true loves, my wife Lise and my daughter Iluna, for supporting and hugging me throughout the project.

List of publications

Study 1

Jensen, P., Kondziella, D., Thomsen, G., Dyssegaard, A., Svarer, C., & Pinborg, L. H. (2015) Anti-NMDAR encephalitis: demonstration of neuroinflammation and the effect of immunotherapy. *Neurology*

Study 2

Jensen, P., Feng, L., Law, I., Svarer, C., Knudsen, G. M., Mikkelsen, J. D., ... Pinborg, L. H. (2015). TSPO imaging in glioblastoma multiforme: A direct comparison between ¹²³I-CLINDE-SPECT, ¹⁸F-FET PET and gadolinium-enhanced MRI. *Journal of Nuclear Medicine*. <https://doi.org/10.2967/jnumed.115.158998>

Study 3

Feng, L*, **Jensen, P.***, Thomsen, G., Dyssegaard, A., Svarer, C., Knudsen, L. V., ... Pinborg, L. H. (2016). The variability of translocator protein signal in brain and blood of genotyped healthy humans using in vivo ¹²³I-CLINDE SPECT imaging – a test-retest study. *Journal of Nuclear Medicine*, jnumed.116.183202.
***Shared 1st author**

Study 4

Jensen P., Feng L., Meden P., Thomsen G., Knudsen L. V., Steglich-Arnholm H., Dyssegaard A., Møller K., Thomsen C., Svarer C., Beliveau V., Ozenne B., Mikkelsen J. D., Knudsen G. M., and Pinborg L. H.. Expression, evolution and prognostic value of Translocator protein in middle cerebral artery stroke patients - A longitudinal ¹²³I-CLINDE-SPECT imaging study. *Un-submitted manuscript*

Abbreviations

2TCM - Two-tissue compartment model

CLINDE - 6-Chloro-2-(4'-¹²³I-Iodophenyl)-3-(N,N-Diethyl)-Imidazo[1,2-a]Pyridine-3-Acetamide

COV - Coefficient of variation

FET – Flouro-ethyl-thyrosine

CE-CT - Contrast enhanced Computed tomography

DAMPs - Damage associated molecular patterns

GAMs - Glioma associated microglia/macrophages

GBM - Glioblastoma multiforme

Gd-MRI - Gadolinium enhanced magnetic resonance imaging

GLS - General least squares

HPLC - High-performance liquid chromatography

ICC - Intraclass correlation coefficient

kDa - Kilo Dalton

LG1 - Leucine-rich glioma inactivated-1

NMDAr - N-methyl-D-aspartate receptor

MRI - Magnetic resonance imaging

PAMPS - Pathogen associated molecular patterns

PBR - Peripheral benzodiazepine receptor

PD - Percentage difference

ROI - Region of interest

SD - Standard deviation

SNR - Signal to noise ratio

SQ - Sørensen-Dice coefficient

SUV - Standard uptake value

TAC - Time activity curve

TSPO - Translocator protein

V_T - Distribution volume

VDAC - Voltage dependent anion channel

Summary in English

The translocator protein (TSPO) is upregulated in reactive glial cells and expression is increased in acute and chronic neuroinflammatory conditions. This thesis focuses on the expression of TSPO imaged by ^{123}I -CLINDE single photon emission computed tomography (SPECT) in four settings: anti-NMDAR encephalitis (study 1), glioma (study 2), healthy volunteers (study 3) and ischemic stroke (study 4).

In study 1, the binding of ^{123}I -CLINDE to TSPO was investigated in a case of anti-NMDA receptor encephalitis. High binding was demonstrated at the initiation of immunotherapy in cortical and subcortical brain regions similar to the distribution of the NMDA receptor. After 7 weeks of treatments, symptoms had subsided and a second scan revealed almost normalized ^{123}I -CLINDE binding compared to a healthy control.

In study 2, ^{123}I -CLINDE-SPECT was investigated in relation to conventional ^{18}F -Flouro-ethyl-tyrosine positron emission tomography (^{18}F -FET PET) and gadolinium-enhanced magnetic resonance imaging (gd-MRI) in three glioma patients. Results were compared to tumor progression on contrast-enhanced structural imaging at follow-up. Results suggested that TSPO imaging may be a predictor of active tumor cell proliferation and tumor progression.

Study 3 is a methodological test-retest study in the variability of ^{123}I -CLINDE SPECT imaging in healthy volunteers. 18 patients were scanned twice. Results revealed that the ^{123}I -CLINDE SPECT scanning modality showed better test-retest variability than the first generation PET tracer ^{11}C -PK11195 and comparable variability to previously tested second generation PET tracers. Furthermore, the study demonstrated the importance of immediate centrifugation of the blood-samples, as ^{123}I -CLINDE is distributed into blood cells if left in the vial, which affects the test-retest variance considerably.

Finally in study 4, a cohort of 12 patients was studied longitudinally at three time-points after ischemic stroke in the middle cerebral artery territory with ^{123}I -CLINDE SPECT, structural MRI and clinical rating. TSPO expression in stroke was furthermore compared to a cohort of 10 healthy volunteers. Results revealed an incredibly dynamic TSPO expression that could not be correlated to recovery after stroke, however the overlap between the lesion on structural MRI and the region of high ^{123}I -CLINDE binding was negatively correlated to the volume of lesion necrosis. Interestingly, regions un-related to the lesion were demonstrated to have lower ^{123}I -

CLINDE binding to TSPO in patients compared to similar regions in healthy volunteers initially and increased to comparable values at later time-points.

In conclusion, the studies of this thesis demonstrate the feasibility of performing research using ¹²³I-CLINDE SPECT imaging in a variety of settings including both healthy volunteers and neurological patients.

Dansk resumé

Translocator proteinet (TSPO) er opreguleret i reaktive gliaceller under akutte samt kroniske neuroinflammatoriske tilstande. Denne afhandling fokuserer på ekspresionen af TSPO målt med den molekylære billeddannende modalitet ^{123}I -CLINDE SPECT i fire forskellige studier: anti-NMDA receptor (NMDAr) encephalitis (studie 1), glioblastoma multiforme (studie 2), raske forsøgspersoner (studie 3) samt apopleksia cerebri (studie 4).

Det første studie undersøger TSPO ekspresion i en patient med anti-NMDAr encephalitis skannet med ^{123}I -CLINDE SPECT to gange: ved behandlingsstart og efter 7 uger. Den første scanning viste forhøjet binding af ^{123}I -CLINDE til TSPO i de samme kortikale og subkortikale hjerneregioner, som udtrykker NMDA receptorer. Ved skanning nummer to var patienten bedret betydeligt og ^{123}I -CLINDE bindingen faldet til næsten samme værdier som hos en raske forsøgsperson.

I studie nummer to blev tre patienter med glioblastoma multiforme undersøgt. Studiet sammenligner ^{123}I -CLINDE SPECT med to konventionelle billeddannende modaliteter ved denne sygdom: ^{18}F -Flouro-Ethyl-Tyrosine positron emission tomography samt magnetisk resonans billeddannelse med kontrast (gd-MRI). Derudover bliver resultaterne sammenlignet med tumortilvækst på opfølgende skanning senere i forløbet. Studiet viste, at der er områder i og omkring tumor med høj ^{123}I -CLINDE binding, og at disse områder udviser potentiale til at prædiktere tumor proliferation og tilvækst.

Studie nummer tre er et metodestudie, der undersøger test-retest variansen af ^{123}I -CLINDE SPECT hos 16 raske forsøgspersoner. Studiet viste en bedre test-retest varians for ^{123}I -CLINDE SPECT end førstegenerations TSPO radioliganden PK-11195 og sammenlignelig varians i forhold til tidligere studier af 2. Generations radioliganderne ^{11}C -PBR28 PET og ^{11}C -DPA-713 PET. Desuden vises der i dette studie, at det har en betydning for aktiviteten i blodplasma i de blodprøver der bliver brugt til at beregne ^{123}I -CLINDE bindingen til TSPO, hvis man venter med at centrifuge blodprøverne.

Det sidste og fjerde studie er en longitudinel undersøgelse af 12 patienter skannet tre gange efter blodprop efter iskæmisk apopleksi i arteria cerebri media territoriet. Data bliver sammenholdt med rehabilitering målt gennem forløbet samt TSPO ekspresionen hos 10 raske forsøgspersoner. Her finder vi at TSPO ekspresionen efter blodprop er meget heterogen og dynamisk. Det bliver undersøgt, om TSPO ekspresionen er en markør for rehabiliteringen men

ikke fundet sammenhæng. Derudover ses der initialt lavere ^{123}I -CLINDE binding i hjerneregioner, som umiddelbart ikke er berørt af, eller anatomisk forbundet med blodproppen når man sammenligner med raske forsøgspersoner. Den afsluttende konklusion på denne afhandling er at ^{123}I -CLINDE SPECT er en god og brugbar metode til at foretage kliniske forskningsprojekter af TSPO ekspression hos både raske og syge.

1. Background

The Translocator Protein – History, localization, structure and function

The link between the translocator protein (TSPO) and the consequences of its expression is complex, poorly understood, and hence still a subject of research and debate. The following text outlines the central history, structure and cellular functions of TSPO with emphasis on the TSPO expressing cells of the brain.

The first discovery of TSPO was made in the late 1970's by Danish biochemist Claus Bræstrup and colleagues. It was originally named the peripheral benzodiazepine receptor (PBR) because of its discovery in non-brain tissues and affinity to benzodiazepines. Later on, the molecule was also identified in brain tissue (Braestrup & Squires, 1977) and almost thirty years later, the PBR nomenclature was changed to TSPO based on discoveries in structure and molecular function (Papadopoulos et al., 2006).

The tertiary molecular structure of TSPO comprises 5 trans-membrane domains that environ the benzodiazepine binding site (Scarf & Kassiou, 2011). The 18 kDa TSPO molecule is primarily located in the outer mitochondrial membrane at contact sites between inner and outer mitochondrial membranes (Papadopoulos et al., 2006; Scarf & Kassiou, 2011). During active cell proliferation and steroid synthesis TSPO has the ability to form oligomers (Delavoie et al., 2003; Lacapère & Papadopoulos, 2003). It has been demonstrated that TSPO is associated with the mitochondrial membrane located voltage dependent anion channel (VDAC) and several other mitochondrial membrane proteins including peripheral benzodiazepine receptor-associated protein 1 (PRAX-1, steroidogenic acute regulatory protein (StAR), peripheral benzodiazepine receptor-associated protein (PAP7) and diazepam binding inhibitor (DBI) (G.-J. Liu et al., 2014), and that the association with proximal proteins can affect the binding of ligand to TSPO towards both higher and lower affinity (Midzak et al., 2015).

TSPO is an evolutionary ancient protein and expressed throughout all tissues but at the highest concentration in steroid synthesising tissues in body and brain. When performing a ¹¹C-PBR28 PET scan of the torso and head, it is apparent that TSPO is present in high concentrations in the

heart and lungs (Kreisl et al., 2010). TSPO is also abundant in monocytes and granulocytes (Canat et al., 1993). The name TSPO was changed from PBR because of its involvement in intracellular movement of protoporphyrins and cholesterol (Papadopoulos et al., 2006). However, more recently this function of mammalian TSPO has been taken up for renewed discussion (Zhao et al., 2016). TSPO has been demonstrated to be involved in numerous cellular processes including steroidogenesis, cell growth and proliferation, bile acid synthesis, calcium flow, heme synthesis, mitochondrial respiration and apoptosis (Chen & Guilarte, 2008).

TSPO and neuroinflammation

In the healthy brain, TSPO is expressed at low levels (Chen & Guilarte, 2008), but upregulation occurs after damage to brain tissue or invasion of pathogens (Martín et al., 2010). TSPO-upregulation has been paralleled with the concept of neuroinflammation, and used as a molecular target for studying human neuroinflammation in vivo by molecular imaging. In early TSPO imaging literature, emphasis was often exaggerated on TSPO upregulation in microglia, but it is now recognised that astrocytes and invading macrophages also make up a substantial part of the TSPO-signal (Martín et al., 2010). Since TSPO upregulation is not specific to types of immunological cells or their active properties, a change in TSPO expression has to be interpreted in the context of the condition that is studied (G.-J. Liu et al., 2014). A description of the TSPO expressing cells of the brain is given below.

Microglia

Microglia are often referred to as the resident macrophages of the brain. However, microglia show very unique properties and do not originate from haematopoietic cells in the bone marrow but rather the yolk sac and enter the brain during early development of the brain (Ginhoux et al., 2010).

Under healthy conditions, microglia are distributed throughout the brain tissue in a ramified phenotype, chemically surveying the local extracellular environment with motile processes emitting from the cellular body (Prinz & Priller, 2014). In this state TSPO is only expressed to a small degree (Chen & Guilarte, 2008).

As a response to neuronal damage or pathogens in the extracellular environment, microglia transform into a “reactive” state and move to the lesion site. Microglia show very diverse properties in this reactive state and play a pivotal role orchestrating astrocyte activation and recruitment of peripheral macrophages (Tang, & Feng, 2011). TSPO is highly upregulated in reactive microglia (Albrecht, et al., 2016).

Historically, microglia activation has been paralleled to macrophage polarization with activation into M1 and M2 phenotypes. This paradigm suggests that microglia can activate in a classical pathway in response to pathogens or neuronal damage leading to a M1 pro-inflammatory phenotype producing proinflammatory cytokines and reactive oxygen species. Alternatively, in response to chemokines, microglia activate into a M2 neuroprotective phenotype that promotes tissue remodelling and produces anti-inflammatory cytokines. (Nakagawa & Chiba, 2015; Prinz & Priller, 2014). It is generally accepted that microglia retain the above-mentioned properties, however, the polarization paradigm is disputed both for macrophages and microglia (Ransohoff, 2016).

Astrocytes

Astrocytes are the most diverse resident cells of the brain and play many structural and functional roles under healthy and pathological conditions (Cekanaviciute & Buckwalter, 2016). Like microglia, astrocytes can transition into a high TSPO expressing reactive state in response to neuronal damage and pro-inflammatory cytokines (Cekanaviciute & Buckwalter, 2016). The upregulation of TSPO in reactive astrocytes usually shows a temporally slower and more prolonged upregulation pattern compared to microglia (Boutin & Pinborg, 2015). TSPO upregulation in astrocytes has been linked to the synthesis of the two neurosteroids pregnenolone and progesterone (Le Goascogne et al., 2000; Schumacher et al., 2000). Activated astrocytes like microglia regulate the local immune response by releasing cytokines and chemokines in the affected tissue. Furthermore, astrocytes acts as a physical barrier by forming astrocytic scars to wall of sites of neuronal injury (Cekanaviciute & Buckwalter, 2016).

Macrophages

Peripheral macrophages have the ability to cross the BBB and infiltrate the brain parenchyma in response to injury or infection (Minogue, 2017) and express TSPO (Canat et al., 1993). The degree of macrophage invasion varies greatly depending on the disease and is generally assumed to be larger in diseases with disruption of the BBB (Albrecht et al., 2016), but the role of infiltrating macrophages in neuroinflammation is unclear and confounded by their similarity to activated microglia in both morphology and phenotype (Minogue, 2017).

TSPO radiotracers

The first generation TSPO radiotracers for molecular imaging were developed in the late 1980's (G.-J. Liu et al., 2014) and since then, more than 50 TSPO tracers have been developed (Ching et al., 2012). One of the first-generation tracers is ^{11}C -PK11195, which is still widely used for PET imaging today. For SPECT imaging, iodinated first-generation analogues exist such as ^{123}I -RO5-4864 and ^{123}I -PK11195 (Gildersleeve et al., 1989; Stevenson et al., 2010). Because of relatively low affinity to TSPO for the first-generation radiotracers, second generation TSPO radiotracers have since been developed. ^{123}I -CLINDE is a second generation radiotracer for SPECT imaging (Arlicot et al., 2008; Mattner et al., 2008).

Currently, the most widespread second generation PET radiotracers are ^{11}C -PBR28 and ^{18}F -DPA714. However, the search for a high affinity radiotracer that is unaffected by the rs6971 polymorphism is still on-going and tracer development is now entering the third generation.

The rs6971 polymorphism

After the development of second generation radiotracers with higher signal to noise ratio, substantial indefinable differences in binding of ligand to TSPO were measured that could not be reproduced with ^{11}C -PK11195 especially for the radiotracer ^{11}C -PBR28 (Kreisl et al., 2010). The cause of the difference remained a mystery until Owen et al. described the effect of the rs6971 polymorphism on the affinity (Owen et al., 2012). The rs6971 single nucleotide polymorphism is an amino acid substitution in the trans-membrane pocket of TSPO at position 147 of Threonine (T) by Alanine (A). This results in a division of subjects into high affinity binders (HABs, TT), mixed affinity binders (MABs, AT) and low affinity binders (LABs, AA). There is large variance in the polymorphism throughout different ethnic populations. In previous studies on white Caucasian populations the incidence of HABs is 65%, MABs 30%, and LABs around 5% (Mizrahi et al., 2012). The rs6971 polymorphism is usually only attributed to differences in the affinity to second generation TSPO tracers, however, an association of the single-nucleotide polymorphism has been made to Bipolar disorder (Colasanti et al., 2013). ^{123}I -CLINDE is a second generation TSPO tracer and thus sensitive to the rs6971 polymorphism (Feng et al., 2014). The rs6971 polymorphism provides a limitation for quantification in TSPO studies using tracers whose affinity to TSPO are affected, and should be accounted for in the study design and analysis (Owen et al., 2015).

TSPO imaging studies in diseases of the human brain

Since the link between TSPO and neuroinflammation was drawn in the early 1980's, in vivo TSPO imaging has been performed in a number of the diseases of the brain where inflammation or other causes for TSPO upregulation (e.g. glioma) are known or hypothesised to play a role. Furthermore, TSPO has been studied in a variety of brain diseases with acute inflammation (stroke, encephalitis, multiple sclerosis and tumor) or chronic inflammation (dementia, Alzheimer's disease, schizophrenia). This thesis includes a more in-depth description on TSPO expression in the studied diseases in the 'description of research projects' section.

2. Objectives

At the initiation of the current PhD project, eleven subjects had been scanned at our site, and the first methodological paper on the quantification of ^{123}I -CLINDE SPECT was in the workings (Feng et al., 2014). The main objective of the current thesis was to further advance ^{123}I -CLINDE SPECT imaging in clinical research. This was done in three ways:

- 1) To perform two proof-of-concept studies with ^{123}I -CLINDE SPECT imaging in challenging clinical settings:
 - a. To investigate the longitudinal dynamics of the TSPO expression at the initiation of treatment and after clinical recovery in an Anti-N-Methyl-D-Aspartate receptor (Anti-NMDAr) encephalitis patient (Study 1).
 - b. In Glioblastoma multiforme (GBM) patients, to compare baseline ^{123}I -CLINDE SPECT with gadolinium-enhanced MRI imaging, ^{18}F -FET PET, and follow-up structural imaging (Study 2).
- 2) To further the validation and development of the ^{123}I -CLINDE SPECT scanning method by performing a test-retest study in healthy volunteers and testing the effect of blood sample handling (Study 3).
- 3) Finally, to perform a clinical study with longitudinal ^{123}I -CLINDE SPECT imaging in stroke patients (Study 4) and investigate the temporal evolution of TSPO expression after stroke, compare results to rehabilitation measures and TSPO expression in healthy volunteers. Here the following hypotheses were tested for the stroke patients:
 - a. Increased perilesional binding of ^{123}I -CLINDE to TSPO at 1-2 weeks after stroke is a biomarker of poor recovery at 25-26 weeks.
 - b. Increased binding of ^{123}I -CLINDE to TSPO in the ipsilesional thalamus and pons at 1-2 weeks after stroke is a biomarker of poor recovery at 25-26 weeks.
 - c. Increased binding of ^{123}I -CLINDE to TSPO in the contralesional thalamus at 5-6 weeks after stroke is a biomarker of good recovery at 25-26 weeks.

3. Description of the research projects

Study 1 – Proof of concept: ¹²³I-CLINDE-SPECT in anti-NMDAr encephalitis

Background

The autoimmune encephalitis (AIE) subtype Anti-NMDAr encephalitis is a relatively newly discovered, but prevalent antibody-mediated disease with neurologic and psychiatric symptoms associated with the limbic regions of the brain (e.g. amnesia, confusion and epileptic seizures) and a mortality of 14 % (Blaabjerg et al., 2015). The two most prevalent autoimmune encephalitis types anti-NMDAr encephalitis and anti-Leucine-rich glioma-inactivated 1-encephalitis (anti-LG1 encephalitis) comprise 80% of all diagnosed AIE's in Denmark (Blaabjerg et al., 2015). Anti-NMDAr encephalitis is associated with production of antibodies towards the glutamate receptor subtype N-methyl-D-aspartate receptor. An underlying cancer diagnosis is made in 40-50 % of anti-NMDAr encephalitis cases (Titulaer et al., 2013). The first description of Anti-NMDAr encephalitis symptoms was in 2005 and the first correlation between symptoms and antibodies was made in 2007. AIE is generally under-diagnosed which greatly influences treatment response and prognosis. Twenty-four months mortality is 9.4% after anti-NMDAr encephalitis onset and 20% have severe loss of function (Blaabjerg et al., 2015).

The current first line treatment for anti-NMDAr encephalitis is high-dose methylprednisolone (1g a day for five days) in combination with plasmapheresis (5-7 treatments during 10-14 days) or intravenous immunoglobulin (2 g pr. Kg bodyweight distributed over 5 days). (Blaabjerg et al., 2015). Around 50% respond to treatment (Titulaer et al., 2013). Furthermore, symptoms and/or underlying cancer diagnosis are addressed separately.

Previously, TSPO has been demonstrated to be upregulated in two human case of Rasmussen's encephalitis using ¹¹C-PK11195 PET, demonstrating both focal and diffuse binding increase in the affected hemisphere (Banati et al., 1999), but no previous human TSPO studies on AIE have been published.

Case description

The patient was a 35-year-old male, originally admitted to the department of psychiatry because of sudden onset of severe psychosis. At the transfer to the department of neurology, the patient suffered from psychosis, amnesia, orofacial dyskinesia, catatonia and autonomic instability. Antibodies for the NMDA receptor were detected in the cerebrospinal fluid (CSF), and the diagnosis of anti-NMDAR encephalitis was confirmed (Dalmau et al., 2011).

The patient was treated with plasmapheresis and methylprednisolone and had a good recovery. Seven weeks after treatment, the patient (Titulaer et al., 2013) was back at work part time, despite mild cognitive symptoms. At 6 months follow-up the patient was back to work full time.

Study design and materials

¹²³I-CLINDE SPECT, T1 weighted MRI, genotyping, post processing and kinetic modelling were performed as described in the general methods section. The patient was scanned twice with ¹²³I-CLINDE SPECT: at 2 days and 7 weeks after initiation of immunotherapy. Results were compared to an age- gender- and genotyped matched (MAB) healthy volunteer.

Study 2 – Proof of concept: ¹²³I-CLINDE SPECT in Glioma

Background

Glioblastoma multiforme remains the most frequent and malignant primary CNS tumor with a median overall survival of 15 months from the time of diagnosis in spite of conventional treatment (Stupp et al., 2005). To visualise and quantify tumor progression and treatment response, GBM patients undergo structural imaging with contrast enhanced MRI (gd-MRI) and molecular imaging with 0-(2-¹²³I-fluoroethyl]-L-tyrosine PET (¹⁸F-FET PET) (Dunet et al., 2012; Pauleit, 2005). However, it is known that ¹⁸F-FET PET is not entirely glioma-specific and that increased ¹⁸F-FET uptake is also present in astrogliosis, secondary to infection, haematoma, ischemia and as a cause of radiation injury (Floeth et al., 2006; Pichler et al., 2010; Salber et al., 2007; Spaeth et al., 2004).

TSPO has been demonstrated to be expressed in glioma cell lines and the density of TSPO has been positively correlated with WHO malignancy grade (Louis et al., 2016), cell proliferation index and mortality (Miettinen et al., 1995; Vlodyavsky & Soustiel, 2007; Winkeler et al., 2012).

In astrocytic brain tumor cell lines, TSPO is expressed primarily by the neoplastic cells and to a small degree in glioma associated microglia/macrophages (GAMs) (Awde et al., 2013; Winkeler et al., 2012). ^{123}I -CLINDE SPECT has been validated for investigation of TSPO expression in a GL26 mouse glioma model (Tsartsalis et al., 2015) and investigated in glioma patients (Feng et al., 2014). Here, no significant changes in ^{123}I -CLINDE binding were found in areas of gadolinium leak on gd-MRI leading to the assumption that ^{123}I -CLINDE binding parameters are not affected by an impaired BBB. The aim of this study was to test the hypothesis that at baseline ^{123}I -CLINDE SPECT is a predictor of tumor progression at follow-up structural imaging.

Study design and demographics

Patients: The study included three patients in advanced state of GBM (Table 3.1). All patients had undergone debulking tumor surgery and received radio- and chemotherapy with temozolomide, bevacizumab and irinotecan before inclusion. At baseline, patients were scanned with ^{123}I -CLINDE SPECT, ^{18}F -FET PET and gd-MRI within two days. At follow-up, patients 1 and 2 were re-scanned with gd-MRI and patient 3 with contrast-enhanced CT (CE-CT). The current study joined in the advanced stage of a larger study with autologous lymphoid effector cells specific against tumor cells (ALECSAT) which was received by patient 2 and 3. No further patients were included because of the termination of the ALECSAT study.

Patient	Sex	Age (y)	Binder status	Rescanning modality	Interval (wk)	^{123}I -CLINDE injected dose (MBq)
1	F	48	MAB	MR imaging	6	191
2	M	65	LAB	MR imaging	17	188
3	M	64	MAB	CT	4	188

Table 3.1. Overview of glioma patients included in the study. Genotype, rescan modality, time intervals between scans and injected ^{123}I -CLINDE dose.

Study 3- Advances in protocol and test-retest variability of ¹²³I-CLINDE SPECT

Background

Performing a test-retest study is a way to test the reproducibility and reliability of a given modality by performing two identical tests and comparing the results. This is useful for the design of future studies and to compare with other similar methods for validation. A method with high reproducibility is good for performing longitudinal studies, since fewer subjects would be required in the study. However, one should bear in mind that a test-retest study does not give a measure on the specificity or sensitivity of the method. If a biological variance occurs that is not taken into account when measuring, a method with high sensitivity would yield a higher test-retest variance. In the current study, the tested modality was ¹²³I-CLINDE SPECT scanning in healthy volunteers. The outcome measures are percentage difference (PD), which is an estimate of test-retest reproducibility and tracer reliability measured as intra-class correlation coefficient (ICC) and coefficient of variation (COV) (see methods for study 3 for definitions).

The test-retest variance has previously been examined in the first generation TSPO tracers ¹¹C-PK1195 (Jučaitė et al., 2012) revealing moderate test-retest variability, and in the second generation tracers ¹¹C-DPA 713 (Coughlin et al., 2014) and ¹¹C-PBR28 (Collste et al., 2015; Park et al., 2015) with moderate to good test-retest variability.

Study design and demographics

Healthy volunteers were screened for the rs6971 genotype before inclusion in order to restrict the inclusion to MABs and HABs. All subjects had a normal neurological examination and blood screen. A total of sixteen healthy controls were included in the study (MABs=8, HABs=8, females=9). Healthy volunteers were ¹²³I-CLINDE SPECT scanned twice and scanned once with T1-weighted MRI. See table 3.2 for an overview of the patients.

Test-retest variability measures were estimated on both brain SUV and V_T 's derived from 2TCM.

In the current study, the variability of ¹²³I-CLINDE was tested independently in both brain and blood. During the study, we discovered that the blood measurements were sensitive to the time from drawing to centrifugation (see the results section for study 3). This is probably because of continuous binding of parent tracer to TSPO in blood cells where monocytes and granulocytes

are known to express abundant levels of TSPO (Canat et al., 1993). This finding made us change the protocol for handling and centrifugation the blood samples. In the old protocol, a batch of blood samples were drawn and stored on ice. They were then transported to the HPLC site and waited for some time before centrifugation. In the worst-case scenario, blood samples were resting on ice for 90 minutes from drawing to centrifugation. This protocol was applied for the first eight healthy volunteers. For the new protocol, a centrifuge was acquired to be in the near vicinity of the scanner, so that blood samples could be centrifuged as fast as possible. This immediate centrifugation was timed to be within 5 minutes from drawing the blood samples to starting the centrifuge. Immediate centrifugation was applied for the remaining eight healthy volunteers. Finally, we implemented a population-based approach based on whole blood curves which theoretically should be unaffected by being kept in the vial for any amount of time.

Table 1 Demographic data and methodological information specified by subject

Subject	Gender	Age (yrs)	Body weight (kg)	TSPO genotype	Injected activity (MBq)	Scan interval (days)	Centrifugation	Purity (%)	Plasma control (%)
1	M	61	80	MAB	120.9 117.8	21	delayed	96.1 93.5	95.4 91.4
2	M	70	92	MAB	112.2 123.6	42	delayed	95.4 94.9	95.4 93.8
3	M	59	76.5	HAB	118.1 112.0	35	delayed	96.4 94.9	94.7 93.2
4	F	38	110	HAB	116.3 114.3	28	delayed	96.0 90.7	95.0 88.4
5	F	62	70	HAB	119.0 119.4	42	delayed	96.1 96.6	95.1 94.0
6	F	58	50	MAB	116.0 119.7	28	delayed	96.1 95.3	96.2 91.4
7	F	68	87	HAB	124.8 115.1	56	delayed	92.3 95.2	90.1 90.5
8	M	52	94	HAB	118.5 124.1	56	delayed	98.1 89.8	93.8 88.5
9	M	42	80	MAB	118.8 115.8	28	immediate	95.7 93.4	94.6 90.3
10	F	45	86.2	MAB	117.4 114.1	56	immediate	95.4 94.9	94.6 94.7
11	M	35	100	HAB	119.9 114.4	56	immediate	93.0 90.7	93.2 89.9
12	F	40	73	MAB	112.0 130.7	7	immediate	92.8 94.7	91.8 94.1
13	M	24	95.6	MAB	115.4 116.0	14	immediate	94.4 92.0	92.2 90.2
14	F	69	83	MAB	123.0 127.1	28	immediate	94.5 94.4	92.7 90.4
15	F	30	68	HAB	105.8 116.0	42	immediate	91.0 91.1	82.9 88.1
16	F	34	74.2	HAB	118.4 116.3	28	immediate	NA NA	NA NA
Mean ±STD		49± 15	82.5± 14.4		117.9± 4.9	35± 15		93.4± 1.7	91.4± 3.2

Table 3.2: The table displays the data for the healthy volunteers included.

Study 4 - Clinical study: ¹²³I-CLINDE SPECT in stroke

Background

Stroke is a large burden to patients and society and the major contributor to inherited disability in developed countries (“WHO | The Atlas of Heart Disease and Stroke,”). Molecular imaging of TSPO after stroke is of particular interest because of upregulation in microglia, macrophages and astrocytes, as a response to brain injury (Chen & Guilarte, 2008). This provides a window into the acute and chronic immune-response after cerebral infarction. Since microglia, macrophages and astrocytes possess both detrimental proinflammatory and neuroprotective properties, TSPO expression after stroke has been proposed to be a biological marker of recovery, a possible therapeutic target and a marker of clinical response to future immunomodulatory therapy (Boutin & Pinborg, 2015).

Animal studies have demonstrated that TSPO is expressed both lesionally and perilesionally in strokes with reperfusion, whereas the core infarct has low TSPO expression in strokes with permanent ischemia. Here TSPO was primarily expressed in the infarct margin and perilesional region. Furthermore, investigation into the temporal profile of TSPO expressing cells has revealed that initially in rodent stroke models TSPO is expressed primarily in microglia and macrophages and slightly later on primarily by astrocytes.(Boutin & Pinborg, 2015)

Previous TSPO imaging studies in human stroke have emphasised a handful of brain regions of interest (Feng et al., 2014; A Gerhard et al., 2000; Alexander Gerhard, Schwarz, Myers, Wise, & Banati, 2005; Gulyas et al., 2012; Gulyás et al., 2012; Jensen et al., 2015; Pappata et al., 2000; Price, 2006; Radlinska et al., 2009; Ramsay et al., 1992; Ribeiro et al., 2014; Thiel et al., 2010) (Figure 3.3). Generally the regions can be divided into three subtypes. Lesion-related regions, regions anatomically connected to the lesion and regions un-related to the lesion: Lesion-related regions are the lesion area and the perilesional area. In these areas, TSPO has been shown to be expressed from 72 hours, peaking between 2-3 weeks and then decreasing gradually. TSPO expression in the perilesional area is of special interest since proinflammatory microglia and macrophages potentially have the ability to be detrimental to potentially salvageable brain tissue (Weinstein et al., 2010).

For MCA strokes, anatomically connected regions are pons and thalamus. Previous studies have shown increased TSPO expression in both the ipsilesional (Gerhard et al., 2005; Pappata et al., 2000) and contralesional thalamus (Gerhard et al., 2005). In the study by Radlinska et al. (2009) TSPO expression caudal to the stroke in the pyramidal tract was demonstrated in patients where the pyramidal tract was affected as seen on Diffusion Tensor Imaging (DTI). Later on in the same patient cohort, Gerhard et al. (2010) demonstrated a negative partial correlation between the follow-up function of the affected upper extremity as measured with the Rivermead motor function scale and TSPO upregulation in the pyramidal tract. It was proposed that TSPO upregulation in connected tissues can be a consequence of Wallerian degeneration. TSPO expression in regions un-related to the lesion are regions supposed to be unaffected by stroke. Typically this would be the cerebellum or contralesional hemisphere and these regions have been used as reference regions in quantification of the binding of tracer to TSPO. Since we use a metabolite corrected input function for quantification of ^{123}I -CLINDE SPECT (see general methods) we found it interesting to examine these regions. There have been no previous reports on an effect of stroke in humans for these regions.

Author	Year	Number of patients	Stroke	Ligand and imaging	Time of PET	Results
Ramsey et al.	1992	1	1 MCA	[¹¹ C]-PK11195 PET CT	6, 13 and 20 days	Increased TSPO expression in hemisphere of stroke on day 13.
Gerhard et al.	2000	5	4 MCA 1 PCA	[¹¹ C]-PK11195 T1 MRI	5-53 days (1 rescanned)	Increased activity in the stroke region as shown on T1W MRI
Pappata et al.	2000	7	MCA	[¹¹ C]-PK11195 PET +T1 MRI	60-365 days	Increased TSPO expression in ipsilesional thalamus, perinfarct areas and capsula interna.
Gerhard et al.	2005	6	4 MCA 1 PCA 1 BS	[¹¹ C]-PK11195 PET +T1 MRI	3-150 days (2 rescanned)	Increased TSPO expression up to 28 days. After 150 days extending to connected ipsilateral and contralesional regions.
Price et al.	2006	4 4 C	MCA + control	[¹¹ C]-PK11195 PET +T1,T2 MRI	2-30 days (3 rescanned)	TSPO expression within 72 hours, rising within a week before some reduction by weeks 3-4.
Radlinska, Thiel et al.	2009	21	Sub-cortical	[¹¹ C]-PK11195 PET +T1 and DTI MRI (3T)	2-20 days	Specific remote caudal TSPO expression in subjects with subcortical infarct in pyramidal tract. (using DTI to delineate fibertracts)
Thiel et al	2010	18	Sub-cortical	[¹¹ C]-PK11195 PET +T1 and DTI MRI (3T)	Within 3 weeks. 6 month follow up	Correlation between PT damage on DTI (R_{FA}) and PK uptake in the brainstem. No correlation between PK uptake in the infarct or brainstem and motor score (RMFT) at follow-up.
Gulyàs et al.	2012	4	Focal	[¹¹ C]-PK11195	28-55 days	Comparative study of [¹¹ C]-PK11195 And [¹¹ C]vinpocetine. Vinpocetine has possible nonspecific binding or different receptor profile than PK.
Gulyàs et al.	2012	9	Cortical and subcortical	[¹¹ C]vinpocetine	7-98 days	Increased TSPO expression in perilesional region for several weeks after stroke
Feng et al	2014	9	3 MCA, 1rescan 2 PCA, 1 rescan	[¹²³ I]CLINDE	28-252 days	Increased TSPO expression in lesional and perilesional region at 4 weeks after stroke, decreasing at later timepoints. One patient with increasing TSPO expression in the contralesional insula at 8 months after stroke.
Ribeiro et al	2014	9	MCA	[¹⁸ F]DPA-714	8-18 days	Increased TSPO expression activation in the lesional and perilesional region

Table 3.3 An overview of Previous TSPO studies in stroke patients

Study design and demographics

Patients: The investigation of stroke patients was designed as a longitudinal study (Figure 3.1). Patients were recruited from Rigshospitalet and Bispebjerg Hospital, Copenhagen University Hospital, in the first week after stroke then and scanned longitudinally with concomitant ¹²³I-CLINDE SPECT and structural MRI three times at, i.e. 1-2, 5-6 and 15-18 weeks after stroke. Furthermore, the patients underwent a clinical rating battery of rehabilitation measures at scan-days and at 25-26 week follow-up.

Patients were included according to the following in- and exclusion criteria:

Inclusion criteria:

- First ever MCA stroke with cortical/subcortical involvement and affection of the contralateral upper extremity
- HAB (TT) or MAB (AT) genotype
- Age above 18

Exclusion criteria:

- Prior relevant neurological impairment or a severe medical condition that prohibiting participation in the study
- Insufficient ability to participate in the study and its informed consent process
- Contraindications for SPECT or MRI imaging

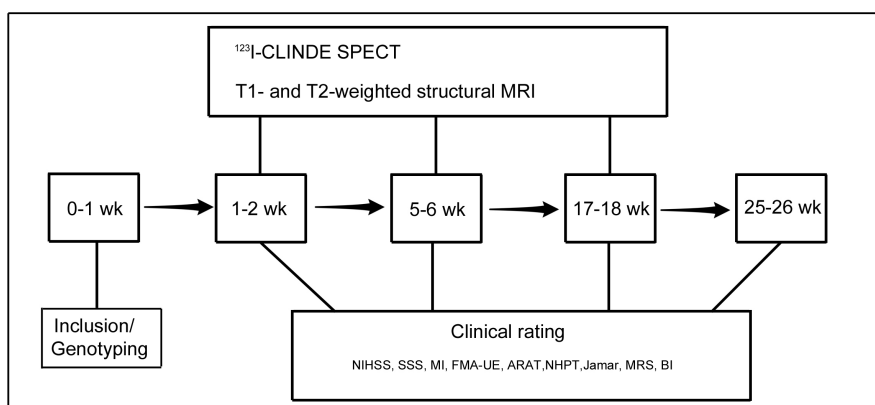


Figure 3.1: Diagram of the study design from study 4.

In total, 12 stroke patients completed the study (Table 3.4). Rehabilitation measures and MRI sequences are detailed in the methods section for study 4.

Healthy volunteers: Genotyping revealed that 10 out of 12 stroke-patients were HAB (Table 3.4). Thus, 10 healthy HAB volunteers were recruited and underwent ^{123}I -CLINDE SPECT and MRI once. Some of the healthy volunteers were also participating in the test-retest study (study 3) and therefore scanned twice. In these cases, the first ^{123}I -CLINDE SPECT scan was used. See table 3.3 for demographics of the healthy volunteers.

Volunteer no.	Gender	Age at inclusion (Years)	Injected activity (MBq)
HV 1	M	49	124.9
HV 2	M	36	119.9
HV 3	F	48	104.5
HV 4	M	25	112.5
HV 5	F	34	115.3
HV 6	F	44	116.2
HV 7	F	30	105.8
HV 8	F	34	118.4
HV 9	F	24	128.2
HV 10	F	21	120.9

Table 3.3: Demographics of the healthy volunteers in study 4

Patient no.	Days after stroke	Gender	Age at inclusion (Years)	lesion side / Artery	Etiology	TSPO Genotype	Injected activity (MBq)	Centrifugation
Pt. 1	10	F	52	Left MCA	ICA dissection (Trauma)	HAB	108.9	Delayed
	38						113.4	Delayed
	101						103.1	Delayed
Pt. 2	10	M	63	Left MCA	ICA dissection - (HT)	HAB	112.3	Delayed
	46						102.5	Delayed
	157						117.5	Immediate
Pt. 3	12	M	57	Left MCA	Thrombo-embolism (HC)	HAB	135.7	Immediate
	40						114.8	Immediate
	130						126.8	Immediate
Pt. 4	15	M	60	Left MCA	Thrombo-embolism (HT+HC)	HAB	110.9	Immediate
	43						115.9	Immediate
	139						128.3	Immediate
Pt. 5	11	F	42	Right MCA	Thrombo-embolism (Contraception)	HAB	127.3	Immediate
	39						114.7	Immediate
	131						108.9	Immediate
Pt. 6	9	M	68	Right MCA	ICA dissection - (HC)	MAB	121.5	Immediate
	35						123.2	Immediate
	135						113.0	Immediate
Pt. 7	7	F	72	Right MCA	Thrombo-embolism (AF)	HAB	118.9	Immediate
	41						117.7	Immediate
	126						108.3	Immediate
Pt. 8	13	F	68	Right MCA	Thrombo-embolism - (HC+HT)	HAB	117.8	Immediate
	41						122.1	Immediate
	125						103.2	Immediate
Pt. 9	10	F	59	Left MCA	Thrombo-embolism (HC)	MAB	137.0	Immediate
	37						117.4	Immediate
	121						122.1	Immediate
Pt. 10	13	F	55	Right MCA	ICA dissection - (HT)	HAB	123.7	Immediate
	41						130.5	Immediate
	132						111.3	Immediate
Pt. 11	10	M	61	Left MCA	Thrombo-embolism (HT)	HAB	113.6	Immediate
	38						112.8	Immediate
	122						114.4	Immediate
Pt. 12	10	M	62	Right MCA	Thrombo-embolism (AF)	HAB	117.6	Immediate
	44						124.9	Immediate
	122						109.9	Immediate

Table 3.4: Demographics of stroke patients in study 4.

4. Methods

Molecular imaging with SPECT

Single-photon emission computed tomography (SPECT) is a molecular imaging modality using photon-emitting isotopes (e.g. ^{123}I , ^{131}I , $^{99\text{m}}\text{Tc}$, ^{111}In) injected or inhaled *in vivo* and measuring the photons from the outside with circulating gamma cameras.

During the acquisition of a SPECT scan, Collimators in front of each of the gamma cameras are selecting projections perpendicular to the head of the gamma camera. After measurement, the tomographic projections are reconstructed into 3-dimensional volumes. Dynamic scans can be obtained by acquiring several volumes consecutively and provide a 4-dimensional image with time as the last dimension. The final post processing part in the quantification of the SPECT signal involves Region of interest (ROI) delineation and quantification of binding using e.g. kinetic modelling. SPECT, albeit lower spatial resolution compared to PET, provides large clinical impact because of the geographically prevalent availability of SPECT tracers since the hospital or clinic is not limited by the need of having a cyclotron available.



Figure 4.1 A photo of the triple head IRIX camera used at the department of neurology at Rigshospitalet for ^{123}I -CLINDE SPECT scanning. To the right in the picture the syringes for blood sampling are displayed.

Radiotracers

A large quantity of radiotracers has been developed to measure a broad range of physiological and biological processes (i.e. blood flow, metabolism, neuroreceptors and transporters). The radioisotope is usually attached to a ligand (e.g. CLINDE), and this ligand has specific affinity to the molecular target of interest. Radioisotopes are administered in tracer doses, meaning that the in vivo concentration occupies a maximum of 10 % of the target sites (Innis et al., 2007). This is enough to measure, but not enough to cause biological effects or saturate the binding sites.

Several conditions need to apply for a radiotracer to be optimal for quantification of molecular targets in the central nervous system (CNS):

- 1) The radiotracer must be able to cross the blood brain barrier (BBB). Compared to most organs, the BBB provides an extra barrier for examining the CNS. Generally the ability to passively cross the BBB depends on the lipophilicity of the radiotracer but too high lipophilicity can increase non-specific binding in brain tissue (Waterhouse, 2003). Radiotracers should cross the BBB by passive diffusion, and there should be no active BBB transport of radiotracer. Finally, radiometabolites and radioactive impurities arising from the tracer production should not cross the BBB.
- 2) High affinity and high selectivity to the molecular target as well as low non-specific binding in tissue are required to get optimal signal to noise ratio.
- 3) The tracer must provide suitable pharmacokinetics for quantification of the signal with kinetic modelling.

2-tissue compartment modelling

The optimal model for quantification of ^{123}I -CLINDE SPECT has been demonstrated to be 2-tissue compartment modelling (2TCM) with metabolite corrected arterial input (Feng et al., 2014). This model is often generally interpreted as gold standard for molecular imaging quantification (Gunn et al., 2001). The 2TCM actually consists of three compartments. (Figure 4.2):

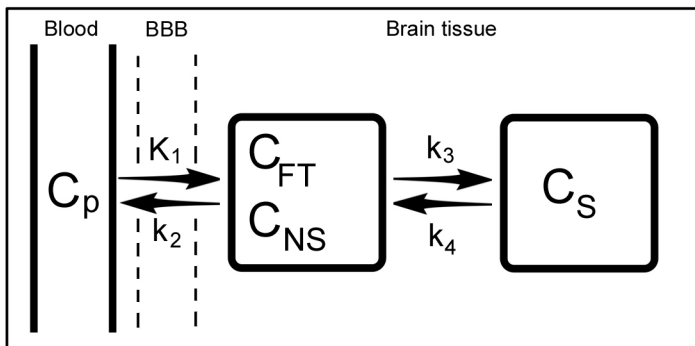


Figure 4.2: A diagram of the 2-tissue compartment model. BBB=blood brain barrier, C_p = plasma concentration, C_{FT} = concentration of free tracer in tissue, C_{NS} = concentration of non-specifically bound tracer in tissue. C_s concentration of tracer bound to target. K_1 , k_2 , k_3 and k_4 are rate constants of diffusion between compartments.

C_p is the concentration of tracer in blood plasma. From the blood, tracer is diffusing into the tissue compartment (C_1), which consists of both free tracer (C_{FT}) and non-specifically bound (C_{NS}). The rate constants describing the diffusion of tracer to and from the plasma are called K_1 and k_2 . Once inside the tissue the tracer can also bind specifically to the target of interest, which is interpreted as an individual compartment (C_S), and the rate constant describing the binding to and from target are denoted (k_3) and (k_4) (Innis et al., 2007).

This system can be described by the following differential equations:

$$\frac{dC_1(t)}{dt} = K_1 C_p(t) - (k_2 + k_3)C_1(t) + k_4 C_S(t)$$

and

$$\frac{dC_2(t)}{dt} = K_3 C_1(t) - k_4 C_S(t)$$

where $C_1 = C_{FT} + C_{NS}$

The metabolite corrected input function ($C_p(t)$) is measured by performing blood sampling and $C_p + C_{ns} + C_{FT} + C_S$ is measured by the SPECT scanner. The rate constants (K_1 , k_2 , k_3 and k_4) are estimated by non-linear fitting. The outcome measure from 2TCM used in ^{123}I -CLINDE SPECT is the distribution volume (V_T), which can be interpreted as the volume fraction of the same amount of tracer in the two tissue compartments divided by the blood compartment. The unit for V_T is cm^3/mL and estimated as:

$$V_T = \frac{K_1}{k_2} + \frac{K_1 \times k_2}{k_2 \times k_4}$$

The ^{123}I -CLINDE SPECT scanning protocol

All studies are performed in accordance with the Helsinki Declaration, and have been approved by the ethical committee of Copenhagen (H-2-2010-086, amendments 35394, 39319, 42262, 51278, 51900 and 55783) and registered to the Danish Data Protection Agency (j.nr. 2012-58-0004 local j.nr. 30-0739). Prior to beginning the experiment, a signed informed consent form was acquired from the subject to be examined.

SPECT scanning

^{123}I -CLINDE is produced by MAP Medical Technologies (Tikkakoski, Finland) calibrated to 185 MBq at 13:00 hours the next day. ^{123}I -CLINDE is transported by flight to Copenhagen. The next morning, the tracer is collected at the airport and transported to Rigshospitalet by a professional courier.

A venous catheter is applied and used to draw venous blood samples to be analysed for standard blood parameters at the Department of Biochemistry, Rigshospitalet. For the analysis of radiometabolites in blood, arterial blood samples are needed, and an arterial catheter is therefore placed in the radial artery by an experienced anaesthesiologist.

A standard blood panel is to be analysed by the Department of Biochemistry at Rigshospitalet. Furthermore, blood is drawn at this time in order to perform plasma standard HPLC, and a blood sample is drawn to keep at -80 degrees Celsius for future cytokine evaluation.

Prior to imaging, subjects receive an intravenous injection of 200 mg potassium perchlorate to block thyroidal uptake of free radioiodine.

The SPECT scanner is a triple head IRIX camera (Phillips Medical, Cleveland USA) fitted with low-energy, general all-purpose, parallel-holed (LEGAP) collimators and a 9.5 mm sodium iodine scintillation crystal (Feng et al., 2014) (Figure 4.1).

The subject is positioned between the scanner heads and a headband is applied to fixate the head during the scan. Between 110-130 MBq ^{123}I -CLINDE is injected into the brachial vein simultaneously with scanner start. The scanner acquires images in two stages, the first stage is 20 minutes consisting of ten 2-minute frames and the second 70-minute stage consists of seven 10-minute frames. In total, a 90 minute dynamic scan is acquired. The first scans we performed (used in study 2) were acquired with a longer second stage of 130 minutes and consequently a total scan-time of 150 minutes. While scanning, 21 blood samples are drawn from the radial artery catheter to count the activity in whole blood and plasma, and eight samples are drawn to perform metabolite analysis using high-performance liquid chromatography (HPLC) by a trained pharmacist.

Post processing of ^{123}I -CLINDE SPECT images and blood measures.

The post processing of ^{123}I -CLINDE SPECT data has changed as the protocol has been evolved and refined during the studies.

To reconstruct the SPECT images and quantify the TSPO signal in different brain regions, the measured raw data undergo a series of post processing steps:

- SPECT images are reconstructed using filtered back projection method for each scan stage and afterwards combined to a single dynamic 90 minute scan.
- Co-registration of the concentration weighted 3-dimensional SPECT image and the T1 MRIs are performed manually using Interactive Image Overlay (IIO) (Willendrup et al., 2004).
- Regions of Interest (ROIs) are delineated from the coregistered structural MRI and SPECT images depending on the specific study. Automatic delineation of regions is performed using the PVE-LAB processing pipeline (Svarer et al., 2005). Time activity curves (TACs) are then extracted from the ROIs.
- Blood TACs are prepared from plasma and whole-blood counts.
- 2-TCM is performed using PMOD 3.0 (PMOD Technologies Inc., Switzerland).

- Firstly, a Hill function (study 1) or an exponential (study 3 and 4) or is fitted to the slope of the metabolite measurements. This estimated function is used to model the metabolite corrected input function from the plasma activity.
- Secondly, the 2-TCM model is fitted to each brain TAC data using non-linear fitting. Rate constants (K_1 , k_2 , k_3 and k_4) are estimated for each brain region and V_T measures are calculated.

Magnetic resonance imaging

For safety reasons, a standard MRI safety questionnaire is filled out for each subject prior to scanning. Structural MRI was performed on all subjects using either a Siemens Verio 1.5 Tesla scanner or a Siemens Prisma 3 Tesla scanner (Siemens, Erlangen). All subjects received T1 and T2 weighted images and gadolinium-enhanced T1 weighted images was also performed in study 1 and 2.

Methods used in study 1

All methods used in this study are described in the “general methods section”. See the study design for study 1 in the ‘Descriptions of research projects’ section.

Methods used in study 2

Acquisition and reconstruction of ^{18}F -FET PET:

All patients fasted for at least six hours before ^{18}F -FET injection. A single-frame static PET acquisition was performed on a 64-slice-CT Biograph TruePoint PET/CT scanner (Siemens, Erlangen, Germany) 20-40 minutes after intravenous injection of 200 MBq ^{18}F -FET and attenuation-corrected using a low dose CT acquired immediately before the PET scan.

Subsequently, PET images were corrected for scatter and dead time and reconstructed with an ordered subset maximization three-dimensional algorithm (6 iterations, 16 subsets) and a 5 mm Gaussian filter.

Regions of interest:

SPECT: To standardize glioma-related high ^{123}I -CLINDE binding ROIs between MAB and HAB, a cerebellar reference approach was applied by firstly defining three adjacent cerebellar regions manually on the coregistered structural MRI image and then estimating the mean

cerebellar count on the SPECT image. Secondly, glioma-related high ^{123}I -CLINDE binding regions were selected by automatically drawing an iso-contour around voxels above 1.5 times the mean cerebellar count.

PET: For $[^{18}\text{F}]\text{FET}$ -PET tumor region delineation, a 3D crescent shaped background ROI encompassing the activity above 70 % of maximum was delineated in healthy appearing grey and white matter of four contiguous brain slices above the insula in the contralateral hemisphere to the tumor. The high uptake $[^{18}\text{F}]\text{FET}$ -PET ROI was auto-contoured in 3D defining tumor tissue at a threshold of above 1.6 of mean SUV (standardized uptake value) in the background ROI. The ROI definition was performed using the Syngo-TrueD software tool (Siemens). This region delineation method is adapted from Pauleit et al. (2005).

Structural Images: Structural tumor ROIs were delineated by outlining the contrast-enhanced areas on gd-MRI or CE-CT. Tumor progression ROIs were defined as the additional contrast-enhanced area from baseline to follow-up scan.

The Sørensen-Dice index

The Sørensen-Dice index (SQ) is a measure of similarity between the overlap of two volumes (or ROIs) in space. See Figure 4.3

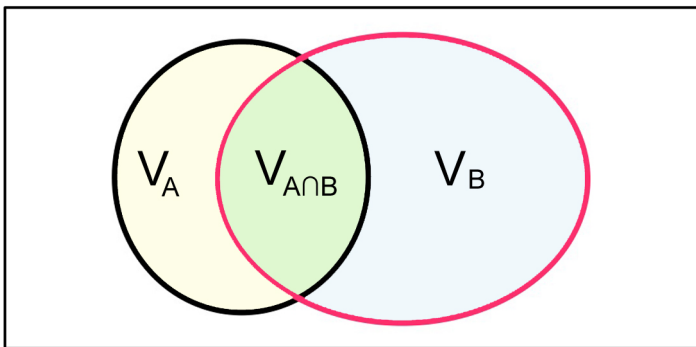


Figure 4.3: Individual and overlapping volumes V_A and V_B is the total volumes of each region and $V_{A \cap B}$ is the common or “overlapping” volume of V_A and V_B .

The SQ is defined as.

$$SQ = \frac{2V_{A \cap B}}{V_A + V_B}$$

with \cap being the symbol for common volume.

A SQ of 1 depicts total similarity and a SQ of 0 depicts no similarity between ROIs.

Methods used in study 3

Several measures of test-retest variability were applied in this study. The study also implements a population based approach to rescue the datasets with delayed centrifugation of blood samples. The population-based data-rescue method is only addressed shortly in the current thesis, as its concentration and data-analysis primarily were done by Ling Feng.

Regions

In this study, mSUV, mSUV₆₀₋₉₀ and V_T were investigated in the following ROIs: Midbrain, Thalamus, Pons, Pallidostriatum, Hippocampus, Cerebellum and Neocortex. ROIs were chosen for comparison with previous test-retest studies in TSPO tracers.

Brain uptake

Brain uptake was estimated separately as the area under the curve of the standard uptake value (mSUV) derived from the brain TAC of the investigated ROIs. mSUV's were estimated for the full 90 minutes and from 60-90 minute mSUV₆₀₋₉₀.

Blood uptake

To test the effect of delayed versus immediate centrifugation and HAB versus MAB in blood, MSUV's were calculated for the plasma to whole blood ratio and parent fraction.

Percentage difference

Percentage difference (PD) is a measure of reproducibility and is calculated for each subject as the test-retest difference divided by the average between test and retest. In study 3, calculations of PD were performed on both brain and blood mSUVs and V_T 's. Furthermore the absolute PD was calculated for brain mSUVs and V_T 's, to compare results with previous studies.

Intraclass correlation coefficient

The intraclass correlation coefficient (ICC) is a reliability measure, as it estimates the within-subject variability relative to the between subject reliability. In a test-retest situation the ICC can be interpreted as whether the variation of measures are derived from the measured group of subjects or from the variation of the measures in individual subject. To calculate this measure, firstly the deviation of measures from the mean is estimated the as the mean sum of squares between subjects (MSS_{btw}) and within subjects (MSS_{within}):

$$MSS_{btw} = \frac{1}{N-1} \sum_{i=1}^N (\bar{V}_{Ti} - \bar{V}_T)^2$$

$$MSS_{within} = \frac{1}{N} \sum_{i=1}^N \sum_{j=1}^k (V_{Tij} - \bar{V}_{Ti})^2$$

\bar{V}_{Ti} : Mean of test and retest measures of subject i , \bar{V}_T : mean of all observations. V_{Tij} : one of the measures of subject i . N : the number of subjects.

From this this ICC can be calculated as follows:

$$ICC = \frac{MSS_{btw} - MSS_{within}}{MSS_{btw} + (k-1)MSS_{within}}$$

k : number of repeated measures ($k=2$).

If $MSS_{btw} = 0$ there is no variation between subjects, thus all variance is described by the within subject variation, there is no reliability, and $ICC=-1$.

If $MSS_{within}=0$ there is no variation within subjects (test and retest values are identical), thus all variance is described by between subject variation, there is maximum reliability, and $ICC=1$.

Coefficient of variation

The coefficient of variation (COV) is the ratio between the standard deviation and the mean.

$$COV = \frac{\sqrt{\frac{1}{n \times t} \times \sum_{n,t} (x_{n,t} - m)^2}}{m}$$

where the mean

$$m = \frac{1}{n \times t} \times \sum_{n,t} x_{n,t}$$

n is the number of subjects, t is time point and $x_{n,t}$ is measure per patient and point of time. COV is calculated on all observations and does not account for the fact that some of the observations are test and retest of the same subjects.

The test-retest variation measures PD, ICC and COV are affected by many factors. The quantification of a SPECT scan relies on several independent measures: Activity in blood and plasma samples, HPLC analysis and the SPECT measure. Furthermore a biological intrasubject variation often occurs (e.g. time of day) and finally, for ICC and COV the intersubject variation also affects the measure.

Previous studies testing the reliability of second generation TSPO tracers (Collste et al., 2015; Coughlin et al., 2014; Park et al., 2015) did not report to have genotyped subjects for the rs6971 polymorphism and thus calculated the ICC value for LABs, MABs and HABs separately. Since binder-status is known to affect the affinity to TSPO for second generation TSPO tracers (David R Owen et al., 2012), bulking all genotypes into one group will increase the MSS_{btw} relative to the MSS_{within} and consequently artificially increase the ICC value. In a clinical study it is not possible to compare HABs and MABs without taking the difference in binding of tracer to TSPO into account. Thus, in study 3 we calculated ICC values for the whole group to compare with previous studies, and separately for HABs and MABs to give a more valid ICC estimate of the tracer.

General least squares model

A general least squares (GLS) model is similar to a standard linear correlation model, but can be modified to account for complex covariance structures (e.g. repeated measures). In study 3, GLS model was applied to test the effect of the following:

- Test versus retest
- Immediate centrifugation versus delayed centrifugation
- HAB versus MAB binder-status

Methods used in study 4

Structural MRI sequences

Stroke patients underwent T1 and T2 weighted structural MRI at all scans using a 3 Tesla Siemens Prisma MRI scanner (Siemens, Erlangen).

Delineation of ROIs

The following ROIs were delineated for the stroke patients:

- Stroke related ROIs: Structural T2-weighted lesion, ^{123}I -CLINDE lesion, ^{123}I -CLINDE perilesional.
- Connected anatomical ROIs: Ipsi- and perilesional thalamus and Pons.
- Anatomical ROIs unrelated to the stroke: Ipsilesional cerebellum and contralesional occipital cortex.

For the healthy volunteers, anatomical ROIs were delineated for occipital cortex and cerebellum

The structural lesion ROI was delineated on the first t2-weighted MRI (scan 1).

The ^{123}I -CLINDE lesion ROI was delineated on the first SPECT scan (scan 1) by automatically selecting voxels in the vicinity of the stroke with a value above 1.5 times the mean cerebellar ^{123}I -CLINDE uptake.

The Perilesional SPECT region was delineated by subtracting the T2-weighted lesion ROI from the ^{123}I -CLINDE lesion ROI.

Automatic delineation of anatomical ROIs is described in the general methods section.

Rehabilitation measures

The rehabilitation measures in this study can be divided into three categories:

- Neurological impairment rating scales
 - National Institute of Health Stroke Scale (NIHSS)
 - Scandinavian Stroke Scale (SSS)
 - Fugl-Meyer Assessment of the Upper Extremity (FMA-UE)
 - Motricity Index (MI)
- Functional rating scales of the upper extremity
 - Action Research Arm Test (ARAT)
 - Nine-Hole Peg Test (NHPT)
 - Grip strength (GS)

- Disability rating scales
 - Barthel Index (BI)
 - Modified Ranking scale (MRS)

Neurological impairment rating scales are clinically used tests that estimate the grade of functional impairment from a neurological deficit perspective (e.g. paresis, sensory loss, aphasia). Functional test is a test of impairment by making the patient perform different tasks and rating or measuring the performance. Disability rating scales are an estimate of the loss of function in daily life.

Statistical analysis

Testing the TSPO expression on absolute values is limited for second-generation TSPO tracers by the rs6971 polymorphism's effect on affinity of tracer to TSPO. Having V_T 's as outcome measure for the TSPO expression, there is no exact workaround for this issue (Owen et al., 2015). When studying longitudinal development one can calculate the relative differences as PD between scans. However, since V_T is a measure of the activity difference between total tissue ($C_{FT}+C_{NS}+C_S$) and blood (C_P), comparing PD measures in pooled populations of genotypes can be biased by free tracer and non-specific binding ($C_{FT}+C_{NS}$) which are not as directly affected by the affinity to the tracer as the specifically bound (C_S) part.

Comparison with healthy volunteers:

In this study, ten of the stroke patients were HABs and two were MABs. Therefore, we decided to do the comparison between stroke and healthy volunteers by comparing the ten stroke HABs at scan 1,2 and 3 with ten healthy volunteer HABs were compared to the V_T 's of cerebellum and occipital cortex in healthy volunteers using Mann-Whitney U tests.

Longitudinal evolution of the TSPO signal in stroke patients:

This was done in two ways. In the ten HAB patients by performing repeated measures ANOVA on all three scans. In all twelve patients, by calculating the PD between scans 1 and 3 and performing a one-sample two-sided t-test.

Correlations between the TSPO signal and rehabilitation measures and lesion necrosis were estimated by performing the following Pearson correlations:

- Initial V_T was correlated with PD of rehabilitation measures between scan 1 and 6 months follow-up.
- Overlap percentage of the T2-weighted lesion ROI by the CLINDE-Lesion ROI was correlated with the volume of lesion necrosis at scan 3 (15-18 weeks after stroke).

PD of rehabilitation measures were calculated as:

Repeated measure ANOVA, t-test, Pearson correlation, and Mann-Whitney U tests were performed using Prism 6.0c (Graphpad Software Inc.). Percentage difference was calculated using Matlab (Mathworks Inc.).

5. Results

Results – study 1

At the beginning of immunotherapy, the patient had high binding of ^{123}I -CLINDE to TSPO in the neocortex ($V_T = 6.3 \text{ mL/cm}^3$) and after 7 weeks the binding of ^{123}I -CLINDE to TSPO had decreased and almost normalised ($V_T = 4.0 \text{ mL/cm}^3$) compared to the healthy volunteer MAB ($V_T = 3.0 \text{ mL/cm}^3$).

Results - study 2

Results are shown in table 5.1.

Baseline

VOIs of increased ^{123}I -CLINDE binding and ^{18}F -FET uptake showed varying degrees of overlap (12-42 %). In all cases, baseline gadolinium-MRI VOIs showed greater similarity to ^{18}F -FET VOIs (SQ 0.54, 0.69 and 0.40) compared to ^{123}I -CLINDE VOIs (SQ 0.05, 0.36 and 0.18). The percentage overlap of gadolinium-MRI baseline VOIs was greater for ^{18}F -FET VOIs (79-93%) than for ^{123}I -CLINDE VOIs (15-30%).

Follow-up

In the two patients where follow-up tumor progression volumes were estimated, the volume with tumor progression at follow-up compared to baseline overlapped to a greater extent with ^{123}I -CLINDE VOIs than with ^{18}F -FET VOIs (21% vs. 8 % and 72% vs. 55%).

A - Volumes (ml)	FET-PET	CLINDE- SPECT	FET-PET \cap CLINDE-SPECT	MRI- contrast (baseline)	MRI/CT - contrast (follow up - baseline)
Pt. 1	17.3	36.6	2.0 (12%)	7.2	97.5
Pt. 2	196.9	97.9	62.6 (32%)	150.5	NA
Pt. 3	180.0	140.7	75.0 (42%)	60.7	44.8
B - Baseline	FET-PET \cap MRI-contrast baseline (ml)	CLINDE-SPECT \cap MRI-contrast baseline (ml)	SQ_{PET+MRI}	SQ_{SPECT+MRI}	
Pt. 1	6.7 (93%)	1.1 (15%)	0.54	0.05	
Pt. 2	120.1 (80%)	44.4 (30%)	0.69	0.36	
Pt. 3	48.0(79%)	18.3 (30%)	0.4	0.18	
C - Follow up (ml)	FET-PET \cap MRI/CT- contrast (follow up - baseline)	CLINDE-SPECT \cap MRI/CT- contrast (follow up - baseline)			
Pt. 1	7.7 (8%)	20.9 (21%)			
Pt. 3	24.6 (55%)	32.3 (72%)			

Table 5.1. (A): volume sizes for ROIs of high ^{18}F -FET uptake ^{123}I -CLINDE binding and tumor ROIs on contrast-enhanced structural imaging at baseline and follow-up. Furthermore, common volumes between ^{18}F -FET PET and ^{123}I -CLINDE SPECT ($\text{FET PET} \cap \text{CLINDE SPECT}$) and their percentage overlap with ^{18}F -FET ROIs as reference is calculated.

(B): Baseline common volumes of $\text{FET PET} \cap \text{gd-MRI}$ and $\text{CLINDE SPECT} \cap \text{gd-MRI}$ common along with Sørensen-Dice coefficients (SQ).

(C): Follow-up common volumes of $\text{FET PET} \cap \text{gd-MRI}$ and $\text{CLINDE SPECT} \cap \text{gd-MRI}$ common volumes are given along with percentage overlap (first mentioned modality as reference).

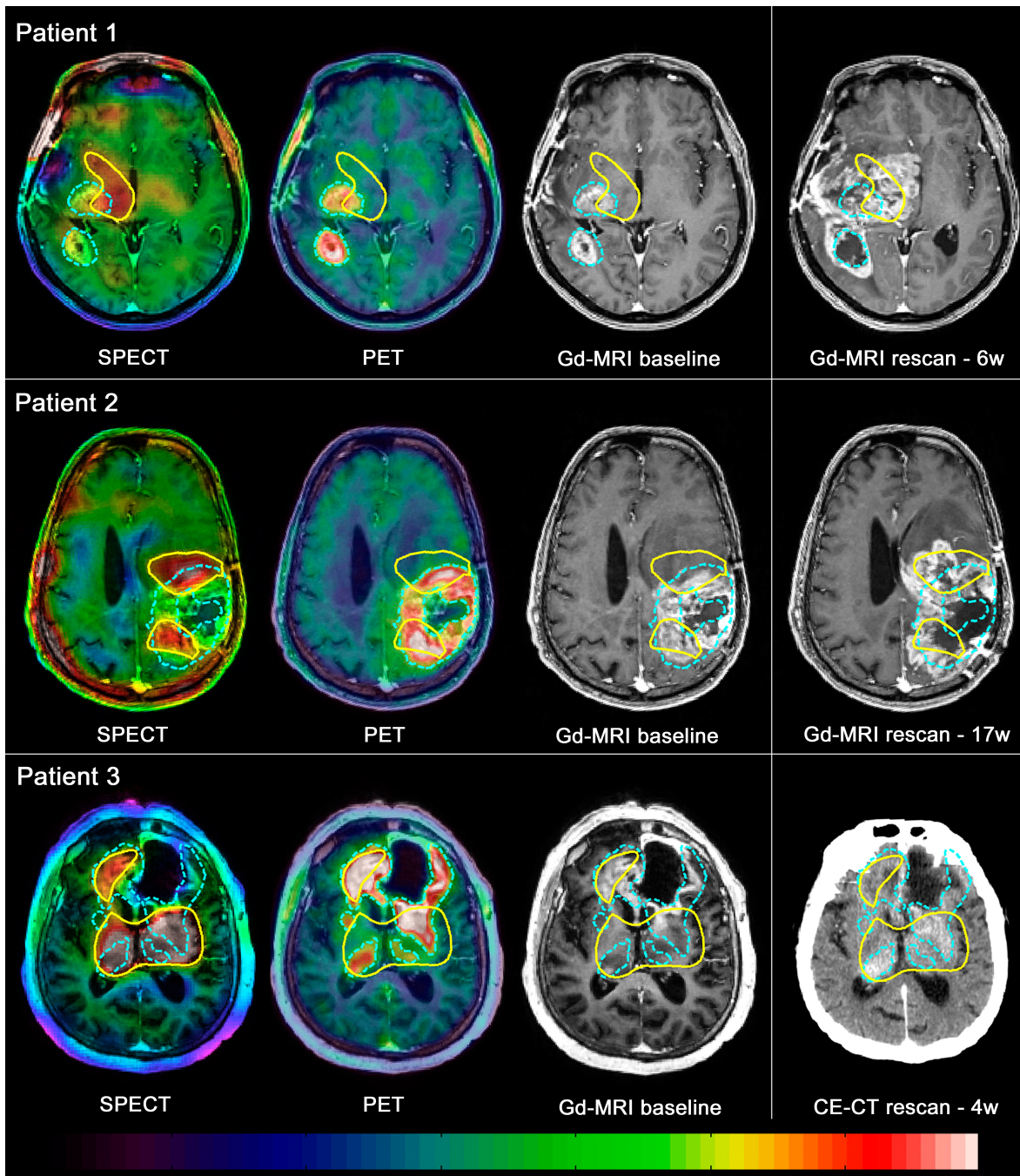


Figure 5.1. ^{123}I -CLINDE SPECT weighted mean images (first column), ^{18}F -FET PET summed scans (second column) and gadolinium-enhanced T1 weighted MRI scans at baseline (third column) for three glioma patients. The last column displays gadolinium enhanced T1 weighted MRI for patient 1 and 2 at follow-up, and follow-up contrast enhanced structural CT for patient 3. Yellow ROIs delineate high ^{23}I -CLINDE binding areas and blue ROIs delineates high ^{18}F -FET uptake. Comparing baseline scans with follow-up, visually reveals that the glioma predominantly expands in high ^{123}I -CLINDE binding areas compared to high ^{18}F -FET uptake areas.

Results - study 3

Test-retest variability of brain uptake and distribution volumes and the effect of genotype on variability measures

Addressing the brain uptake (mSUV), we found high correlation between test and retest mSUV for the same subjects, with correlation coefficients of 0.86 ± 0.07 ($p < 0.05$, $N=16$).

On average (GLS model, age and gender adjusted), the PD was $-3.6 \pm 8.1\%$ for MABs and $-7.0 \pm 7.8\%$ for HABs. No significant PD difference in mSUV between MABs and HABs was found. ICC values for mSUV of MABs and HABs are given in table 5.2

COV was $20.0 \pm 2.3\%$ in MABs and $9.2 \pm 2.0\%$ in HABs.

A significant difference between MABs and HABs was found both in ICC ($p = 2.29e-05$) and COV ($p = 1.38e-05$) with a MAB:HAB ratio of 1.8 for ICC and 2.2 for COV.

Test-retest variability measures for the V_T estimates were calculated both separately and combined with regard to the eight immediately centrifuged and the eight delayed centrifuged population adjusted datasets. (Table 5.2)

On average Test-retest PD of V_T 's for all subjects across 7 ROIs was $-12.1 \pm 8.3\%$ for HABs and $-11.7 \pm 8.6\%$ for MABs when evaluated as a repeated measure in an age and gender adjusted GLS.

The average COV of V_T 's was $-12.1 \pm 8.3\%$ for HABs and $-11.7 \pm 8.6\%$ for MABs.

ICC values are presented for each region in table 5.2.

Regions	V_T using population-adjusted input function of delayed centrifugation N=8			V_T of immediate centrifugation N=8			V_T of all subjects N=16					Brain uptake N=16				
	PD (%)	Absolute PD (%)	ICC	PD (%)	Absolute PD (%)	ICC	PD (%)	Absolute PD (%)	ICC of MABs	ICC of HABs	ICC of all	PD (%)	Absolute PD (%)	ICC of MAB	ICC of HAB	ICC of all
Midbrain	2.8 ± 14.5	12.4	0.96	-1.5 ± 15.6	11.8	0.86	0.6 ± 14.8	12.1	0.41	0.91	0.93	-2.5 ± 11.5	10.1	0.72	0.39	0.71
Thalamus	11.0 ± 10.5	12.8	0.94	-12.3 ± 13.3	12.7	0.86	-0.7 ± 16.7	12.8	0.68	0.84	0.90	-4.7 ± 14.6	11.6	0.74	0.53	0.71
Pons	-2.3 ± 14.2	9.6	0.90	-8.2 ± 23.8	18.9	0.72	-5.3 ± 19.2	14.2	0.54	0.60	0.82	-2.7 ± 12.4	11.0	0.81	0.52	0.77
Pallidostriatum	5.8 ± 21.9	17.6	0.85	-7.0 ± 19.0	14.1	0.87	-0.6 ± 20.9	15.8	0.22	0.79	0.85	-2.2 ± 13.7	11.1	0.79	0.50	0.74
Hippocampus	14.9 ± 17.3	15.7	0.75	-5.9 ± 11.8	9.7	0.91	4.5 ± 17.9	12.7	0.58	0.78	0.83	-2.0 ± 15.2	12.3	0.57	0.23	0.56
Cerebellum	9.6 ± 9.4	10.2	0.94	-4.9 ± 10.0	8.2	0.96	2.3 ± 12.0	9.2	0.76	0.88	0.95	-1.5 ± 9.4	7.8	0.90	0.45	0.87
Neocortex	5.8 ± 12.6	10.2	0.92	-3.2 ± 12.8	10.5	0.92	1.3 ± 13.2	10.4	0.88	0.79	0.92	-2.8 ± 9.6	8.5	0.91	0.57	0.85

Table 5.2: Results study 3 - Test-retest variability measures of V_T s and mSUV

Effect of centrifugation on plasma to whole-blood ratio

Applying a GLS model adjusted for genotype on the mSUV of the plasma to whole-blood ratio (PoB) showed an increase from 0.95 to 1.07 ($p=0.0003$) when changing from delayed to immediate centrifugation. This results in a 12.4% decrease in PoB when delaying the time to centrifugation (Figure 5.2). This shift may be caused by radioactivity leaving the plasma-phase as the sample is waiting in the vial, and will consequently cause the input function to be underestimated and the V_T to be over-estimated.

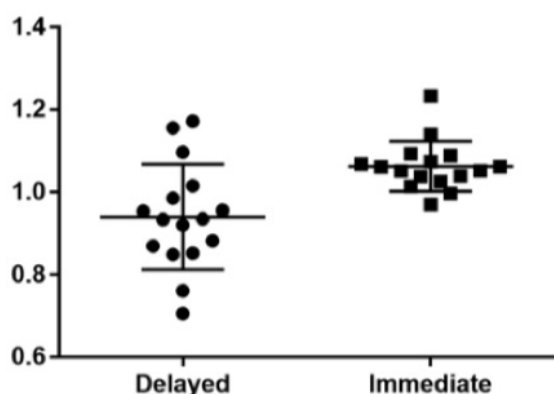


Figure 5.2 Effect of time to centrifugation on the plasma to whole blood ratio.

Effect of genotype on the parent fraction, brain uptake and distribution volumes

Parent fraction: As mentioned in the study-design, this study only included MAB and HAB genotypes. The testing of genotype differences in mSUV of the parent fraction was performed on the immediately centrifuged group applying a GLS model adjusted for age and gender.

The mSUV of parent fraction was significantly different between MAB and HAB both before ($p=0.0006$) and after ($p=0.0002$) parent fraction adjustment.

Parent fraction mSUV was 0.37 ± 0.07 , mean \pm SE in MAB and 0.22 ± 0.05 , mean \pm SE in HAB, with a MAB:HAB ratio of 1.65.

The parent fraction time curves between HABs and MABs were also different. After adjustment of parent fraction, the mean starting point for MABs was 94% intact ^{123}I -CLINDE and 77% for HABs. Mean intact ^{123}I -CLINDE for MABs versus HABs at 20 minutes post injection was 53%(MAB) and 36% (HAB). At 90 minutes they were 38%(MAB) versus 27%(HAB).

mSUV: When applying a GLS with different residual variances on all scans and 7 ROIs, the mSUV of a 49 year old male HABs was 16.8% higher than a MAB, and for mSUV_{60-90min} a HAB was 27.6% higher than an MAB. The binder-status difference between MAB and HAB was borderline for mSUV (p=0.0535) and significant for mSUV_{60-90min} (p=0.0105).

Distribution volumes of HABs were 65% higher on average than MABs when applying a GLS model on V_Ts of 7 ROIs from scans with both immediately and population-based adjusted, delayed centrifuged blood samples (32 scans). The average V_T of a 49 year old male HAB was 7.5±1.4 mL/cm³ (mean ±SE), and 4.6±1.4 mL/cm³ (mean ±SE) for a MAB (Figure 5.3).

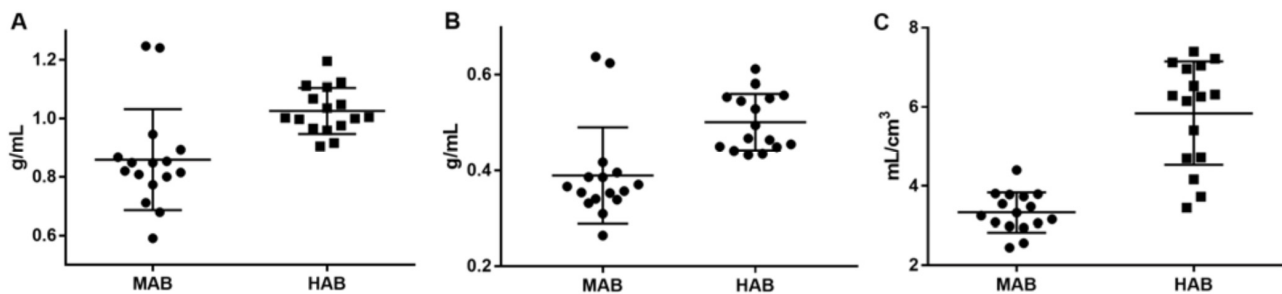


Figure 5.3: The effect of genotype in mSUV, mSUV₆₀₋₉₀ and V_T's

Results - study 4

This study generally showed that the TSPO expression after MCA stroke is remarkably dynamical. Lesional and perilesional size and intensity of the CLINDE uptake was very different for the patients at scan 1 and the expression varied substantially in the following scans (Figure 5.4).

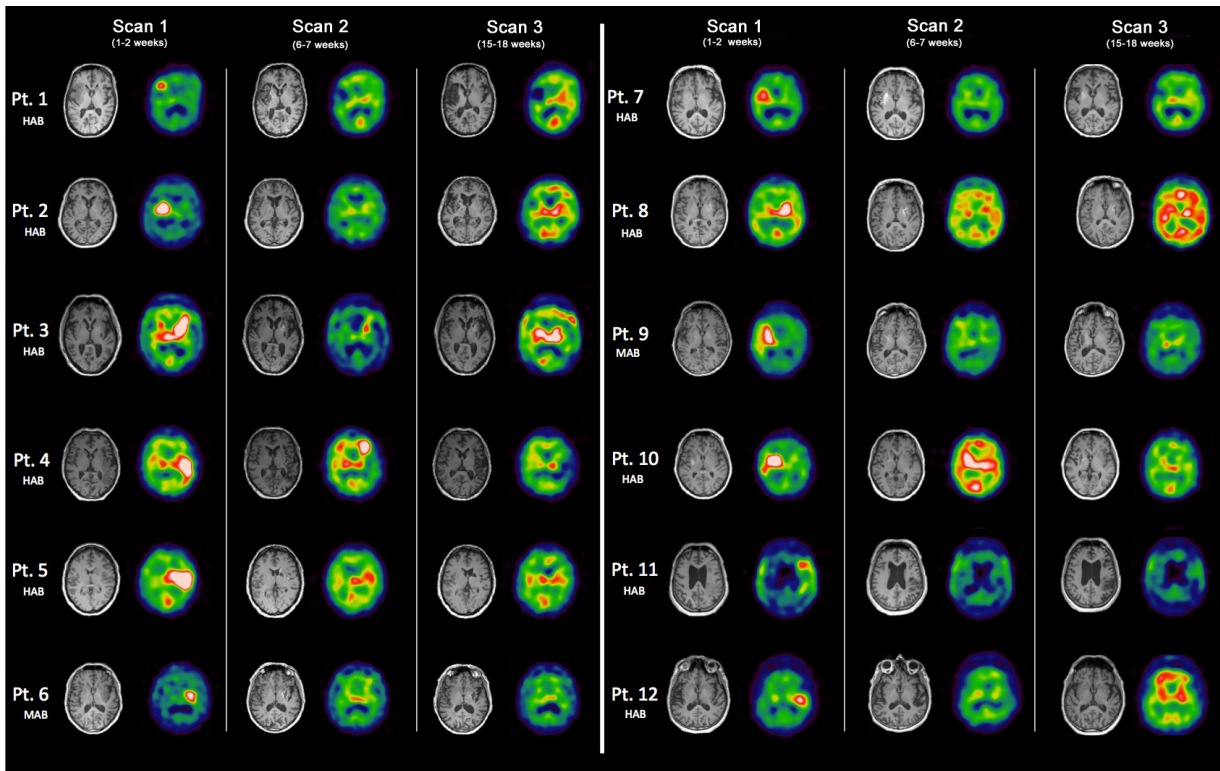


Figure 5.4: *T1-Weighted MRI and ^{123}I -CLINDE SPECT in stroke. ^{123}I -CLINDE SPECT is normalised by weight and injected ^{123}I -CLINDE dose for each patient*

TSPO expression in lesion-related ROIs

For the ten HAB patients, when performing repeated measures ANOVA, V_T 's decreased lesionally over the three scans ($p=0.004$) with a relative decrease between scans 1 and 3 of 34.7%. A trend towards a perilesional decrease ($p=0.07$) was found (Figure 5.5). Performing a one-sided two-tailed t-test PD of V_T on all 12 patients lesionally and perilesionally revealed a significant mean decrease of 22.6 % lesionally ($p=0.04$) and 21.3 % perilesionally ($p=0.001$). See table 5.3 for descriptive data.

Correlations between TSPO expression, clinical outcome measures and necrosis

We found no significant correlation between the PD of rehabilitation measures between scan 1 and the 25-26 week follow-up and any of the ROIs. (Figure 5.5). Furthermore, we also did not find a correlation between the V_T of the contralesional thalamus measured at 5-6 weeks and the PD of rehabilitation measures between 5-6 weeks and 25-26 weeks. However, the percentage overlap between lesional-SPECT and the T2-weighted structural lesion at scan 1 correlated negatively with volume of lesion necrosis at scan 3 ($p=0.001$).

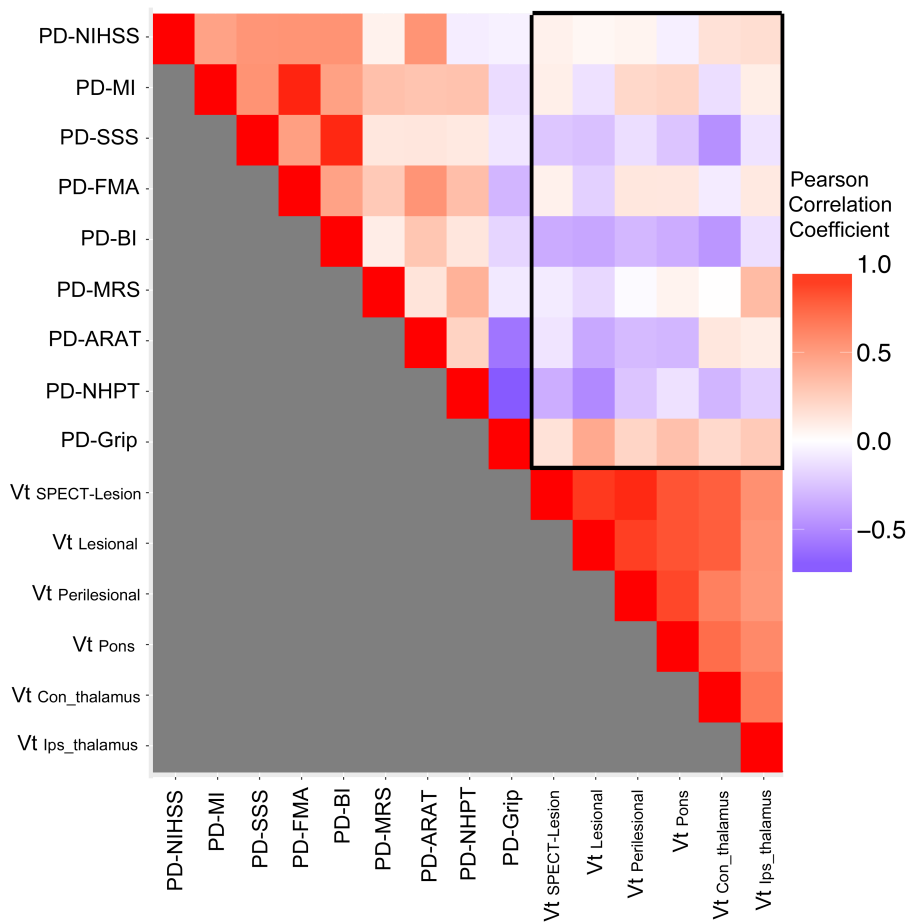


Figure 5.5: Plot of V_T 's at 1-2 weeks after stroke correlated to the PD of rehabilitation measures tested in the study using Pearson correlation. Abbreviations: Percentage difference (PD), National Institutes of Health Stroke Scale (NIHSS), Scandinavian Stroke Scale (SSS), Fugl-Meyer Assessment of the Upper Extremity (FMA-UE), Motricity Index (MI), Action Research Arm Test (ARAT), Nine-Hole Peg Test (NHPT), Grip strength (Grip), Modified Ranking Scale (MRS) and Barthel Index (BI).

TSPO expression in ROIs unrelated to the lesion

For the HAB patients, mean V_T in the ipsilesional cerebellum and the perilesional occipital cortex increased by 72.3% ($p=0.01$) and 51.4% ($p=0.002$). Comparing HABs of healthy volunteers with stroke patients (ten in each group) by Mann-Whitney U test, revealed a significantly lower binding of ^{123}I -CLINDE to TSPO for stroke patients at scan 1 ($p=0.001$ and $p=0.002$). No significant differences at scan 2 ($p=0.11$ and $p=0.52$) and 3 ($p=0.45$ and $p=0.31$) were found. See figure 5.6 for examples of low initial TSPO expression compared to healthy volunteers, figure 5.7 for graphical representation of data, and table 5.3 for descriptive data.

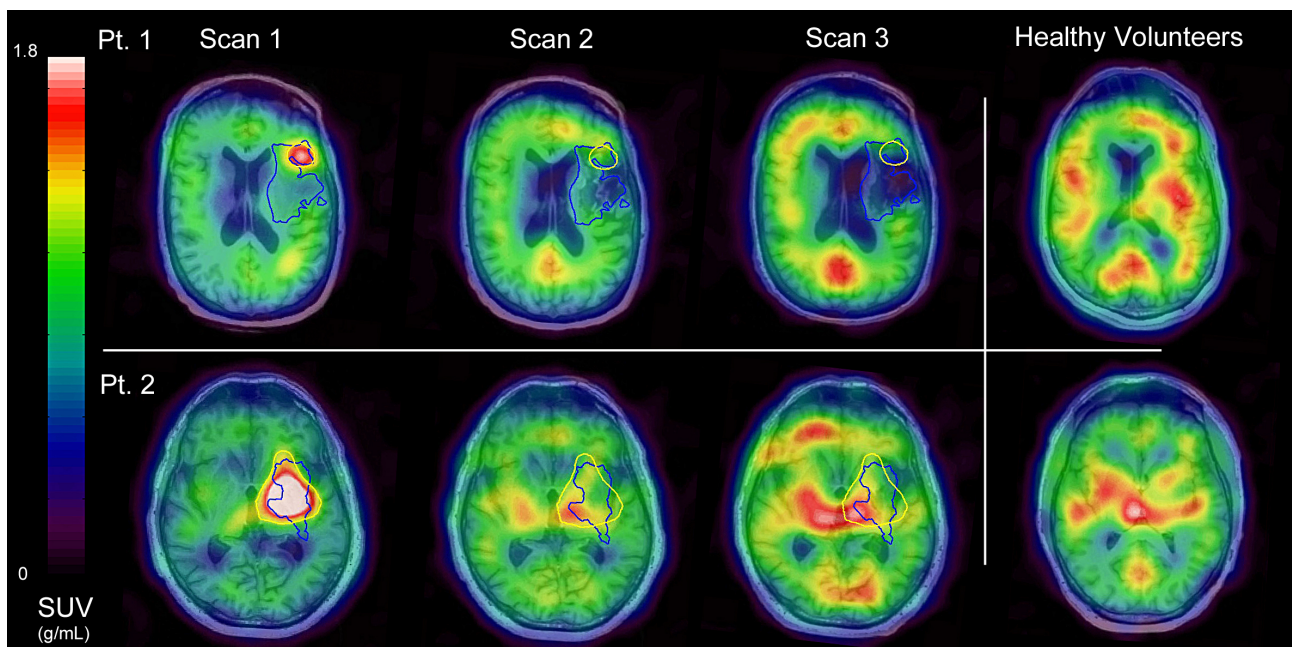


Figure 5.6 T1-weighted MRI overlaid by ^{123}I -CLINDE normalised by bodyweight and injected ^{123}I -CLINDE dose. Yellow ROIs depict the lesional SPECT upregulation and blue ROIs depict the structural lesion delineated on T2-weighted MRI (not shown) on scan 1. The initially low TSPO expression in regions not related to the lesion is apparent when compared to two healthy HAB controls. Pt.1 developed a large area of lesion necrosis and had a small initial TSPO expression ROI whereas Pt.2 had a large area of TSPO expression initially, and only a minor part of the lesion necrotized.

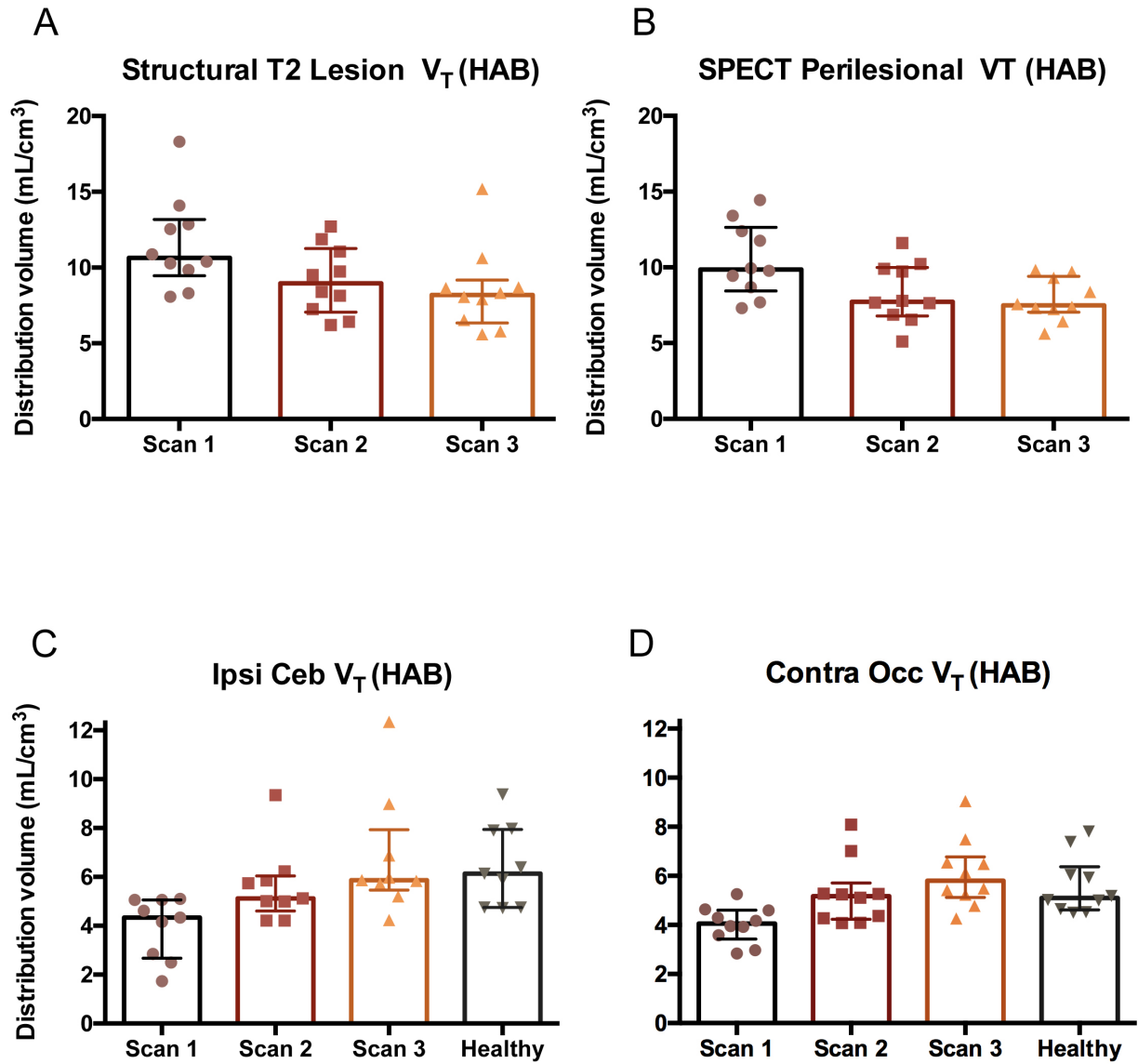


Figure 5.7: V_T 's in ten HAB patients (A-D) and ten HAB healthy volunteers (C-D). Columns represent median values and brackets span the interquartile range. Lesional V_T 's decreased (A) as well as a trend towards a decrease in the perilesional SPECT ROI (B). The ipsilesional cerebellum (C) and contralesional occipital cortex (D) ROIs were initially lower than similar regions in healthy volunteers at scan 1 and increased towards normal values at scan 3.

Descriptive data	Unit	Median	Quartiles [1st;3rd]	Range
Patient age	Years	60.7	[55.9;66.7]	[41.7;71.7]
Healthy volunteer age	Years	33.6	[24.3;45.5]	[21.4;49.0]
NIHSS at stroke onset	Points	17.5	[13.3;19.8]	[8;22]
NIHSS at scan 1	Points	6.5	[4.3;10.0]	[1;12]
NIHSS at follow-up	Points	1.5	[1.0;4.5]	[0;5]
T2 lesion volume at scan 1	mL	40.5	[25.1;63.8]	[17.5;76.1]
T1 necrosis volume at scan 3	mL	4.7	[3.1;15.9]	[2.0;50.8]
Overlap: SPECT Lesion/ T2 Lesion	%	68.8	[51.6;80.0]	[6.4;90.4]
V _T lesional scan 1 (HAB)	mL/cm ³	10.2	[8.6;12.6]	[7.5;15.0]
V _T lesional scan 2 (HAB)	mL/cm ³	8.0	[6.3;10.5]	[5.4;11.0]
V _T Lesional scan 3 (HAB)	mL/cm ³	7.1	[6.2;7.8]	[4.6;8.5]
V _T Con Occ cortex scan 1 (HAB)	mL/cm ³	4.1	[3.4;4.6]	[2.8;5.3]
V _T Con Occ cortex scan 2 (HAB)	mL/cm ³	5.2	[4.2;5.7]	[4.1;8.1]
V _T Con Occ cortex scan 3 (HAB)	mL/cm ³	5.8	[5.1;6.8]	[4.3;9.1]
V _T Occ cortex (healthy volunteers) (HAB)	mL/cm ³	5.1	[4.6;6.4]	[4.5;7.8]

Table 5.3 Descriptive data for the patients

6. Discussion and perspectives

Study 1

To our knowledge, this is the first reported human TSPO imaging study of anti-NMDAR encephalitis. The binding of ^{123}I -CLINDE to TSPO expression was initially increased. The patient responded well to treatment, and demonstrated almost normal values at the follow-up scan after 7 weeks. This implies that TSPO imaging in anti-NMDAR encephalitis has the potential to monitor treatment response in anti-NMDAR encephalitis. This could be a valuable tool since it only about 50% of anti-NMDAR encephalitis patients responds to initial treatment (Titulaer et al., 2013). If treatment non-responders could be identified and earlier given earlier secondary treatment, potentially resulting in a better prognosis.

The current study furthermore proves the feasibility of performing ^{123}I -CLINDE SPECT in anti-NMDAR encephalitis patients. The study is limited to a single patient, and further investigation into the diagnostic and monitoring role of TSPO imaging in AIE in general is warranted.

Study 2

This is the first study in GBM patients to address the clinical value of TSPO imaging with ^{123}I -CLINDE SPECT in combination with ^{18}F -FET PET and contrast-enhanced structural imaging. The study by Pauleit (2005) demonstrated the added diagnostic value of ^{18}F -FET PET to gd-MRI and this has subsequently been standard in therapy planning and monitoring of treatment response for glioma patients in many countries including Denmark. An aim for the present study was therefore to investigate if ^{123}I -CLINDE SPECT provides new and possible valuable information when compared to ^{18}F -FET PET and gd-MRI. Due to the limited number of subjects (i.e. three) in this study, testing the prognostic value of TSPO imaging was not reasonable. Comparing ^{123}I -CLINDE and ^{18}F -FET ROIs, we found only limited overlap, indicating that TSPO binding and amino-acid uptake reflect different aspect of gliomas. We hypothesize that ^{18}F -FET positive, but ^{123}I -CLINDE negative regions primarily reflect reactive astrocytosis rather than glioma tumor cells since ^{18}F -FET is known not to be entirely glioma-specific (Floeth et al., 2006; Pichler et al., 2010; Salber et al., 2007; Spaeth et al., 2004). A marker of GBM proliferation and spatial progression would be a very valuable clinical tool in the planning of

debulking surgery and radiotherapy. This further makes TSPO a possible therapeutical target. Further research into TSPO as a marker of tumor proliferation and progression is warranted, preferably correlated with analysis of tumor biopsies.

A limitation of the study is that the patients in this study consisted of one LAB and two MABs which does not make a direct comparison of CLINDE binding to TSPO between patients possible with V_T 's as an outcome measure (Owen et al., 2015).

To compare the different scan modalities, the method of quantification was carried out as a ROI analysis. ^{123}I -CLINDE ROIs were standardized as tumor-related regions at a value above 1.5 times the mean cerebellar value. This “cerebellar threshold method” for quantification has limitations when comparing results across genotypes.

Study 3

The test-retest variance of V_T in ^{123}I -CLINDE SPECT

The V_T is the primary outcome measure for the binding of ^{123}I -CLINDE to TSPO. The ICC values for ^{123}I -CLINDE SPECT were higher than previously reported for ^{11}C -PK11195 PET (Jučaitė et al., 2012) and comparable to second generation TSPO tracers ^{11}C -DPA-713 PET (Coughlin et al., 2014) and ^{11}C -PBR28 PET (Collste et al., 2015). The compared ICC values are based upon pooled groups of HABs and MABs. This artificially increases the estimated ICC values as described in the methods section for study 4. ICC values are considerably lower when estimated separately for HABs and MABs. We were not able to compare these more factual ICC values to other second-generation TSPO tracers, as they have not been reported. The first-generation TSPO tracer ^{11}C -PK11195 is not susceptible to the rs6971 genotype, which could explain part of the lower ICC values for this tracer.

In our study, ICC and COV were slightly higher for HABs than for MABs. This may be because of better signal-to-background conditions in HABs. The PD and absolute PD of V_T 's for ^{123}I -CLINDE SPECT were slightly smaller than previously reported for ^{11}C -PBR28 PET (Collste et al., 2015).

Estimating brain uptake with mSUV and mSUV_{60-90}

Investigating the test-retest variance and genotype difference of brain uptake by estimating mSUV and mSUV_{60-90} was also done in this study. When estimating mSUV arterial blood sampling is avoided which would reduce the complexity of the scanning protocol. When comparing the mean difference in HABs and MABs, it became apparent that the V_T estimates

were more sensitive to genotype effect than mSUV and mSUV₆₀₋₉₀. Thus, in situations where a change in binding of ¹²³I-CLINDE to TSPO is pursued, the V_T measure is the superior measure. Other ways to avoid blood sampling is by population-based input functions, this may be a subject for a future study.

Effect of blood centrifugation

This study shows that PoB is decreasing if blood samples are not centrifuged immediately. Our hypothesis for this phenomenon is that parent ¹²³I-CLINDE continuously binds to TSPO in blood cells after the blood sample has been drawn, as TSPO is known to be expressed abundantly in granulocytes and monocytes, and to a lesser degree in the remaining blood cells (Canat et al., 1993). Tracer metabolites are not assumed to have this time dependent effect, as they are usually confined to the plasma phase because of lower lipophilicity and thus inability to cross cell membranes.

A lower measured plasma radioactivity because of delayed centrifugation will lead to an underestimation of the plasma input function. When performing kinetic analysis with 2TCM using a metabolite corrected arterial input function, a false low input function will result in an overestimation of V_T. In a test-retest setting an uncontrolled time to centrifugation will greatly affect the test-retest variability measures providing higher PD and lower ICC. In our protocol, the fastest possible time to centrifugation of the blood samples was within 5 minutes. It is suspected that these 5 minutes will still have an effect on the estimate of plasma and HPLC measures, especially in the first minutes after tracer injection. An important concern is therefore, firstly to be as fast as possible with the centrifugation of blood-samples and secondly, to be as consistent as possible in the time to centrifugation.

This finding will probably affect all high-affinity TSPO tracers, but it is unknown to what amount and could be a subject for further investigation.

Study 4

TSPO expression and stroke recovery

The hypothesis of the current study with regard to TSPO being a biomarker of recovery after stroke was falsified. The main reason for this negative finding may be that the TSPO signal is a combination of different reactive cell types (microglia, macrophages and astrocytes) with both pro- and anti-inflammatory properties.

On a group level, the expression of TSPO was initially high lesionally and perilesionally at 1-2 weeks and then gradually decreased perilesionally at 5-6 and 15-18 weeks. This corresponds to other studies examining the TSPO expression between 1-4 weeks after stroke (Boutin & Pinborg, 2015).

However, on an individual level the longitudinal TSPO expression was found to be exceedingly dynamic and heterogeneous. It is a known fact that microglia cells react immediately upon damage to the brain tissue (Davalos et al., 2005). However, TSPO upregulation is first seen after 72 hours by in vivo imaging in human stroke with ^{11}C -PK11195 (Price, 2006). This time discrepancy between microglial activation and TSPO upregulation infers that there is no direct link between microglial function and TSPO expression in stroke. Another well-known limitation is that rehabilitation measures often show floor and ceiling effects which can impede the estimation of recovery especially in mild to moderate stroke (Jensen et al., 2015; Lindemann et al., 2012).

TSPO expression and lesion necrosis

A negative correlation was made between the initial percentage of T2-weighted lesion delineated overlapped by the ^{123}I -CLINDE ROI and the volume of lesion necrosis. This result infers that less TSPO in the lesion results in necrosis. Low TSPO expression in the core of the infarct further implies that the area is too ischemic for the TSPO expressing cells to survive and / or that the lack of perfusion hinders the arrival of tracer to target. We did not perform blood perfusion imaging (e.g. perfusion weighted MRI) to quantify the perfusion of the lesioned area. This could be of interest to investigate further, especially the overlap between perilesional TSPO expression and the ischemic penumbra. Since no lesional blood perfusion estimate was made one cannot be sure about the perfusion status of the lesion, however large necrosis of a lesion suggests permanent ischemia. Thus the results from this study seem to be in agreement with clinical studies in stroke with permanent ischemia. In these studies TSPO is primarily expressed in the

infarct margin and perilesionally initially after stroke, while the infarct core show low TSPO expression (Boutin & Pinborg, 2015).

TSPO expression in stroke compared to healthy volunteers

Ipsilesional cerebellum and contralateral occipital cortex had significantly lower binding of ¹²³I-CLINDE to TSPO when compared to cerebellar and occipital TSPO expression in healthy volunteers. This finding suggests a global TSPO decrease in regions not related to the lesion.

Several biological processes occurring after stroke may cause this initial down regulation:

- The brain tissue could be globally affected by anti-inflammatory cytokines (e.g. IL-10) released by the high TSPO expressing reactive glial cells in the region of the lesion (Doll, Barr, & Simpkins, 2014).
- It is well known, but poorly understood that a systemic immunomodulatory process occurs after stroke (Santos et al., 2016). This could potentially affect the TSPO everywhere in the body.
- The low TSPO can be the result of low availability of TSPO expressing glia and perivascular macrophages, because they have migrated to the site of the lesion. However, TSPO is generally understood to be expressed at low concentration in healthy brain (Chen & Guilarte, 2008).

Previously, low TSPO expression in platelets was linked to anxiety and major depression with anxiety disorder which is hypothesised to be because of the involvement of TSPO in the production of neusteroids (Rupprecht et al., 2010). Nearly 30 % of stroke patients develop post-stroke depression (Paolucci, 2008). It could be of interest to further study this relationship.

Future analyses for the current study

Several future aims for the data analysis of the current study exist: Firstly, to further investigate the hypotheses of the study using more advanced statistics (e.g. latent variable models). This could provide more information on the initial TSPO expression and recovery after stroke.

Secondly, additional fMRI data using a hand activation paradigm have been collected for the stroke patients and await analysis. Other unexplored data is blood samples for peripheral cytokine analysis, which was collected and stored but have yet to be analysed.

7. Conclusions

Conclusions on the studies

Study 1

Study 1 shows increased binding of ^{123}I -CLINDE to TSPO in anti-NMDAR encephalitis at treatment start and a decrease after 7 weeks of immunotherapy.

Study 2

Several conclusions were drawn from study 2:

- TSPO imaging is a sensitive and specific marker of GBM.
- TSPO imaging in glioma may be a predictor of tumor cell proliferation and tumor progression.
- ^{123}I -CLINDE SPECT may be less susceptible to changes in BBB permeability than ^{18}F -FET PET.

Study 3

The conclusions drawn from study 3 were the following:

- The test-retest variability of ^{123}I -CLINDE SPECT is favourable compared to the first generation TSPO PET tracer ^{11}C -PK11195 and comparable to the second generation PET tracers ^{11}C -DPA713 and ^{11}C -PBR28.
- Brain SUV estimates compared to V_T estimated from 2TCM have limitations compared to V_T .
- Immediate centrifugation of blood samples is essential for correct estimation of tracer activity.

Study 4

The following conclusions could be drawn from the final study:

- TSPO expression after stroke is remarkably heterogeneous, both initially after stroke and longitudinally.
- No correlation between initial TSPO expression and patient recovery between 2 weeks and 6 months could be made. This may be because of the heterogeneous TSPO expression in reactive glial cells with both pro- and anti-inflammatory properties.
- A negative correlation between lesional overlap percentage of ^{123}I -CLINDE with the volume of tissue necrosis was made. This corresponds to findings from animal studies and may be the result of an ischemic environment where TSPO expressing cells cannot survive and that the tracer is unavailable because the tissue is not perfused.
- Finally, when comparing regions un-related to the stroke to similar regions in healthy volunteers, the binding of ^{123}I -CLINDE to TSPO is significantly lower in stroke patients. This may be because of anti-inflammatory cytokine release from lesion-related reactive glia or a proxy to post stroke immunomodulation.

Conclusions on the thesis objective

The main objective of the current thesis was to further advance ^{123}I -CLINDE SPECT imaging for clinical research. The following conclusions can be drawn:

- It is feasible to investigate TSPO expression research in anti-NMDAr encephalitis and glioma using ^{123}I -CLINDE SPECT and both studies points towards larger clinical studies of tumor progression in GBM and treatment response in anti-NMDAr encephalitis.
- ^{123}I -CLINDE SPECT is a tracer with comparable properties in test-retest variance to other second-generation TSPO PET tracers. This makes it a usable tracer for research on the same terms as other second-generation TSPO tracers.
- It is feasible to conduct larger research projects in patients with the current ^{123}I -CLINDE SPECT setup and protocol (study 4).
- The clinical study (study 4) implies that the expression of TSPO is exceedingly heterogeneous after brain damage and may represent a multitude of both anti- and proinflammatory properties of the TSPO expressing cells. This is an issue when conducting studies in functional effects of TSPO dynamics.

8. References

- Albrecht, D. S., Granziera, C., Hooker, J. M., & Loggia, M. L. (2016). In Vivo Imaging of Human Neuroinflammation. *ACS Chemical Neuroscience*, 7(4), 470–483. <https://doi.org/10.1021/acscchemneuro.6b00056>
- Arlicot, N., Katsifis, A., Garreau, L., Mattner, F., Vergote, J., Duval, S., ... Chalon, S. (2008). Evaluation of CLINDE as potent translocator protein (18 kDa) SPECT radiotracer reflecting the degree of neuroinflammation in a rat model of microglial activation. *European Journal of Nuclear Medicine and Molecular Imaging*, 35(12), 2203–2211. <https://doi.org/10.1007/s00259-008-0834-x>
- Awde, A. R., Boisgard, R., Thézé, B., Dubois, A., Zheng, J., Dollé, F., ... Winkeler, A. (2013). The Translocator Protein Radioligand 18F-DPA-714 Monitors Antitumor Effect of Erufosine in a Rat 9L Intracranial Glioma Model. *Journal of Nuclear Medicine*, 54(12), 2125–2131. <https://doi.org/10.2967/jnumed.112.118794>
- Banati, R. B., Goerres, G. W., Myers, R., Gunn, R. N., Turkheimer, F. E., Kreutzberg, G. W., ... Duncan, J. S. (1999). [11C](R)-PK11195 positron emission tomography imaging of activated microglia in vivo in Rasmussen's encephalitis. *Neurology*, 53(9), 2199–2199. <https://doi.org/10.1212/WNL.53.9.2199>
- Blaabjerg, M., Mærsk-Møller, C. C., Kondziella, D., Somnier, F., Celicanin, M., Andersen, H., ... Pinborg, L. H. (2015). [Workup and treatment of autoimmune encephalitis]. *Ugeskrift for Læger*, 177(45), V05150448.
- Boutin, H., & Pinborg, L. H. (2015). TSPO imaging in stroke: from animal models to human subjects. *Clinical and Translational Imaging*, 1–13. <https://doi.org/10.1007/s40336-015-0146-7>
- Braestrup, C., & Squires, R. F. (1977). Specific benzodiazepine receptors in rat brain characterized by high-affinity (3H) diazepam binding. *Proceedings of the National Academy of Sciences*, 74(9), 3805–3809.
- Canat, X., Carayon, P., Bouaboula, M., Cahard, D., Shire, D., Roque, C., ... Casellas, P. (1993). Distribution profile and properties of peripheral-type benzodiazepine receptors on human hemopoietic cells. *Life Sciences*, 52(1), 107–118.
- Cekanaviciute, E., & Buckwalter, M. S. (2016). Astrocytes: Integrative Regulators of Neuroinflammation in Stroke and Other Neurological Diseases. *Neurotherapeutics*, 13(4), 685–701. <https://doi.org/10.1007/s13311-016-0477-8>
- Chen, M.-K., & Guilarte, T. R. (2008). Translocator protein 18 kDa (TSPO): Molecular sensor of brain injury and repair. *Pharmacology & Therapeutics*, 118(1), 1–17. <https://doi.org/10.1016/j.pharmthera.2007.12.004>
- Ching, A. S. C., Kuhnast, B., Damont, A., Roeda, D., Tavitian, B., & Dollé, F. (2012). Current paradigm of the 18-kDa translocator protein (TSPO) as a molecular target for PET imaging in neuroinflammation and neurodegenerative diseases. *Insights into Imaging*, 3(1), 111–119. <https://doi.org/10.1007/s13244-011-0128-x>
- Colasanti, A., Owen, D. R., Grozeva, D., Rabiner, E. A., Matthews, P. M., Craddock, N., & Young, A. H. (2013). Bipolar Disorder is associated with the rs6971 polymorphism in the gene encoding 18kDa Translocator Protein (TSPO). *Psychoneuroendocrinology*, 38(11), 2826–2829. <https://doi.org/10.1016/j.psyneuen.2013.07.007>
- Collste, K., Forsberg, A., Varrone, A., Amini, N., Aeinehband, S., Yakushev, I., ... Cervenka, S. (2015). Test–retest reproducibility of [11C]PBR28 binding to TSPO in healthy control subjects. *European Journal of Nuclear Medicine and Molecular Imaging*, 1–11. <https://doi.org/10.1007/s00259-015-3149-8>

- Coughlin, J. M., Wang, Y., Ma, S., Yue, C., Kim, P. K., Adams, A. V., ... Pomper, M. G. (2014). Regional brain distribution of translocator protein using [11C]DPA-713 PET in individuals infected with HIV. *Journal of NeuroVirology*, 20(3), 219–232. <https://doi.org/10.1007/s13365-014-0239-5>
- Dalmau, J., Lancaster, E., Martinez-Hernandez, E., Rosenfeld, M. R., & Balice-Gordon, R. (2011). Clinical experience and laboratory investigations in patients with anti-NMDAR encephalitis. *Lancet Neurology*, 10(1), 63–74. [https://doi.org/10.1016/S1474-4422\(10\)70253-2](https://doi.org/10.1016/S1474-4422(10)70253-2)
- Davalos, D., Grutzendler, J., Yang, G., Kim, J. V., Zuo, Y., Jung, S., ... Gan, W.-B. (2005). ATP mediates rapid microglial response to local brain injury in vivo. *Nature Neuroscience*, 8(6), 752–758. <https://doi.org/10.1038/nn1472>
- Delavoie, F., Li, H., Hardwick, M., Robert, J.-C., Giatzakis, C., Péranzi, G., ... Papadopoulos, V. (2003). In Vivo and in Vitro Peripheral-Type Benzodiazepine Receptor Polymerization: Functional Significance in Drug Ligand and Cholesterol Binding[†]. *Biochemistry*, 42(15), 4506–4519. <https://doi.org/10.1021/bi0267487>
- Doll, D. N., Barr, T. L., & Simpkins, J. W. (2014). Cytokines: Their Role in Stroke and Potential Use as Biomarkers and Therapeutic Targets. *Aging and Disease*, 5(5), 294–306. <https://doi.org/10.14336/AD.2014.0500294>
- Dunet, V., Rossier, C., Buck, A., Stupp, R., & Prior, J. O. (2012). Performance of 18F-Fluoro-Ethyl-Tyrosine (18F-FET) PET for the Differential Diagnosis of Primary Brain Tumor: A Systematic Review and Metaanalysis. *Journal of Nuclear Medicine*, 53(2), 207–214. <https://doi.org/10.2967/jnumed.111.096859>
- Feng, L., Svarer, C., Thomsen, G., de Nijs, R., Larsen, V. A., Jensen, P., ... Pinborg, L. H. (2014). In Vivo Quantification of Cerebral Translocator Protein Binding in Humans Using 6-Chloro-2-(4'-123I-Iodophenyl)-3-(N,N-Diethyl)-Imidazo[1,2-a]Pyridine-3-Acetamide SPECT. *Journal of Nuclear Medicine*. <https://doi.org/10.2967/jnumed.114.143727>
- Floeth, F. W., Pauleit, D., Sabel, M., Reifenberger, G., Stoffels, G., Stummer, W., ... Langen, K.-J. (2006). 18F-FET PET Differentiation of Ring-Enhancing Brain Lesions. *Journal of Nuclear Medicine*, 47(5), 776–782.
- Gerhard, A., Neumaier, B., Elitok, E., Glatting, G., Ries, V., Tomczak, R., ... Reske, S. N. (2000). In vivo imaging of activated microglia using [11C]PK11195 and positron emission tomography in patients after ischemic stroke. *Neuroreport*, 11(13), 2957–2960.
- Gerhard, A., Schwarz, J., Myers, R., Wise, R., & Banati, R. B. (2005). Evolution of microglial activation in patients after ischemic stroke: a [11C](R)-PK11195 PET study. *NeuroImage*, 24(2), 591–595. <https://doi.org/10.1016/j.neuroimage.2004.09.034>
- Gildersleeve, D. L., Lin, T.-Y., Wieland, D. M., Ciliax, B. J., Olson, J. M. M., & Young, A. B. (1989). Synthesis of a high specific activity 125I-labeled analog of PK 11195, potential agent for SPECT imaging of the peripheral benzodiazepine binding site. *International Journal of Radiation Applications and Instrumentation. Part B. Nuclear Medicine and Biology*, 16(4), 423–429. [https://doi.org/10.1016/0883-2897\(89\)90111-6](https://doi.org/10.1016/0883-2897(89)90111-6)
- Ginhoux, F., Greter, M., Leboeuf, M., Nandi, S., See, P., Gokhan, S., ... Merad, M. (2010). Fate Mapping Analysis Reveals That Adult Microglia Derive from Primitive Macrophages. *Science (New York, N.Y.)*, 330(6005), 841–845. <https://doi.org/10.1126/science.1194637>
- Gulyás, B., Tóth, M., Schain, M., Airaksinen, A., Vas, Á., Kostulas, K., ... Halldin, C. (2012). Evolution of microglial activation in ischaemic core and peri-infarct regions after stroke: A PET study with the TSPO molecular imaging biomarker [11C]vinpocetine. *Journal of the Neurological Sciences*, 320(1–2), 110–117. <https://doi.org/10.1016/j.jns.2012.06.026>

- Gulyas, B., Toth, M., Vas, A., Shchukin, E., Hillert, J., & Halldin, C. (2012). Visualising Neuroinflammation in Post-Stroke Patients: A Comparative PET Study with the TSPO Molecular Imaging Biomarkers [¹¹C]PK11195 and [¹¹C]vinpocetine. *Current Radiopharmaceuticalse*, 5(1), 19–28. <https://doi.org/10.2174/1874471011205010019>
- Gunn, R. N., Gunn, S. R., & Cunningham, V. J. (2001). Positron emission tomography compartmental models. *Journal of Cerebral Blood Flow & Metabolism*, 21(6), 635–652.
- Innis, R. B., Cunningham, V. J., Delforge, J., Fujita, M., Gjedde, A., Gunn, R. N., ... Carson, R. E. (2007). Consensus nomenclature for in vivo imaging of reversibly binding radioligands. *Journal of Cerebral Blood Flow & Metabolism*, 27(9), 1533–1539. <https://doi.org/10.1038/sj.jcbfm.9600493>
- Jensen, P., Meden, P., Knudsen, L. V., Knudsen, G. M., Thomsen, C., Feng, L., & Pinborg, L. H. (2015). [Golf handicap score is a suitable scale for monitoring rehabilitation after apoplexia cerebri]. *Ugeskrift for Laeger*, 177(52).
- Jučaite, A., Cselényi, Z., Arvidsson, A., Åhlberg, G., Julin, P., Varnäs, K., ... Farde, L. (2012). Kinetic analysis and test-retest variability of the radioligand [11C](R)-PK11195 binding to TSPO in the human brain - a PET study in control subjects. *EJNMMI Research*, 2(1), 1–13. <https://doi.org/10.1186/2191-219X-2-15>
- Kreisl, W. C., Fujita, M., Fujimura, Y., Kimura, N., Jenko, K. J., Kannan, P., ... Innis, R. B. (2010). Comparison of [11C]-(R)-PK 11195 and [11C]PBR28, Two Radioligands for Translocator Protein (18 kDa) in Human and Monkey: Implications for Positron Emission Tomographic Imaging of this Inflammation Biomarker. *NeuroImage*, 49(4), 2924–2932. <https://doi.org/10.1016/j.neuroimage.2009.11.056>
- Lacapère, J.-J., & Papadopoulos, V. (2003). Peripheral-type benzodiazepine receptor: structure and function of a cholesterol-binding protein in steroid and bile acid biosynthesis. *Steroids*, 68(7–8), 569–585. [https://doi.org/10.1016/S0039-128X\(03\)00101-6](https://doi.org/10.1016/S0039-128X(03)00101-6)
- Le Goascogne, C., Eychenne, B., Tonon, M.-C., Lachapelle, F., Baumann, N., & Robel, P. (2000). Neurosteroid progesterone is up-regulated in the brain of jimpy and shiverer mice. *Glia*, 29(1), 14–24. [https://doi.org/10.1002/\(SICI\)1098-1136\(20000101\)29:1<14::AID-GLIA2>3.0.CO;2-N](https://doi.org/10.1002/(SICI)1098-1136(20000101)29:1<14::AID-GLIA2>3.0.CO;2-N)
- Lindemann, U., Jamour, M., Nicolai, S. E., Benzinger, P., Klenk, J., Aminian, K., & Becker, C. (2012). Physical activity of moderately impaired elderly stroke patients during rehabilitation. *Physiological Measurement*, 33(11), 1923–1930. <https://doi.org/10.1088/0967-3334/33/11/1923>
- Liu, G.-J., Middleton, R. J., Hatty, C. R., Kam, W. W.-Y., Chan, R., Pham, T., ... Banati, R. B. (2014a). The 18 kDa Translocator Protein, Microglia and Neuroinflammation: TSPO, Microglia and Neuroinflammation. *Brain Pathology*, 24(6), 631–653. <https://doi.org/10.1111/bpa.12196>
- Liu, W., Tang, Y., & Feng, J. (2011). Cross talk between activation of microglia and astrocytes in pathological conditions in the central nervous system. *Life Sciences*, 89(5–6), 141–146. <https://doi.org/10.1016/j.lfs.2011.05.011>
- Louis, D. N., Perry, A., Reifenberger, G., von Deimling, A., Figarella-Branger, D., Cavenee, W. K., ... Ellison, D. W. (2016). The 2016 World Health Organization Classification of Tumors of the Central Nervous System: a summary. *Acta Neuropathologica*, 131(6), 803–820. <https://doi.org/10.1007/s00401-016-1545-1>
- Martín, A., Boisgard, R., Thézé, B., Van Camp, N., Kuhnast, B., Damont, A., ... Tavitian, B. (2010). Evaluation of the PBR/TSPO radioligand [18F]DPA-714 in a rat model of focal cerebral ischemia. *Journal of Cerebral Blood Flow and Metabolism: Official Journal of the International Society of Cerebral Blood Flow and Metabolism*, 30(1), 230–241. <https://doi.org/10.1038/jcbfm.2009.205>

- Mattner, F., Mardon, K., & Katsifis, A. (2008). Pharmacological evaluation of [123I]-CLINDE: a radioiodinated imidazopyridine-3-acetamide for the study of peripheral benzodiazepine binding sites (PBBS). *European Journal of Nuclear Medicine and Molecular Imaging*, 35(4), 779–789. <https://doi.org/10.1007/s00259-007-0645-5>
- Midzak, A., Zirkin, B., & Papadopoulos, V. (2015). Translocator protein: pharmacology and steroidogenesis. *Biochemical Society Transactions*, 43(4), 572–578. <https://doi.org/10.1042/BST20150061>
- Miettinen, H., Kononen, J., Haapasalo, H., Helén, P., Sallinen, P., Harjuntausta, T., ... Alho, H. (1995). Expression of Peripheral-Type Benzodiazepine Receptor and Diazepam Binding Inhibitor in Human Astrocytomas: Relationship to Cell Proliferation. *Cancer Research*, 55(12), 2691–2695.
- Minogue, A. M. (2017). Role of infiltrating monocytes/macrophages in acute and chronic neuroinflammation: Effects on cognition, learning and affective behaviour. *Progress in Neuro-Psychopharmacology and Biological Psychiatry*. <https://doi.org/10.1016/j.pnpbp.2017.02.008>
- Mizrahi, R., Rusjan, P. M., Kennedy, J., Pollock, B., Mulsant, B., Suridjan, I., ... Houle, S. (2012). Translocator protein (18 kDa) polymorphism (rs6971) explains in-vivo brain binding affinity of the PET radioligand [18F]-FEPPA. *Journal of Cerebral Blood Flow & Metabolism*, 32(6), 968–972.
- Nakagawa, Y., & Chiba, K. (2015). Diversity and plasticity of microglial cells in psychiatric and neurological disorders. *Pharmacology & Therapeutics*, 154, 21–35. <https://doi.org/10.1016/j.pharmthera.2015.06.010>
- Owen, D. R., Guo, Q., Rabiner, E. A., & Gunn, R. N. (2015). The impact of the rs6971 polymorphism in TSPO for quantification and study design. *Clinical and Translational Imaging*, 3(6), 417–422. <https://doi.org/10.1007/s40336-015-0141-z>
- Owen, D. R., Yeo, A. J., Gunn, R. N., Song, K., Wadsworth, G., Lewis, A., ... Rubio, J. P. (2012). An 18-kDa Translocator Protein (TSPO) polymorphism explains differences in binding affinity of the PET radioligand PBR28. *Journal of Cerebral Blood Flow & Metabolism*, 32(1), 1–5. <https://doi.org/10.1038/jcbfm.2011.147>
- Paolucci, S. (2008). Epidemiology and treatment of post-stroke depression. *Neuropsychiatric Disease and Treatment*, 4(1), 145–154.
- Papadopoulos, V., Baraldi, M., Guilarte, T. R., Knudsen, T. B., Lacapère, J.-J., Lindemann, P., ... Gavish, M. (2006). Translocator protein (18kDa): new nomenclature for the peripheral-type benzodiazepine receptor based on its structure and molecular function. *Trends in Pharmacological Sciences*, 27(8), 402–409. <https://doi.org/10.1016/j.tips.2006.06.005>
- Pappata, S., Levasseur, M., Gunn, R. N., Myers, R., Crouzel, C., Syrota, A., ... Banati, R. B. (2000). Thalamic microglial activation in ischemic stroke detected in vivo by PET and [11C]PK1195. *Neurology*, 55(7), 1052–1054.
- Park, E., Gallezot, J.-D., Delgado, A., Liu, S., Planeta, B., Lin, S.-F., ... Pelletier, D. (2015). 11C-PBR28 imaging in multiple sclerosis patients and healthy controls: test-retest reproducibility and focal visualization of active white matter areas. *European Journal of Nuclear Medicine and Molecular Imaging*, 42(7), 1081–1092. <https://doi.org/10.1007/s00259-015-3043-4>
- Pauleit, D. (2005). O-(2-[18F]fluoroethyl)-L-tyrosine PET combined with MRI improves the diagnostic assessment of cerebral gliomas. *Brain*, 128(3), 678–687. <https://doi.org/10.1093/brain/awh399>
- Pichler, R., Wurm, G., Nussbaumer, K., Kalev, O., Silyé, R., & Weis, S. (2010). Sarcoidosis and radiation-induced astrogliosis causes pitfalls in neuro-oncologic positron emission

- tomography imaging by O-(2-[18F]fluoroethyl)-L-tyrosine. *Journal of Clinical Oncology: Official Journal of the American Society of Clinical Oncology*, 28(36), e753-755. <https://doi.org/10.1200/JCO.2010.30.5763>
- Price, C. J. S. (2006). Intrinsic Activated Microglia Map to the Peri-infarct Zone in the Subacute Phase of Ischemic Stroke. *Stroke*, 37(7), 1749–1753. <https://doi.org/10.1161/01.STR.0000226980.95389.0b>
- Prinz, M., & Priller, J. (2014). Microglia and brain macrophages in the molecular age: from origin to neuropsychiatric disease. *Nature Reviews Neuroscience*, 15(5), 300–312. <https://doi.org/10.1038/nrn3722>
- Radlinska, B. A., Ghinani, S. A., Lyon, P., Jolly, D., Soucy, J.-P., Minuk, J., ... Thiel, A. (2009). Multimodal microglia imaging of fiber tracts in acute subcortical stroke. *Annals of Neurology*, 66(6), 825–832. <https://doi.org/10.1002/ana.21796>
- Ramsay, S. C., Weiller, C., Myers, R., Cremer, J. E., Luthra, S. K., Lammertsma, A. A., & Frackowiak, R. S. J. (1992). Monitoring by PET of macrophage accumulation in brain after ischaemic stroke. *The Lancet*, 339(8800), 1054–1055. [https://doi.org/10.1016/0140-6736\(92\)90576-O](https://doi.org/10.1016/0140-6736(92)90576-O)
- Ransohoff, R. M. (2016). A polarizing question: do M1 and M2 microglia exist? *Nature Neuroscience*, 19(8), 987–991. <https://doi.org/10.1038/nn.4338>
- Ribeiro, M.-J., Vercouillie, J., Debiais, S., Cottier, J.-P., Bonnaud, I., Camus, V., ... Guilloteau, D. (2014). Could 18 F-DPA-714 PET imaging be interesting to use in the early post-stroke period? *EJNMMI Research*, 4, 28. <https://doi.org/10.1186/s13550-014-0028-4>
- Rupprecht, R., Papadopoulos, V., Rammes, G., Baghai, T. C., Fan, J., Akula, N., ... Schumacher, M. (2010). Translocator protein (18 kDa) (TSPO) as a therapeutic target for neurological and psychiatric disorders. *Nature Reviews Drug Discovery*, 9(12), 971–988. <https://doi.org/10.1038/nrd3295>
- Salber, D., Stoffels, G., Pauleit, D., Oros-Peusquens, A.-M., Shah, N. J., Klauth, P., ... Langen, K.-J. (2007). Differential uptake of O-(2-18F-fluoroethyl)-L-tyrosine, L-3H-methionine, and 3H-deoxyglucose in brain abscesses. *Journal of Nuclear Medicine: Official Publication, Society of Nuclear Medicine*, 48(12), 2056–2062. <https://doi.org/10.2967/jnumed.107.046615>
- Santos Samary, C., Pelosi, P., Leme Silva, P., & Rieken Macedo Rocco, P. (2016). Immunomodulation after ischemic stroke: potential mechanisms and implications for therapy. *Critical Care*, 20(1). <https://doi.org/10.1186/s13054-016-1573-1>
- Scarf, A. M., & Kassiou, M. (2011). The Translocator Protein. *Journal of Nuclear Medicine*, 52(5), 677–680. <https://doi.org/10.2967/jnumed.110.086629>
- Schumacher, M., Akwa, Y., Guennoun, R., Robert, F., Labombarda, F., Désarnaud, F., ... Baulieu, E.-E. (2000). Steroid synthesis and metabolism in the nervous system: Trophic and protective effects. *Journal of Neurocytology*, 29(5–6), 307–326. <https://doi.org/10.1023/A:1007152904926>
- Spaeth, N., Wyss, M. T., Weber, B., Scheidegger, S., Lutz, A., Verwey, J., ... Buck, A. (2004). Uptake of 18F-fluorocholine, 18F-fluoroethyl-L-tyrosine, and 18F-FDG in acute cerebral radiation injury in the rat: implications for separation of radiation necrosis from tumor recurrence. *Journal of Nuclear Medicine: Official Publication, Society of Nuclear Medicine*, 45(11), 1931–1938.
- Stevenson, L., Tavares, A. A. S., Brunet, A., McGonagle, F. I., Dewar, D., Pimlott, S. L., & Sutherland, A. (2010). New iodinated quinoline-2-carboxamides for SPECT imaging of the translocator protein. *Bioorganic & Medicinal Chemistry Letters*, 20(3), 954–957. <https://doi.org/10.1016/j.bmcl.2009.12.061>

- Stupp, R., Mason, W. P., van den Bent, M. J., Weller, M., Fisher, B., Taphoorn, M. J. B., ... Mirimanoff, R. O. (2005). Radiotherapy plus Concomitant and Adjuvant Temozolomide for Glioblastoma. *New England Journal of Medicine*, 352(10), 987–996. <https://doi.org/10.1056/NEJMoa043330>
- Svarer, C., Madsen, K., Hasselbalch, S. G., Pinborg, L. H., Haugbøl, S., Frøkjær, V. G., ... Knudsen, G. M. (2005). MR-based automatic delineation of volumes of interest in human brain PET images using probability maps. *NeuroImage*, 24(4), 969–979. <https://doi.org/10.1016/j.neuroimage.2004.10.017>
- Thiel, A., Radlinska, B. A., Paquette, C., Sidel, M., Soucy, J.-P., Schirmacher, R., & Minuk, J. (2010). The Temporal Dynamics of Poststroke Neuroinflammation: A Longitudinal Diffusion Tensor Imaging-Guided PET Study with ¹¹C-PK11195 in Acute Subcortical Stroke. *Journal of Nuclear Medicine*, 51(9), 1404–1412. <https://doi.org/10.2967/jnumed.110.076612>
- Titulaer, M. J., McCracken, L., Gabilondo, I., Armangué, T., Glaser, C., Iizuka, T., ... Dalmau, J. (2013). Treatment and prognostic factors for long-term outcome in patients with anti-NMDA receptor encephalitis: an observational cohort study. *The Lancet Neurology*, 12(2), 157–165. [https://doi.org/10.1016/S1474-4422\(12\)70310-1](https://doi.org/10.1016/S1474-4422(12)70310-1)
- Tsartsalis, S., Dumas, N., Tournier, B. B., Pham, T., Moulin-Sallanon, M., Grégoire, M.-C., ... Millet, P. (2015). SPECT imaging of glioma with radioiodinated CLINDE: evidence from a mouse GL26 glioma model. *EJNMMI Research*, *\$metaTagArticleVolume*(1), 9. <https://doi.org/10.1186/s13550-015-0092-4>
- Vlodavsky, E., & Soustiel, J. F. (2007). Immunohistochemical expression of peripheral benzodiazepine receptors in human astrocytomas and its correlation with grade of malignancy, proliferation, apoptosis and survival. *Journal of Neuro-Oncology*, 81(1), 1–7. <https://doi.org/10.1007/s11060-006-9199-9>
- Waterhouse, R. (2003). Determination of lipophilicity and its use as a predictor of blood–brain barrier penetration of molecular imaging agents. *Molecular Imaging & Biology*, 5(6), 376–389. <https://doi.org/10.1016/j.mibio.2003.09.014>
- Weinstein, J. R., Koerner, I. P., & Möller, T. (2010). Microglia in ischemic brain injury. *Future Neurology*, 5(2), 227–246. <https://doi.org/10.2217/fnl.10.1>
- WHO | The Atlas of Heart Disease and Stroke. (n.d.). Retrieved July 24, 2013, from http://www.who.int/cardiovascular_diseases/resources/atlas/en/
- Willendrup, P., Pinborg, L. H., Hasselbalch, S. G., Adams, K. H., Stahr, K., Knudsen, G. M., & Svarer, C. (2004). Assessment of the precision in co-registration of structural MR images and PET images with localized binding. *International Congress Series*, 1265, 275–280. <https://doi.org/10.1016/j.ics.2004.04.065>
- Winkeler, A., Boisgard, R., Awde, A. R., Dubois, A., Thézé, B., Zheng, J., ... Tavitian, B. (2012). The translocator protein ligand [¹⁸F]DPA-714 images glioma and activated microglia in vivo. *European Journal of Nuclear Medicine and Molecular Imaging*, 39(5), 811–823. <https://doi.org/10.1007/s00259-011-2041-4>
- Zhao, A. H., Tu, L. N., Mukai, C., Sirivelu, M. P., Pillai, V. V., Morohaku, K., ... Selvaraj, V. (2016). Mitochondrial Translocator Protein (TSPO) Function Is Not Essential for Heme Biosynthesis. *The Journal of Biological Chemistry*, 291(4), 1591–1603. <https://doi.org/10.1074/jbc.M115.686360>

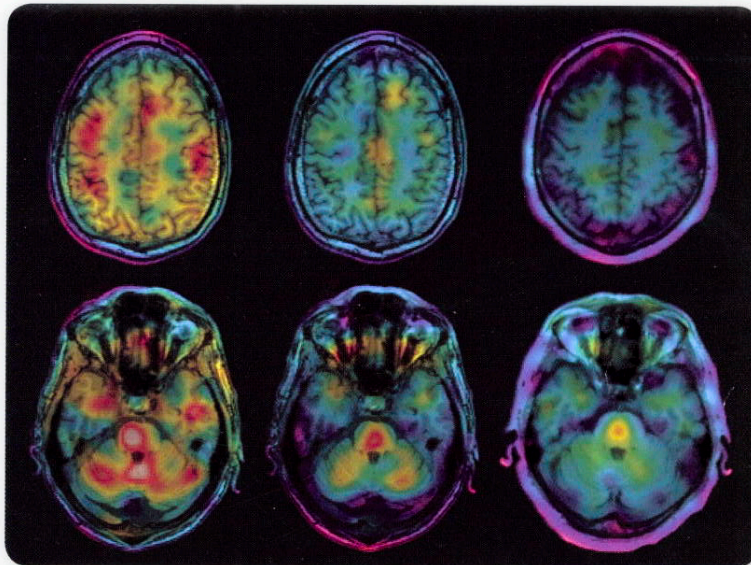
Appendix

Study 1

Neurology®

Volume 84, Number 8, February 24, 2015
Neurology.org

AMERICAN ACADEMY OF
NEUROLOGY®



Thalamus structure and function determine severity of cognitive impairment in multiple sclerosis, **p 776**

Placebo effect of medication cost in Parkinson disease: A randomized double-blind study, **p 794**

Subclinical cardiac dysfunction increases the risk of stroke and dementia: The Rotterdam Study, **p 833**

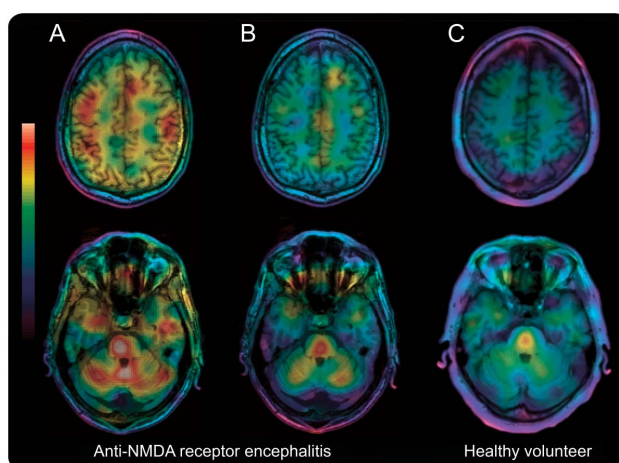
Read Neurology® on your iPad®!
Convenient... portable...
engaging... interactive!

The most widely read and highly cited peer-reviewed neurology journal
THE OFFICIAL JOURNAL OF THE AMERICAN ACADEMY OF NEUROLOGY

Anti-NMDAR encephalitis

Demonstration of neuroinflammation and the effect of immunotherapy

Figure $[^{123}\text{I}]\text{CLINDE}$ -SPECT and coregistered MRI in a patient with anti-NMDA receptor encephalitis



At the start of immunotherapy, (A) $[^{123}\text{I}]\text{CLINDE}$ -binding to TSPO was strongly increased (neocortical distribution volume $[V_T] = 6.3 \text{ mL/cm}^3$), but almost normalized ($V_T = 4.0 \text{ mL/cm}^3$) after 7 weeks of immunotherapy (B) compared to a healthy volunteer (C) ($V_T = 3.0 \text{ mL/cm}^3$).

A 35-year-old man presented with perceptual difficulties and delusions. At presentation, there were orofacial dyskinesias, catatonia, and autonomic instability. Anti-NMDA receptor (NMDAR) antibodies were detected in CSF.¹ Cerebral MRI was unremarkable. At the start of immunotherapy (methylprednisolone and plasmapheresis), $[^{123}\text{I}]\text{CLINDE}$ -SPECT demonstrated a strongly increased binding to TSPO in cortical and subcortical brain regions similar to the distribution of NMDAR in the brain and different from FDG-PET changes reported in the literature (figure, A). TSPO is present on activated microglia and used as a measure of regional neuroinflammation.² After 7 weeks of immunotherapy (figure, B), TSPO binding was close to normal values (figure, C) and the patient was back to work part time as a computer scientist despite mild cognitive problems.

Per Jensen, MD, Daniel Kondziella, MD, PhD, Gerda Thomsen, BS, Agnete Dyssegaard, MS, Claus Svarer, PhD, Lars H. Pinborg, MD, PhD

From Department of Neurology, Rigshospitalet, København, Denmark.

Author contributions: Per Jensen: acquired and analyzed the data. Daniel Kondziella, Gerda Thomsen, and Agnete Dyssegaard: acquired data and revised the manuscript. Claus Svarer: prepared the figure, analyzed data, and revised the manuscript. Lars H. Pinborg: designed the concept, analyzed data, and wrote the clinical summary.

Study funding: Supported by the European Union's Seventh Framework Programme (FP7/2007-2013) under grant agreement HEALTH-F2-2011-278850 (INMiND) and the Danish Research Agency.

Disclosure: The authors report no disclosures relevant to the manuscript. Go to Neurology.org for full disclosures.

Correspondence to Dr. Pinborg: lars.pinborg@nru.dk

1. Dalmau J, Lancaster E, Martinez-Hernandez E, Rosenfeld MR, Balice-Gordon R. Clinical experience and laboratory investigations in patients with anti-NMDAR encephalitis. *Lancet Neurol* 2011;10:63–74.
2. Jacobs AH, Tavitian B. Noninvasive molecular imaging of neuroinflammation. *J Cereb Blood Flow Metab* 2012;32:1393–1415.

TSPO Imaging in Glioblastoma Multiforme: A Direct Comparison Between ^{123}I -CLINDE SPECT, ^{18}F -FET PET, and Gadolinium-Enhanced MR Imaging

Per Jensen¹, Ling Feng¹, Ian Law², Claus Svare¹, Gitte M. Knudsen¹, Jens D. Mikkelsen¹, Robin de Nijs², Vibeke A. Larsen³, Agnete Dyssegaard¹, Gerda Thomsen¹, Walter Fischer⁴, Denis Guilloteau⁵, and Lars H. Pinborg^{1,6}

¹Neurobiology Research Unit, Rigshospitalet, Copenhagen, Denmark; ²Department of Clinical Physiology, Nuclear Medicine, and PET, Rigshospitalet, Copenhagen, Denmark; ³Department of Radiology, Rigshospitalet, Copenhagen, Denmark; ⁴Department of Neurosurgery, Rigshospitalet, Copenhagen, Denmark; ⁵Université François-Rabelais de Tours, INSERM U930 "Imaging and Brain," Tours, France; and ⁶Epilepsy Clinic, Department of Neurology, Rigshospitalet, Copenhagen, Denmark

Here we compare translocator protein (TSPO) imaging using 6-chloro-2-(4'- ^{123}I -iodophenyl)-3-(*N,N*-diethyl)-imidazo[1,2-*a*]pyridine-3-acetamide SPECT (^{123}I -CLINDE) and amino acid transport imaging using *O*-(2- ^{18}F -fluoroethyl)-L-tyrosine PET (^{18}F -FET) and investigate whether ^{123}I -CLINDE is superior to ^{18}F -FET in predicting progression of glioblastoma multiforme (GBM) at follow-up. **Methods:** Three patients with World Health Organization grade IV GBM were scanned with ^{123}I -CLINDE SPECT, ^{18}F -FET PET, and gadolinium-enhanced MR imaging. Molecular imaging data were compared with follow-up gadolinium-enhanced MR images or contrast-enhanced CT scans. **Results:** The percentage overlap between volumes of interest (VOIs) of increased ^{18}F -FET uptake and ^{123}I -CLINDE binding was variable (12%–42%). The percentage overlap of MR imaging baseline VOIs was greater for ^{18}F -FET (79%–93%) than ^{123}I -CLINDE (15%–30%). In contrast, VOIs of increased contrast enhancement at follow-up compared with baseline overlapped to a greater extent with baseline ^{123}I -CLINDE VOIs than ^{18}F -FET VOIs (21% vs. 8% and 72% vs. 55%). **Conclusion:** Our preliminary results suggest that TSPO brain imaging in GBM may be a useful tool for predicting tumor progression at follow-up and may be less susceptible to changes in blood-brain barrier permeability than ^{18}F -FET. Larger studies are warranted to test the clinical potential of TSPO imaging in GBM, including presurgical planning and radiotherapy.

Key Words: neurooncology; SPECT; PET; MRI

J Nucl Med 2015; 56:1386–1390

DOI: 10.2967/jnumed.115.158998

Glioblastoma multiforme (GBM) remains the most common and aggressive primary tumor of the central nervous system. With conventional radiotherapy, chemotherapy, and debulking surgery, mean survival from diagnosis is 14.6 mo (*1*).

GBM lesions are strongly enhanced on contrast-enhanced structural imaging (CT or MR imaging), but populations of glioma

cells are also present in the peritumoral environment. Thus, in clinical trials the volume for radiotherapy has been defined as the region of enhancement plus an isotropic margin of 2–3 cm (*1*). The combination of MR imaging and *O*-(2- ^{18}F -fluoroethyl)-L-tyrosine PET (^{18}F -FET) improves the sensitivity and specificity of tumor tissue detection (*2,3*). However, ^{18}F -FET is not entirely glioma-specific, and increased uptake has been documented in astrogliosis secondary to infection, ischemia, radiation injury, demyelination, and hematoma (*4–7*). The 18-kDa translocator protein (TSPO) is a component of the mitochondrial permeability transition pore and is strongly expressed by glioma cell lines (*8*). In tissue resected from patients with astrocytoma, TSPO density correlates positively with malignancy and cell proliferation index and negatively with survival (*9*). 6-chloro-2-(4'- ^{123}I -iodophenyl)-3-(*N,N*-diethyl)-imidazo[1,2-*a*]pyridine-3-acetamide SPECT (^{123}I -CLINDE; MAP Medical Technologies) has been validated as a second-generation TSPO tracer for use in humans (*10*) and recently in a GL26 mouse model of glioma (*11*). We present ^{123}I -CLINDE SPECT, ^{18}F -FET PET, and gadolinium-enhanced MR imaging results from 3 GBM patients at baseline compared with contrast-enhanced structural imaging at follow-up and hypothesize that ^{123}I -CLINDE SPECT at baseline is an imaging biomarker of GBM progression.

MATERIALS AND METHODS

The study was performed in accordance with the ethical standards of the Declaration of Helsinki and approved by the ethical committee of the Copenhagen Capital Region (approval H-2-2010-086, amendment 39319). All subjects signed an informed consent form. Three patients in an advanced state of GBM (World Health Organization grade IV) were included and genotyped for the rs6971 polymorphism to determine the TSPO binder status as described previously (*10*). Before inclusion, all patients had undergone surgery and received radiotherapy and chemotherapy with temozolomide, bevacizumab and irinotecan. In addition, patients 2 and 3 had been treated with a cell-based immunotherapy. Patient 2 had undergone surgical resection between baseline and follow-up MR imaging. The patients were scanned with ^{123}I -CLINDE, ^{18}F -FET, and MR imaging within 2 d. Patients 1 and 2 were rescanned with MR imaging after 6 and 17 wk, respectively, and patient 3 was rescanned with CT after 4 wk. The patients received no treatment with angiogenesis-inhibiting drugs for 6 wk before the scans and no radiochemotherapy between scans.

Received Apr. 8, 2015; revision accepted Jul. 6, 2015.
For correspondence or reprints contact: Lars H. Pinborg, Neurobiology Research Unit, Copenhagen University Hospital, Building 6931, Blegdamsvej 9, DK-2100 Copenhagen, Denmark.
E-mail: pinborg@nru.dk
Published online Jul. 16, 2015.
COPYRIGHT © 2015 by the Society of Nuclear Medicine and Molecular Imaging, Inc.

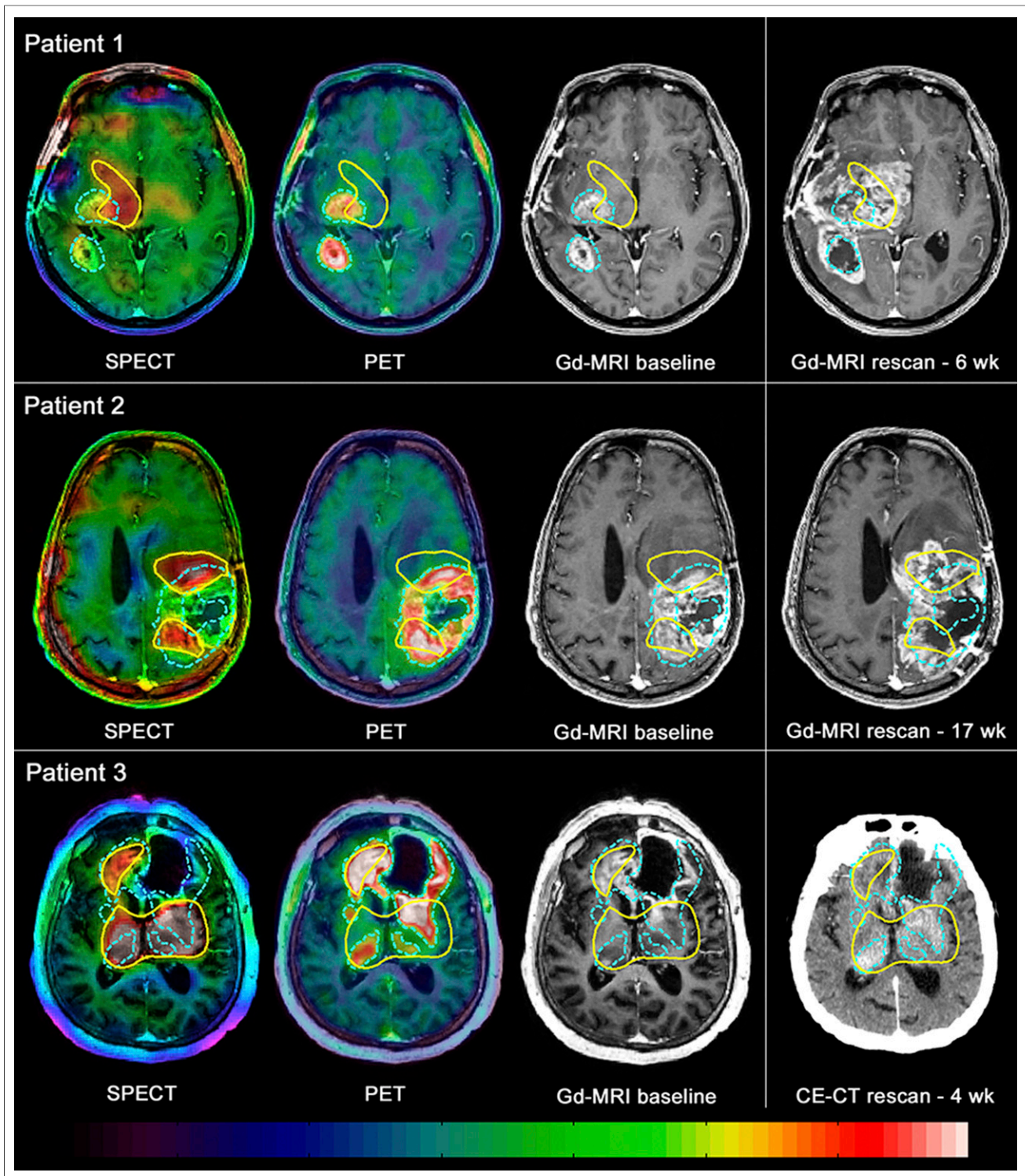


FIGURE 1. Weighted mean 0- to 150-min ^{123}I -CLINDE SPECT scans, summed 20- to 40-min ^{18}F -FET PET scans, and gadolinium- or contrast-enhanced (CE) structural scans at baseline and at rescanning. Blue VOIs show high ^{18}F -FET tumor uptake, and yellow VOIs high ^{123}I -CLINDE binding. Comparison of baseline and rescanning structural scans reveals that tumor expands predominantly in areas of high ^{123}I -CLINDE binding.

TABLE 1
Patients

Patient	Sex	Age (y)	Binder status	Rescanning modality	Interval (wk)	¹²³ I-CLINDE injected dose (MBq)
1	F	48	MAB	MR imaging	6	191
2	M	65	LAB	MR imaging	17	188
3	M	64	MAB	CT	4	188

TABLE 2
VOIs

Patient	¹⁸ F-FET	¹²³ I-CLINDE	¹⁸ F-FET ∩ ¹²³ I-CLINDE	MR imaging (baseline)	MR imaging/CT (follow up – baseline)
1	17.3	36.6	2 (12%)	7.2	97.5
2	196.9	97.9	62.6 (32%)	150.5	NA
3	180	140.7	75 (42%)	60.7	44.8

NA = not applicable.
Data are in milliliters.

TABLE 3
Volumes in Common Between Baseline Structural Imaging and ¹²³I-CLINDE or ¹⁸F-FET PET

Patient	¹⁸ F-FET (mL)	¹²³ I-CLINDE (mL)	Sørensen–Dice coefficient between...	
			¹⁸ F-FET and MR imaging	¹²³ I-CLINDE and MR imaging
1	6.7 (93%)	1.1 (15%)	0.54	0.05
2	120.1 (80%)	44.4 (30%)	0.69	0.36
3	48.0 (79%)	18.3 (30%)	0.4	0.18

TABLE 4
Volumes in Common Between Tumor Progression
at Follow-up Structural Imaging and Baseline
¹⁸F-FET PET or ¹²³I-CLINDE

Patient	¹⁸ F-FET (mL)	¹²³ I-CLINDE (mL)
1	7.7 (8%)	20.9 (21%)
3	24.6 (55%)	32.3 (72%)

Patients

Patient data, genotype, rescan modality, scan–rescan time intervals, and injected ¹²³I-CLINDE dose are presented in Table 1.

Image Acquisition

After bolus injection of ¹²³I-CLINDE, dynamic SPECT images were acquired with a triple-head IRIX camera (Philips Medical) for 2.5 h as previously described (10), and weighted mean images were generated for region analysis.

A single-frame static PET acquisition was performed 20–40 min after intravenous injection of approximately 200 MBq of ¹⁸F-FET on a 64-slice-CT Biograph TruePoint PET/CT scanner (Siemens). All PET scans were attenuation-corrected using low-dose CT performed immediately before the PET scan and were subsequently corrected for scatter and dead time. Images were reconstructed with an ordered-subsets expectation maximization 3-dimensional algorithm (6 itera-

tions, 16 subsets) and a 5-mm gaussian filter. All patients fasted for at least 6 h before ¹⁸F-FET injection.

T1-weighted MR imaging was performed on a 3-T MR Verio scanner (Siemens). Gadolinium was used in a dose of 0.1 mmol/kg of body weight (Multihance [Bracco] or Gadovist [Schering]). Patient 3 was rescanned using a CT scanner (Siemens) and a CT contrast agent containing 70 mL of iodine (350 mg/mL) (Omnipaque; GE Healthcare).

Data Processing

The weighted mean ¹²³I-CLINDE SPECT image was coregistered to the MR image of the same patient using interactive image overlay (12). ¹⁸F-FET PET images and the follow-up MR images were coregistered to the first MR image of the same subject, applying the automatic rigid-body model included with Statistical Parametric Mapping, version 8 (13).

The definition of volumes of interest (VOIs) with high ¹²³I-CLINDE binding was standardized for all patients by automatically selecting voxels with a value above 1.5 times the mean cerebellar count. The delineation of high-uptake ¹⁸F-FET volumes was standardized as previously described (2). A trained neuroradiologist supervised delineation of the MR imaging volumes. Baseline MR imaging VOIs were delineated manually as the contrast-enhanced areas of the coregistered baseline MR image. Blood vessels were omitted. Volumes for SPECT, PET, and MR imaging were determined, along with common volumes. Furthermore, the Sørensen–Dice coefficient for SPECT, PET, and baseline MR imaging was calculated as $\frac{2V_{A \cap B}}{V_A + V_B}$, with ∩ being the symbol of common volume. Volume of tumor progression was

defined as the additional contrast-enhanced volume from baseline to follow-up. For patient 2, follow-up volume analysis was not performed because of surgical resection between the baseline and follow-up scans.

RESULTS

Table 2 shows the sizes of the ^{18}F -FET and ^{123}I -CLINDE VOIs as well as the volumes in common for high-binding ^{123}I -CLINDE VOIs and high-uptake ^{18}F -FET VOIs. The VOIs of increased ^{123}I -CLINDE binding and ^{18}F -FET uptake showed varying degrees of overlap (12%–42%). Binder status does not appear to determine the volume of ^{123}I -CLINDE VOIs.

Table 3 shows the volumes in common between baseline structural imaging and ^{123}I -CLINDE or ^{18}F -FET PET. In all cases, baseline MR imaging VOIs showed greater similarity to ^{18}F -FET VOIs (Sørensen–Dice coefficients, 0.54, 0.69, and 0.40) than to ^{123}I -CLINDE VOIs (Sørensen–Dice coefficients, 0.05, 0.36, and 0.18). The percentage overlap of MR imaging baseline VOIs was greater for ^{18}F -FET VOIs (79%–93%) than for ^{123}I -CLINDE VOIs (15%–30%).

Table 4 shows the volumes in common between tumor progression at follow-up structural imaging and baseline ^{18}F -FET PET or ^{123}I -CLINDE. In the 2 patients for whom follow-up tumor progression volumes were estimated, the volume with de novo contrast enhancement at follow-up overlapped to a greater extent with ^{123}I -CLINDE VOIs than with ^{18}F -FET VOIs (21% vs. 8% and 72% vs. 55%).

DISCUSSION

This study follows 4 previous studies demonstrating TSPO in 1–3 patients with GBM using the TSPO PET tracer ^{11}C -PK11195 PET (14–17). To our knowledge, this is the first study to address the clinical value of TSPO imaging in GBM patients by comparing the second-generation TSPO SPECT tracer ^{123}I -CLINDE with ^{18}F -FET PET and contrast-enhanced structural imaging.

The first aim of the present study was to evaluate the similarity of ^{123}I -CLINDE and ^{18}F -FET VOIs. We found only limited VOI overlap, indicating that imaging of amino acid uptake and TSPO binding reflects different aspects of GBM pathology. Increased ^{18}F -FET uptake has been documented experimentally and clinically in reactive astrogliosis secondary to infection, ischemia, radiation injury, demyelination, and hematoma, indicating that ^{18}F -FET is not entirely glioma-specific (4–7). In contrast, no TSPO expression was found in reactive astrogliosis in a recent study in untreated human glioma patients (17). In addition to binding to glioma cells, TSPO tracers bind to myeloid cell lines, including glioma-associated microglia and macrophages (18). In contrast, uptake of ^{18}F -FET is not increased in areas of infiltrating activated macrophages and activated microglia in experimental abscesses (4,19). It may be hypothesized that TSPO-negative but ^{18}F -FET-positive areas represent primarily reactive astrocytosis, predicting a less aggressive development, but biopsy control confirmation is needed.

The second aim was to evaluate the correspondence between the VOIs of increased ^{18}F -FET uptake, the VOIs of increased ^{123}I -CLINDE binding, and volumes of MR imaging contrast enhancement at baseline. We found that ^{18}F -FET VOIs overlapped more (93%, 80%, 79%) with contrast-enhanced VOIs than with ^{123}I -CLINDE VOIs (15%, 30%, 30%). Contrast enhancement reflects a disturbed blood–brain barrier and could be related to treatment and tissue necrosis and not glioma cell proliferation per se (20).

The binding of ^{123}I -CLINDE to TSPO does not appear to be significantly increased in areas of disrupted blood–brain barrier (10). It is known that glioma cells diffusely infiltrate brain tissue without disrupting the blood–brain barrier (21).

The third aim was to evaluate how ^{18}F -FET and ^{123}I -CLINDE VOIs overlap with VOIs representing tumor progression from baseline to follow-up on contrast-enhanced structural imaging. Follow-up VOI analysis was not performed for patient 2 because debulking surgery had taken place between baseline and follow-up scans and extravasation of gadolinium was highly increased in the area around the operation cavity on the follow-up scan. It appears that the VOIs of increased ^{123}I -CLINDE at baseline are a good visual predictor of tumor progression at follow-up (Fig. 1). In line with the visual interpretation, the percentage overlap with VOIs representing tumor progression is higher for ^{123}I -CLINDE than for ^{18}F -FET (21% vs. 8% and 72% vs. 55%) in patients 1 and 3. The findings correspond to previous reports demonstrating the contribution of TSPO to the uncontrolled cellular proliferation of glioma cells (22) and the correlation between TSPO density in surgically removed glioma tissue with clinical parameters such as survival time and tumor cell proliferation index (8,9). TSPO is expressed in glioma cells, suggesting that this method may be a more sensitive and specific marker of ongoing tumor cell proliferation and progression than conventional imaging methods. In addition, glioma-associated macrophages and monocytes contributing to tumor progression through the release of proinflammatory and proangiogenic factors may also add to the TSPO signal (23). Thus, the addition of TSPO imaging to ^{18}F -FET PET has the potential to add information about areas of very active tumor cell proliferation in GBM. This may explain why low-grade gliomas have few or no TSPO binding sites (17).

CONCLUSION

These preliminary results from 3 patients with advanced GBM suggest that TSPO imaging is a sensitive and specific marker of GBM and that regional binding predicts areas of active tumor cell proliferation in GBM. Favorable implications can be foreseen for planning surgery and radiotherapy and monitoring the effect of oncologic therapy. ^{123}I -CLINDE SPECT appears to be less susceptible to blood–brain barrier disruption than ^{18}F -FET PET. However, to determine the exact role of TSPO imaging compared with imaging of amino acid transport, further studies are warranted.

DISCLOSURE

The costs of publication of this article were defrayed in part by the payment of page charges. Therefore, and solely to indicate this fact, this article is hereby marked “advertisement” in accordance with 18 USC section 1734. This work was financially supported by the European Union’s Seventh Framework Programme (FP7/2007-2013), the Danish Council for Independent Research, the Research Committee of Rigshospitalet, and Desirée and Niels Yde’s foundation. No other potential conflict of interest relevant to this article was reported.

ACKNOWLEDGMENTS

We acknowledge Svitlana Olsen and Melanie Ganz-Benjaminson for technical assistance.

REFERENCES

- Stupp R, Mason WP, van den Bent MJ, et al. Radiotherapy plus concomitant and adjuvant temozolomide for glioblastoma. *N Engl J Med*. 2005;352:987–996.
- Pauleit D. O-(2-[¹⁸F]fluoroethyl)-L-tyrosine PET combined with MRI improves the diagnostic assessment of cerebral gliomas. *Brain*. 2005;128:678–687.
- Dunet V, Rossier C, Buck A, Stupp R, Prior JO. Performance of ¹⁸F-fluoro-ethyl-tyrosine (¹⁸F-FET) PET for the differential diagnosis of primary brain tumor: a systematic review and metaanalysis. *J Nucl Med*. 2012;53:207–214.
- Salber D, Stoffels G, Pauleit D, et al. Differential uptake of O-(2-¹⁸F-fluoroethyl)-L-tyrosine, L-³H-methionine, and ³H-deoxyglucose in brain abscesses. *J Nucl Med*. 2007;48:2056–2062.
- Spaeth N, Wyss MT, Weber B, et al. Uptake of ¹⁸F-fluorocholine, ¹⁸F-fluoroethyl-L-tyrosine, and ¹⁸F-FDG in acute cerebral radiation injury in the rat: implications for separation of radiation necrosis from tumor recurrence. *J Nucl Med*. 2004;45:1931–1938.
- Pichler R, Wurm G, Nussbaumer K, Kalev O, Silyé R, Weis S. Sarcoidosis and radiation-induced astrogliosis causes pitfalls in neuro-oncologic positron emission tomography imaging by O-(2-[¹⁸F]fluoroethyl)-L-tyrosine. *J Clin Oncol*. 2010;28:e753–e755.
- Floeth FW, Pauleit D, Sabel M, et al. ¹⁸F-FET PET differentiation of ring-enhancing brain lesions. *J Nucl Med*. 2006;47:776–782.
- Winkler A, Boisgard R, Awde AR, et al. The translocator protein ligand [¹⁸F]DPA-714 images glioma and activated microglia in vivo. *Eur J Nucl Med Mol Imaging*. 2012;39:811–823.
- Miettinen H, Kononen J, Haapasalo H, et al. Expression of peripheral-type benzodiazepine receptor and diazepam binding inhibitor in human astrocytomas: relationship to cell proliferation. *Cancer Res*. 1995;55:2691–2695.
- Feng L, Svarer C, Thomsen G, et al. In vivo quantification of cerebral translocator protein binding in humans using 6-chloro-2-(4'-¹²³I-iodophenyl)-3-(N,N-diethyl)-imidazo[1,2-a]pyridine-3-acetamide SPECT. *J Nucl Med*. 2014;55:1966–1972.
- Tsartsalis S, Dumas N, Tournier BB, et al. SPECT imaging of glioma with radioiodinated CLINDE: evidence from a mouse GL26 glioma model. *EJNMMI Res*. 2015;5:9.
- Willendrup P, Pinborg LH, Hasselbalch SG, et al. Assessment of the precision in co-registration of structural MR images and PET images with localized binding. *Int Congr Ser*. 2004;1265:275–280.
- Ashburner J, Friston K. Multimodal image coregistration and partitioning: a unified framework. *Neuroimage*. 1997;6:209–217.
- Junck L, Olson JMM, Ciliax BJ, et al. PET imaging of human gliomas with ligands for the peripheral benzodiazepine binding site. *Ann Neurol*. 1989;26:752–758.
- Pappata S, Cornu P, Samson Y, et al. PET study of carbon-11-PK 11195 binding to peripheral type benzodiazepine sites in glioblastoma: a case report. *J Nucl Med*. 1991;32:1608–1610.
- Su Z, Herholz K, Gerhard A, et al. [¹¹C]-(R)PK11195 tracer kinetics in the brain of glioma patients and a comparison of two referencing approaches. *Eur J Nucl Med Mol Imaging*. 2013;40:1406–1419.
- Su Z, Roncaroli F, Durrenberger PF, et al. The 18-kDa mitochondrial translocator protein in human gliomas: an ¹¹C-(R)PK11195 PET imaging and neuropathology study. *J Nucl Med*. 2015;56:512–517.
- Batarseh A, Papadopoulos V. Regulation of translocator protein 18 kDa (TSPO) expression in health and disease states. *Mol Cell Endocrinol*. 2010;327:1–12.
- Kaim AH, Weber B, Kurrer MO, et al. ¹⁸F-FDG and ¹⁸F-FET uptake in experimental soft tissue infection. *Eur J Nucl Med Mol Imaging*. 2002;29:648–654.
- Brandma D, van den Bent MJ. Pseudoprogression and pseudoreponse in the treatment of gliomas. *Curr Opin Neurol*. 2009;22:633–638.
- Wen PY, Macdonald DR, Reardon DA, et al. Updated response assessment criteria for high-grade gliomas: response assessment in neuro-oncology working group. *J Clin Oncol*. 2010;28:1963–1972.
- Austin CJD, Kahlert J, Kassiu M, Rendina LM. The translocator protein (TSPO): a novel target for cancer chemotherapy. *Int J Biochem Cell Biol*. 2013;45:1212–1216.
- Seyfried TN, Flores R, Poff AM, D'Agostino DP, Mukherjee P. Metabolic therapy: a new paradigm for managing malignant brain cancer. *Cancer Lett*. 2015;356(2 Pt A):289–300.

Study 3

Downloaded from jnm.snmjournals.org by Koebenhavns Universitetsbibliotek Nord on November 14, 2016. For personal use only.



The variability of translocator protein signal in brain and blood of genotyped healthy humans using in vivo ^{123}I -CLINDE SPECT imaging – a test-retest study

Ling Feng, Per Jensen, Gerda Thomsen, Agnete Dyssegaard, Claus Svarer, Lars Vestergaard Knudsen, Kirsten Møller, Carsten Thomsen, Jens Damsgaard Mikkelsen, Denis Guilloteau, Gitte Moos Knudsen and Lars H. Pinborg

J Nucl Med.

Published online: November 10, 2016.

Doi: 10.2967/jnumed.116.183202

This article and updated information are available at:

<http://jnm.snmjournals.org/content/early/2016/11/09/jnumed.116.183202>

Information about reproducing figures, tables, or other portions of this article can be found online at:

<http://jnm.snmjournals.org/site/misc/permission.xhtml>

Information about subscriptions to JNM can be found at:

<http://jnm.snmjournals.org/site/subscriptions/online.xhtml>

JNM ahead of print articles have been peer reviewed and accepted for publication in *JNM*. They have not been copyedited, nor have they appeared in a print or online issue of the journal. Once the accepted manuscripts appear in the *JNM* ahead of print area, they will be prepared for print and online publication, which includes copyediting, typesetting, proofreading, and author review. This process may lead to differences between the accepted version of the manuscript and the final, published version.

The Journal of Nuclear Medicine is published monthly.
SNMMI | Society of Nuclear Medicine and Molecular Imaging
1850 Samuel Morse Drive, Reston, VA 20190.
(Print ISSN: 0161-5505, Online ISSN: 2159-662X)

© Copyright 2016 SNMMI; all rights reserved.

The variability of translocator protein signal in brain and blood of genotyped healthy humans
using in vivo ¹²³I-CLINDE SPECT imaging – a test-retest study

Ling Feng^{1*}, Per Jensen^{1,2*}, Gerda Thomsen¹, Agnete Dyssegaard¹, Claus Svarer¹, Lars V.
Knudsen¹, Kirsten Møller³, Carsten Thomsen⁴, Jens D. Mikkelsen^{1,2}, Denis Guilloteau⁵, Gitte M.
Knudsen^{1,2} and Lars H. Pinborg^{1,2,6}

1 Neurobiology Research Unit, Rigshospitalet, Copenhagen Denmark

2 Faculty of Health and Medicine, University of Copenhagen, Denmark

3 Department of Neuroanaesthesiology, Rigshospitalet, Copenhagen Denmark

4 Department of Radiology, Rigshospitalet, Copenhagen Denmark

5 UFR de Médecine, Université François Rabelais de Tours, France

6 Epilepsy Clinic, Department of Neurology, Rigshospitalet, Copenhagen Denmark

* Per Jensen and Ling Feng contributed equally to this study.

Corresponding author:

Ling Feng MSc. Ph.D

Neurobiology Research Unit, Rigshospitalet, Copenhagen Denmark

Email: ling.feng@nru.dk, Tlf: +45 3545 6718, Fax: +45 3545 6713

Reprints are not available.

Word Count: 5489

Financial support: This work was financially supported by the European Union's Seventh Framework Programme (FP7/2007-2013) under grant agreement n° HEALTH-F2-2011-278850 (INMiND) and the Danish Council for Independent Research (grant ID: 0602-0228-8B).

Running Title: Test-retest variability of ^{123}I -CLINDE

The aim of the current study was to examine the test-retest reproducibility measured as PD and reliability measured as ICC and COV of ^{123}I -CLINDE binding in healthy subjects based on the brain SUV and 2TCM with arterial blood as the input function.

MATERIALS AND METHODS

Subjects and genotyping

This study was conducted in accordance with the Declaration of Helsinki at the Copenhagen University Hospital, Rigshospitalet, Denmark. The ethical committee of the Copenhagen Capital Region (H-2-2010-086) approved the study protocol. All subjects provided written informed consent.

Due to low TSPO signal in glioblastoma tissue from a patient who was a low affinity binder (LAB) (12), we did not expect to obtain reliable TSPO signals in healthy LABs. Consequently, after screening for the rs6971 polymorphism (12), 16 healthy subjects (MAB:HAB=1:1, 9 females) were included and SPECT scanned twice with an interval of 35 ± 15 days. All healthy subjects had normal physical and neurological examinations, and blood tests. Table 1 shows a summary of age, gender, TSPO genotype and scan information.

Arterial blood sampling and centrifugation

From a radial arterial cannula, blood samples for measuring radioactivity in plasma and whole blood were drawn manually at 0.25, 0.5, 0.75, 1, 1.5, 2, 2.5, 3, 4, 6, 8, 10, 12, 15, 20, 25, 30, 35, 45, 65 and 85 min post injection of ^{123}I -CLINDE. Additionally, samples were drawn at 0.5, 4, 10, 20, 30, 45, 65 and 85 min for metabolite analysis by radio-high performance liquid chromatography (radio-HPLC) (16). Fractions of HPLC eluent were collected using a fraction collector device (Foxy Jr FC144, Teledyne Isco) and counted off-line in a well-counter (2480 Wizard2 Gamma Counter, Perkin Elmer) for accurate measurements of parent tracer. For the

first eight subjects the blood was stored on ice for an estimated 30-90 min until centrifugation (Eppendorf centrifuge 5800R with 3500 rpm at 4° C in 7 min). During the course of the study, we discovered that ^{123}I -CLINDE continued to bind to TSPO in formed blood cells, presumably the monocytes, until separating plasma from the sample by centrifugation. For the remaining 8 subjects, all blood samples were stored on ice and centrifuged within max. 5 min. Total radioactivity in plasma and whole-blood was measured in a well-counter (Cobra 5003; Packard Instruments) and data were decay-corrected to the time of injection. Further, the radioligand *purity* was measured for each batch of ^{123}I -CLINDE, and trapping efficiency of the HPLC column (*plasma control*) was determined for each scan by spiking water and blank plasma with ^{123}I -CLINDE. All equipment was cross-calibrated to the SPECT scanner. Blood screening including white blood cell differential count was performed at each scan.

Image acquisition

To block thyroidal uptake of free radioiodine, 200 mg of potassium perchlorate was administered intravenously 20 min before injection of ^{123}I -CLINDE. A headband was applied to minimize head movements during scanning. Dynamic SPECT scanning with a triple-head IRIX camera (Philips Medical) was started simultaneously with a bolus injection of ^{123}I -CLINDE (MAP Medical Technologies), and lasted for 90 mins. The protocol consisted of 10x2-minute frames, followed by 7x10-minute frames.

T1-weighted magnetic resonance imaging (MRI) was acquired once for each subject using a 3T Siemens Prisma MR scanner 3 ± 49 (mean \pm standard deviation, median=0) days after the corresponding SPECT scan. All brain scans were normal as interpreted by a neuroradiologist.

Image analysis

Image preprocessing. For each subject the weighted mean SPECT image was co-registered to the T1-weighted MRI by interactive image overlay (17). Automatic delineation of volumes of interest (VOIs) was performed using probability maps and a data processing pipeline (18). Due to the limited spatial resolution of SPECT images, no segmentation of grey matter, white matter and cerebrospinal fluid was attempted. Seven VOIs were investigated in this study: midbrain, thalamus, pons, striatum, hippocampus, cerebellum (without vermis) and neocortex. These VOIs were defined as volume-weighted means of either the left- and the right-hemisphere or of smaller VOIs: striatum as the mean of caudate nucleus and putamen; and neocortex as the mean of frontal cortex, superior temporal gyrus, medial inferior temporal gyrus, parietal cortex, sensory motor cortex and occipital cortex.

Brain and blood uptake. The radioactive concentrations in blood and brain were studied independently to investigate the test and retest variability. Therefore, percentage difference of the mean SUV (mSUVs) was calculated, where SUV (g/ml) was defined as TAC (kBq/ml) in blood or brain VOIs normalized by the injected dose per body weight (in MBq/kg) (19), and mSUV is defined as the area under the SUV curve normalized by time length.

Kinetic modelling. A 2TCM with arterial plasma function as input (K_1 to k_4 with a fixed blood volume in brain tissue of 5%) was used to quantify ^{123}I -CLINDE binding as distribution volume (V_T), as this has previously been demonstrated to be the optimal method (12).

The arterial input function was generated in two ways, depending on the blood sample centrifugation.

Method 1: For studies with immediate centrifugation of blood samples

To account for tracer purity and trapping efficiency the measured parent fraction (PF) from the fraction collector was first fitted by a multi-exponential function and adjusted as below:

$$PF(t) = a_1 \cdot e^{-b_1 t} + a_2 \cdot e^{-b_2 t} + a_3 \quad \text{eq. 1}$$

$$PF_adj(t) = (PF(t) + \text{purity} - \text{plasma std}) / \text{purity}$$

The difference between ¹²³I-CLINDE purity and plasma control indicates the part failed to be trapped by the extraction column of the radio HPLC.

Then the metabolite-corrected plasma input function was calculated as the product of the plasma TAC $C_p(t)$ and the adjusted parent fraction $PF_adj(t)$:

$$C_{mcp}(t) = C_p(t) \cdot PF_adj(t) \quad \text{eq. 2}$$

Method 2: For studies with delayed centrifugation of blood samples

Plasma to whole-blood ratio (PoB) and adjusted parent fraction as a function of time were generated for all scans that were accompanied by blood samples undergoing immediate centrifugation. The mean of these functions, respectively, were generated as population-based PoB (PB_PoB) and population-based parent fraction (PB_PF):

$$PoB_i(t) = a_i \cdot (1 - e^{-b_i t}) + c_i$$

$$PB_PoB(t) = \sum_{i=1}^N PoB_i(t) / N \quad \text{eq. 3}$$

$$PB_PF(t) = \sum_{i=1}^N PF_adj_i(t) / N$$

where N is the number of scans. To generate metabolite-corrected plasma input function (C_{mcp}) these two functions were then applied on the measured whole-blood TAC (C_w) of the studies with delayed centrifugation as below:

$$C_{mcp}(t) = C_w(t) \cdot PB_PoB(t) \cdot PB_PF(t) \quad \text{eq. 4}$$

Image and data pre-processing were performed using MATLAB 8.1 (R2013a, Mathworks Inc., MA) and kinetic modelling was done using PMOD (version 3.0; PMOD Technologies Inc., Switzerland).

Statistical analysis

To evaluate the test-retest reproducibility and variability of ¹²³I-CLINDE the following four matrices were used: PD, absolute PD, ICC and COV.

PD: test-retest reproducibility was calculated as the difference between test and retest outcome measures divided by their average, outcome measures being mSUV of blood or brain uptake, and V_T . The absolute PD was also calculated for comparison to other studies.

ICC: ICC evaluates the reliability by measuring within-subject variability relative to between-subject variability as below:

$$ICC = \frac{MSS_{btw} - MSS_{within}}{MSS_{btw} + (k - 1)MSS_{within}} \quad \text{eq. 5}$$

$$\text{where } MSS_{btw} = \frac{1}{N-1} \sum_{i=1}^N (\bar{V}_{Ti} - \bar{V}_T)^2 \quad MSS_{within} = \frac{1}{N} \sum_{i=1}^N \sum_{j=1}^k (V_{Tij} - \bar{V}_{Ti})^2 \quad \text{eq. 6}$$

\bar{V}_{Ti} is the mean of test and retest measures of subject i , and \bar{V}_T is the mean of all observations (test and retest of all subjects). V_{Tij} is one of the measures of subject i . N is the number of subjects, and k is the number of repeated measures ($k=2$). If $MSS_{btw}=0$ there is no reliability, and $ICC=-1$; if $MSS_{within}=0$ there is maximum reliability, and $ICC=1$.

COV: The COV of outcome measures was calculated as the standard deviation divided by the mean across all observations for each VOI.

To test effects of centrifugation, genotype or the test-retest, a linear model fitting using generalized least squares (GLS) was performed in R (version 3.2.2). In general, a GLS model performs similar to a standard linear model, but can furthermore account for a complex

covariance structure between observations. In our case the GLS model allows for different variances between residuals in repeated measures and for correlation between them, unless otherwise stated.

Details about each model applied will be given in the results section. For GLS models, mean and standard error (SE) are given. In other cases, mean and standard deviation are given. Paired-sample t-test, Wilcoxon rank sum test and Pearson's linear correlation were performed using MATLAB 8.1 (R2013a, Mathworks Inc.).

RESULTS

The injected radioactivity in test and retest scans was not statistically different; neither was ^{123}I -CLINDE purity or plasma control, for details see (Table 1).

Delayed centrifugation and discrepancy between blood and brain PD.

In the first eight subjects with delayed centrifugation of blood samples, we found a large test-retest PD of mSUV in the plasma parent compound ($1.0 \pm 31.3\%$), but much lower PD in the brain ($0.7 \pm 8.0\%$ - $2.2 \pm 18.8\%$ in 7 VOIs).

Effect of genotype

In subjects with immediately centrifuged samples, the parent fraction mSUV was higher in MAB (0.37 ± 0.07 , mean \pm SE) than in HAB (0.22 ± 0.05 , mean \pm SE; $p=0.0006$, GLS model, age and gender adjusted), with a MAB:HAB ratio of 1.65. A genotype-related difference was also observed in PoB (Supplemental Fig. 1). The mean PoB TAC of HAB ($N=2 \times 3$) and that of MAB ($N=2 \times 5$) had different kinetics, especially during the first 20 min, however the difference was not significant. Mean $\text{SUV}_{0-20\text{min}}$ of MABs correlated negatively with monocyte counts ($p=0.0341$, $R^2=0.4486$). A negative trend was also observed for HABs ($p=0.1938$).

Arterial input function

Immediately centrifuged blood samples. After parent fraction adjustment using eq. 1, the parent fraction between MAB and HAB was still significantly different ($p=0.0002$, GLS model, age and gender adjusted). Furthermore, the parent fraction curves had different starting points: 94% intact ^{123}I -CLINDE left for MABs, and 77% for HABs; and at 20 min post injection, 53% for MABs, and 36% for HABs; and at 90 min 38% left for MABs and 27% for HABs.

The arterial input function of a MAB and a HAB (Figs. 1C and 1D) showed faster washout in the HAB. Due to the observed differences between genotypes, population-based PoB functions and population-based PF functions were generated separately for these two genetic groups. Before applying the population-based functions to adjust data with delayed centrifugation, method validation was done on the data with immediate centrifugation using a leave-one-out procedure, where population-based functions were generated excluding the scan that the functions were applied on.

These PB_PoB functions were applied to the whole-blood TAC C_w first to estimate the plasma TAC C_p . The differences between estimated C_p and the measured data were $0.2\pm 4.3\%$ for MABs ($N=2\times 5$), and $0.6\pm 10.8\%$ for HABs ($N=2\times 3$), none were significant. Thereafter, PB_PF was applied to C_p to estimate the metabolite-corrected plasma input function C_{mcp} . Differences between population-adjusted estimates and measured C_{mcp} were $0.6\pm 9.1\%$ for MABs and $0.5\pm 8.0\%$ for HABs, none were significant.

Delayed centrifuged blood samples. Immediate centrifugation increased the mSUV of PoB from 0.95 to 1.07 ($p=0.0003$, GLS model, genotype adjusted), which was 12.4% more than the mSUV of PoB from subjects whose samples underwent delayed centrifugation; see descriptive data of PoB in (Fig. 2)). Thus, the arterial input functions were underestimated in scans with

delayed centrifugation of blood samples (Figs. 1A and 1B). Therefore, population-adjusted input functions were calculated in these cases.

After adjustment using PB_PoB and PB_PF on C_w , test-retest PD of C_p decreased from $-22.7\pm 27.6\%$ to $-9.4\pm 15.2\%$ (absolute PD of C_p decreased from 27.7% to 14.4%), and PD of C_{mcp} changed from $-2.5\pm 34.6\%$ to $-6.4\pm 15.5\%$ (absolute PD of C_{mcp} decreased from 28.0% to 14.1%) (Supplemental Fig. 2).

Test-retest variability

Brain uptake. Brain mSUV of 7 VOIs were studied. The mSUV of a male HAB and a male MAB at age 49 years (mean age) were 1.03 ± 0.14 g/ml and 0.88 ± 0.15 g/ml (mean \pm SE) respectively, and the difference was borderline significant ($p=0.0535$, GLS with different residual variances). The higher binding in HABs than in MABs was also shown in (Fig. 1) illustrated as SUVs of neocortex with slower washout in HABs. Mean SUV of HABs was 16.8% higher than MABs, see descriptive data in (Fig. 3A). Ten of 16 subjects had lower brain mSUV in test than retest scans.

Since the beginning of a brain TAC can be influenced by blood flow, $mSUV_{60-90min}$ was also studied. The $mSUV_{60-90min}$ of a male HAB and a male MAB at age 49 years were 0.55 ± 0.09 g/ml and 0.43 ± 0.09 g/ml (mean \pm SE) respectively ($p=0.0105$, GLS with different residual variances), and the $mSUV_{60-90min}$ of HABs was 27.6% higher than MABs, see descriptive data in (Fig. 3B).

The PDs of brain mSUVs across all subjects in 7 VOIs are shown in (Table 2). Test and retest mSUV of the same subject correlated to a high degree, with correlation coefficients of 0.86 ± 0.07 ($p<0.05$, $N=16$). The PD of MABs was on average $-3.6\pm 8.1\%$ while that of HABs was $-7.0\pm 7.8\%$, however, the difference was not significant (GLS model, age and gender adjusted), and the absolute PD was neither sensitive to genotype. ICC values for MABs and HABs and the total

samples are given in (Table 2). COV was $20.0 \pm 2.3\%$ in MABs and $9.2 \pm 2.0\%$ in HABs.

Furthermore, ICC and COV differed between MABs and HABs ($p = 2.29e-05$, $p = 1.38e-05$, respectively), with a MAB:HAB ratio of 1.8 for ICC and 2.2 for COV.

Distribution volumes. The V_{TS} of 7 VOIs derived from 2TCM modelling of scans with immediately and delayed centrifuged blood samples, with and without population-based adjustment of the input functions, are given in (Supplemental Table 1, 2 and 3). Figure 1 illustrates the 2TCM fitting using the measured or population-based adjusted input functions.

The V_{TS} of scans with delayed centrifuged blood samples (16 scans, 7 VOIs) before and after population-based adjustment was significantly different ($p = 0.0176$, GLS with different residual variances) with a V_T value of $5.3 \pm 1.1 \text{ mL/cm}^3$ before the adjustment and $4.7 \pm 1.1 \text{ mL/cm}^3$ (mean \pm SE) after the adjustment. Delayed centrifugation of samples led to an underestimation of input functions and therefore caused an overestimation of the V_{TS} by 12.4% on average.

Using population-based adjusted input functions in scans with delayed blood centrifugation and measured input functions in scans with immediate blood centrifugation, the V_T (32 scans, 7 VOIs) of a male HAB and a male MAB at age 49 years (mean age) was $7.5 \pm 1.4 \text{ mL/cm}^3$ and $4.6 \pm 1.4 \text{ mL/cm}^3$ (mean \pm SE) respectively ($p = 0.0001$, GLS with different residual variances). V_T of HABs was on average 65% higher than MABs, and there was no test-retest difference, see descriptive data in (Fig. 3C). Test-retest variability measures were calculated for the immediately centrifuged scans and the population-adjusted delayed centrifuged scans both separately and combined (Table 2). For subject 16 the measured purity and plasma standard were not available, thus no adjustment was done.

For the immediately centrifuged scans, test V_T was 0.28 mL/cm^3 lower than retest V_T across all 7 VOIs ($p = 0.0122$, GLS model, age and gender adjusted). This GLS model assumes a

homogeneous test-retest difference across VOIs, since there were no interactions between the 7 VOIs and test-retest scans.

The PD between test-retest of all subjects ($N=16$) across all 7 VOIs evaluated as repeated measures was on average $-11.7\pm 8.6\%$ for MABs and $-12.1\pm 8.3\%$ for HABs, and the difference was not significant (GLS, age and gender adjusted). COV of MABs was $16.7\pm 3.4\%$, and of HABs was $26.5\pm 7.7\%$. Opposite to the brain mSUV, ICC and COV estimated by the V_{TS} were borderline significantly higher for HABs than MABs ($p= 0.0533$, $p= 0.0492$, respectively), with a HAB:MAB ratio of 1.6 for ICC and 1.7 for COV.

DISCUSSION

In this study we investigated the test-retest variability of the second-generation TSPO SPECT ligand, ^{123}I -CLINDE, in a group of 16 healthy volunteers.

Population-based approach

We used a population-based approach to adjust data from subjects with delayed blood centrifugation. The feasibility of the approach was validated on the immediately centrifuged data in a leave-one-out manner to avoid bias. After adjustment, the test-retest difference decreased in blood components. If time-dependent binding to blood cells is also observed in other TSPO ligands, this approach could be applied to data if centrifugation is delayed. Furthermore, this approach has the potential to reduce the complexity and time consumption associated with blood handling and determination of metabolites, since only whole blood counts are needed.

^{123}I -CLINDE SPECT variability

ICC values of V_{TS} were higher for ^{123}I -CLINDE SPECT than previously reported in healthy controls for the first-generation TSPO tracer ^{11}C -PK11195 PET (7) and comparable to second-generation TSPO tracers like ^{11}C -PBR28 (9) and ^{11}C -DPA-713 (8). ICC is a statistical analysis to

compare the between-subject variation with the within-subject variation. If HAB and MAB subjects are pooled and not measured separately for each genetic group, ICC values will be higher and not only reflect the variability of the method but also a known biological difference in affinity. In contrast to previous studies in second-generation TSPO tracers we also calculated ICC and COV separately for each genetic group, revealing higher ICC and COV values for HABs than MABs. A plausible explanation for a generally modest reliability when subdividing into genotypes is that the TSPO signal, due to its non-prominent presence under healthy conditions, has a relatively low signal-to-background ratio compared to a disease situation with an amplified TSPO signal driven by disease-related activated glial cells. For MABs the signal-to-background ratio is lower than for HABs, consequently leading to a comparably lower reliability. Percentage difference of brain mSUV and V_T and the absolute PD for ^{123}I -CLINDE SPECT were slightly smaller than previously reported for ^{11}C -PBR28 (9).

SUV as a semi-quantitative measure

In a clinical setting, SUV is often used as a semi-quantitative surrogate measure to V_T . This is due to several complications related to the complexity of the blood sampling and analysis. In this paper we studied the genotype difference and test-retest variability using both SUV and V_T , to investigate the feasibility of using SUV as an outcome measure for a TSPO ligand. From the brain mSUV it is possible to differentiate MAB and HAB, (Fig. 4), with HABs having ~17% higher binding than MABs when quantified using mSUV of the whole TAC, and ~28% higher when quantified using mSUV_{60-90min}. However, HABs had on average 65% higher binding than MABs using V_T estimated by 2TCM modelling. This can be explained by higher affinity of radioligand to TSPO in HABs and the binding of radiotracer to the abundant TSPO in both blood

and peripheral tissues. Thus, less free radioligand would be available in plasma of HABs compared to MABs which would remain undetected using brain SUV as an outcome. In a clinical setting, patients can have a longitudinally varying disease related peripheral immune response and thereby varying peripheral TSPO binding sites. This may cause changing concentrations of parent TSPO tracer in the plasma, which as a consequence influences the brain uptake. In (20) SUV was compared to V_T in quantifying TSPO changes in baboons' brain caused by lipopolysaccharide using ^{11}C -PBR28, and SUV failed to detect neuroinflammation as indicated by V_T changes. It might be ascribed to the violation of assumptions: 1) the arterial input TAC has a consistent pattern from study to study, and 2) the area under the curve of TAC is proportional to the injected dose/body weight. Our study clearly indicated the violation of these assumptions in the case of TSPO imaging. Therefore, only using brain SUV to quantify TSPO binding has its limitations.

Effect of blood centrifugation

Switching to immediate centrifugation improved the test-retest reliability in blood significantly. Since TSPO is also expressed in blood e.g. in monocytes (2), we hypothesize that ^{123}I -CLINDE continues to bind to TSPO in blood cells and intact ^{123}I -CLINDE in a blood sample will gradually bind to blood cells causing an underestimation of plasma radioactivity. Our hypothesis is supported by the increase in PoB ratio by immediate centrifugation. The negative correlation between PoB in MABs and monocyte counts also indicate that CLINDE binding is related to TSPO expression in blood. Additionally, the lower starting point of PoB TAC of HABs than TAC of MABs (Supplemental Fig. 1) indicates that binding of CLINDE to blood cells is dependent on the affinity/TSPO polymorphism (21). Previously, in (22) an extra compartment was proposed to describe TSPO ligand binding to the vascular walls. Based on our observations,

the “endothelial compartment” may additionally include binding TSPO in blood cells. However, fast and systematic centrifugation of blood samples will still be required to produce consistent results.

CONCLUSION

The variability of ^{123}I -CLINDE binding was investigated in a test-retest setting with 16 healthy subjects. The test-retest variability estimated by ICC and percentage difference was very favourable compared to the first-generation TSPO ligand ^{11}C -PK11195, and comparable to or slightly better than second-generation TSPO ligands ^{11}C -DPA-713 and ^{11}C -PBR28. SUV as a surrogate of the output measure V_T from ‘gold standard’-2TCM has its limitations. Immediate centrifugation of blood samples is essential and can prevent underestimation of the plasma input function. A population-based method could efficiently recover data with delayed centrifugation, and has the potential to be applied to studies using other TSPO ligands.

DISCLOSURE

There is no conflict of interest.

ACKNOWLEDGMENTS

We acknowledge Svitlana Olsen and Glenna Skouboe for technical assistance and Brice Ozenne for his assistance in statistical analysis. This work was financially supported by the European Union's Seventh Framework Programme (FP7/2007-2013) under grant agreement n° HEALTH-F2-2011-278850 (INMiND) and the Danish Council for Independent Research (grant ID: 0602-0228-8B).

Reference list

1. Papadopoulos V, Baraldi M, Guilarte TR, et al. Translocator protein (18kDa): new nomenclature for the peripheral-type benzodiazepine receptor based on its structure and molecular function. *Trends Pharmacol Sci.* 2006;27:402-409.
2. Canat X, Carayon P, Bouaboula M, et al. Distribution profile and properties of peripheral-type benzodiazepine receptors on human hemopoietic cells. *Life Sci.* 1993;52:107-118.
3. Chen MK, Guilarte TR. Translocator protein 18 kDa (TSPO): molecular sensor of brain injury and repair. *Pharmacol Ther.* 2008;118:1-17.
4. Papadopoulos V, Lecanu L. Translocator protein (18 kDa) TSPO: an emerging therapeutic target in neurotrauma. *Exp Neurol.* 2009;219:53-57.
5. Takano A, Piehl F, Hillert J, et al. In vivo TSPO imaging in patients with multiple sclerosis: a brain PET study with [18F]FEDAA1106. *EJNMMI Res.* 2013;3:30.
6. Winkeler A, Boisgard R, Awde AR, et al. The translocator protein ligand [(1)(8)F]DPA-714 images glioma and activated microglia in vivo. *Eur J Nucl Med Mol Imaging.* 2012;39:811-823.
7. Jucaite A, Cselenyi Z, Arvidsson A, et al. Kinetic analysis and test-retest variability of the radioligand [11C](R)-PK11195 binding to TSPO in the human brain - a PET study in control subjects. *EJNMMI Res.* 2012;2:15.
8. Coughlin JM, Wang Y, Ma S, et al. Regional brain distribution of translocator protein using [(11)C]DPA-713 PET in individuals infected with HIV. *J Neurovirol.* 2014;20:219-232.
9. Collste K, Forsberg A, Varrone A, et al. Test-retest reproducibility of [(11)C]PBR28 binding to TSPO in healthy control subjects. *Eur J Nucl Med Mol Imaging.* 2016;43:173-183.
10. Park E, Gallezot JD, Delgadillo A, et al. (11)C-PBR28 imaging in multiple sclerosis patients and healthy controls: test-retest reproducibility and focal visualization of active white matter areas. *Eur J Nucl Med Mol Imaging.* 2015;42:1081-1092.
11. Arlicot N, Katsifis A, Garreau L, et al. Evaluation of CLINDE as potent translocator protein (18 kDa) SPECT radiotracer reflecting the degree of neuroinflammation in a rat model of microglial activation. *Eur J Nucl Med Mol Imaging.* 2008;35:2203-2211.
12. Feng L, Svarer C, Thomsen G, et al. In vivo quantification of cerebral translocator protein binding in humans using 6-chloro-2-(4'-123I-iodophenyl)-3-(N,N-diethyl)-imidazo[1,2-a]pyridine-3-acetamide SPECT. *J Nucl Med.* 2014;55:1966-1972.

13. Jensen P, Feng L, Law I, et al. TSPO Imaging in Glioblastoma Multiforme: A Direct Comparison Between 123I-CLINDE SPECT, 18F-FET PET, and Gadolinium-Enhanced MR Imaging. *J Nucl Med*. 2015;56:1386-1390.
14. Jensen P, Kondziella D, Thomsen G, Dyssegaard A, Svarer C, Pinborg LH. Anti-NMDAR encephalitis: demonstration of neuroinflammation and the effect of immunotherapy. *Neurology*. 2015;84:859.
15. Owen DR, Yeo AJ, Gunn RN, et al. An 18-kDa translocator protein (TSPO) polymorphism explains differences in binding affinity of the PET radioligand PBR28. *J Cereb Blood Flow Metab*. 2012;32:1-5.
16. Gillings N. A restricted access material for rapid analysis of [(11)C]-labeled radiopharmaceuticals and their metabolites in plasma. *Nucl Med Biol*. 2009;36:961-965.
17. Willendrup P, Pinborg LH, Hasselbalch SG, et al. Assessment of the precision in co-registration of structural MR images and PET images with localized binding. *International Congress Series*. 2004;1265:275-280.
18. Svarer C, Madsen K, Hasselbalch SG, et al. MR-based automatic delineation of volumes of interest in human brain PET images using probability maps. *Neuroimage*. 2005;24:969-979.
19. Thie JA. Understanding the standardized uptake value, its methods, and implications for usage. *J Nucl Med*. 2004;45:1431-1434.
20. Yoder KK, Territo PR, Hutchins GD, et al. Comparison of standardized uptake values with volume of distribution for quantitation of [(11)C]PBR28 brain uptake. *Nucl Med Biol*. 2015;42:305-308.
21. Kanegawa N, Collste K, Forsberg A, et al. In vivo evidence of a functional association between immune cells in blood and brain in healthy human subjects. *Brain Behav Immun*. 2016;54:149-157.
22. Rizzo G, Veronese M, Tonietto M, Zanotti-Fregonara P, Turkheimer FE, Bertoldo A. Kinetic modeling without accounting for the vascular component impairs the quantification of [(11)C]PBR28 brain PET data. *J Cereb Blood Flow Metab*. 2014;34:1060-1069.

Figure 1 The effect of population-based (PB) approach to adjust input functions (IF) with delayed centrifugation (A, B) and the standard uptake values (SUV) of IF and a brain region of mixed affinity binders (MAB) (A, C) and high affinity binders (HAB) (B, D). (A) and (B) show the SUVs of a MAB (Subj 6) and a HAB (Subj 3), separately, both with delayed centrifugation of blood samples. Two tissue compartment model (2TCM) fitting to neocortex using the input functions (red curves) were also given. (C) and (D) show the SUVs of a MAB (Subject 10) and a HAB (Subject 14), both with immediate centrifugation of blood samples.

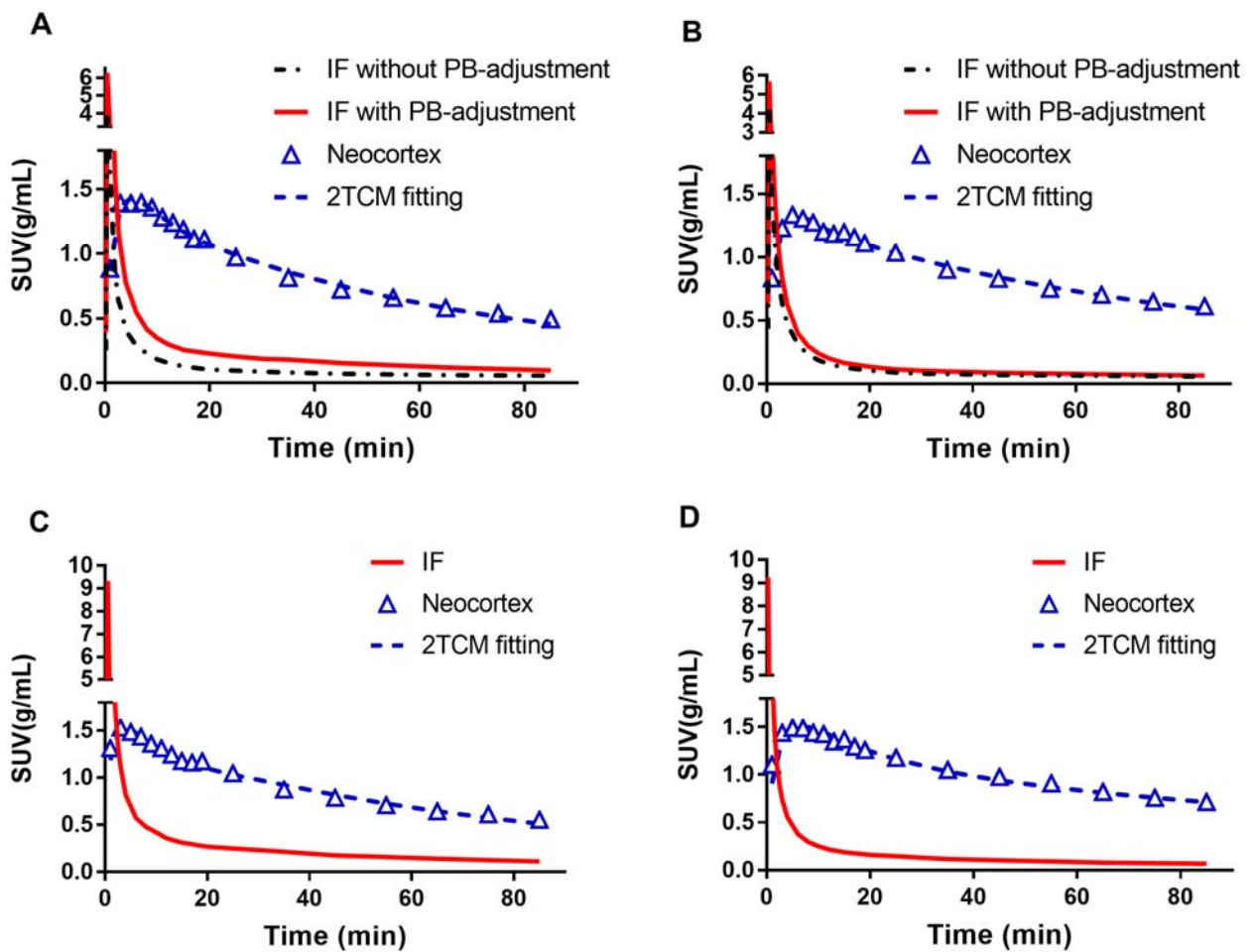


Figure 2 Effect of immediate centrifugation of blood samples on plasma to whole-blood ratio (PoB)

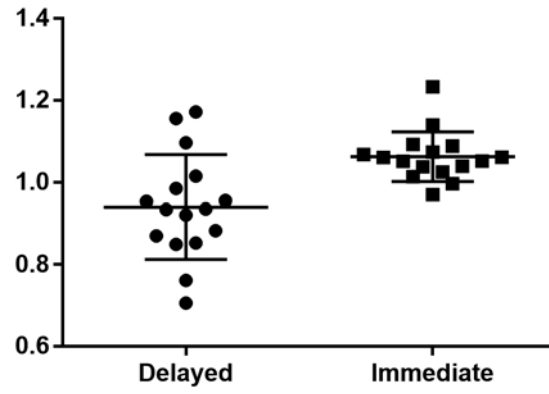


Figure 3 Cerebellar brain mean standard uptake values (mSUV) (A), mSUV from 60 to 90 min (B) and distribution volume V_T (C) categorized by genotype: mixed affinity binder (MAB) and high affinity binder (HAB)

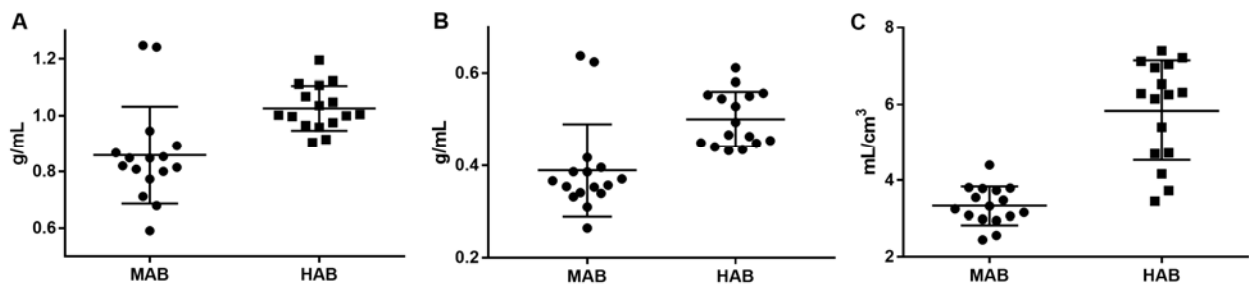


Figure 4 Brain mean standard uptake values (mSUVs) of a typical mixed affinity binder (MAB): subject 12 and a high affinity binder (HAB): subject 11.

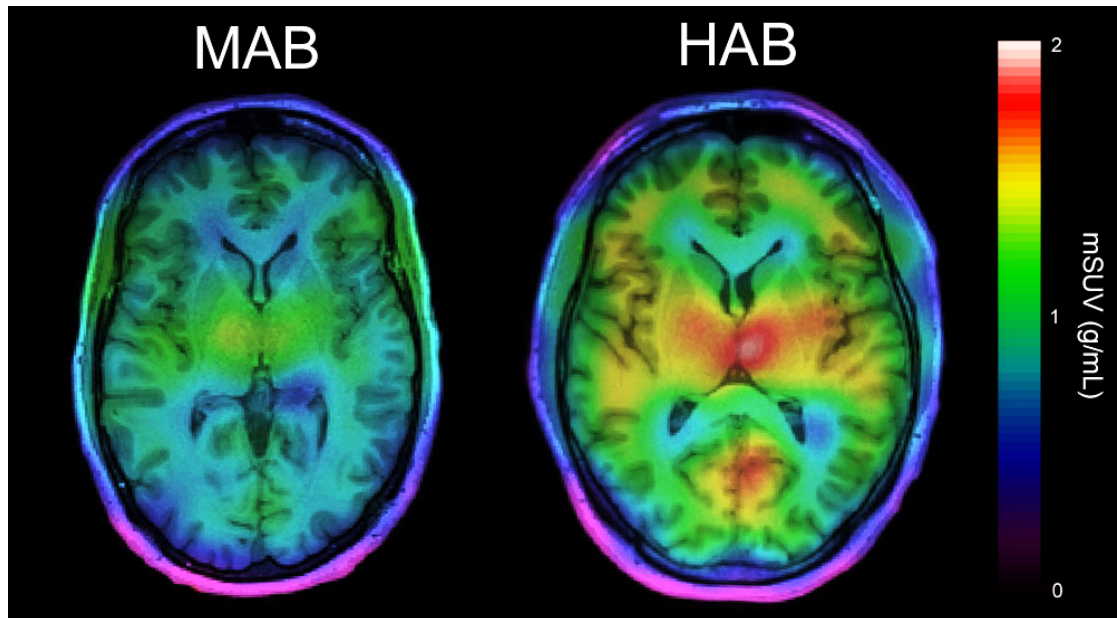


Table 1 Demographic data and methodological information specified by subject

Subject	Gender	Age (yrs)	Body weight (kg)	TSPO genotype	Injected activity (MBq)	Scan interval (days)	Centrifugation	Purity (%)	Plasma control (%)
1	M	61	80	MAB	120.9	21	delayed	96.1	95.4
					117.8			93.5	91.4
2	M	70	92	MAB	112.2	42	delayed	95.4	95.4
					123.6			94.9	93.8
3	M	59	76.5	HAB	118.1	35	delayed	96.4	94.7
					112.0			94.9	93.2
4	F	38	110	HAB	116.3	28	delayed	96.0	95.0
					114.3			90.7	88.4
5	F	62	70	HAB	119.0	42	delayed	96.1	95.1
					119.4			96.6	94.0
6	F	58	50	MAB	116.0	28	delayed	96.1	96.2
					119.7			95.3	91.4
7	F	68	87	HAB	124.8	56	delayed	92.3	90.1
					115.1			95.2	90.5
8	M	52	94	HAB	118.5	56	delayed	98.1	93.8
					124.1			89.8	88.5
9	M	42	80	MAB	118.8	28	immediate	95.7	94.6
					115.8			93.4	90.3
10	F	45	86.2	MAB	117.4	56	immediate	95.4	94.6
					114.1			94.9	94.7
11	M	35	100	HAB	119.9	56	immediate	93.0	93.2
					114.4			90.7	89.9
12	F	40	73	MAB	112.0	7	immediate	92.8	91.8
					130.7			94.7	94.1
13	M	24	95.6	MAB	115.4	14	immediate	94.4	92.2
					116.0			92.0	90.2
14	F	69	83	MAB	123.0	28	immediate	94.5	92.7
					127.1			94.4	90.4
15	F	30	68	HAB	105.8	42	immediate	91.0	82.9
					116.0			91.1	88.1
16	F	34	74.2	HAB	118.4	28	immediate	NA	NA
					116.3			NA	NA
Mean		49±	82.5±		117.9±	35±		93.4±	91.4±
±STD		15	14.4		4.9	15		1.7	3.2

Note: HAB: high affinity binder; MAB: mixed affinity binder; STD: standard deviation; NA: not available.

Table 2 Test-retest variability

Regions	V _T using population-adjusted input function of delayed centrifugation N=8			V _T of immediate centrifugation N=8			V _T of all subjects N=16			Brain uptake N=16						
	PD (%)	Absolute PD (%)	ICC	PD (%)	Absolute PD (%)	ICC	PD (%)	Absolute PD (%)	ICC of MABs	PD (%)	Absolute PD (%)	ICC of HAB	ICC of all			
Midbrain	2.8 ± 14.5	12.4	0.96	-1.5 ± 15.6	11.8	0.86	0.6 ± 14.8	12.1	0.41	0.91	0.93	-2.5 ± 11.5	10.1	0.72	0.39	0.71
Thalamus	11.0 ± 10.5	12.8	0.94	-12.3 ± 13.3	12.7	0.86	-0.7 ± 16.7	12.8	0.68	0.84	0.90	-4.7 ± 14.6	11.6	0.74	0.53	0.71
Pons	-2.3 ± 14.2	9.6	0.90	-8.2 ± 23.8	18.9	0.72	-5.3 ± 19.2	14.2	0.54	0.60	0.82	-2.7 ± 12.4	11.0	0.81	0.52	0.77
Pallidostriatum	5.8 ± 21.9	17.6	0.85	-7.0 ± 19.0	14.1	0.87	-0.6 ± 20.9	15.8	0.22	0.79	0.85	-2.2 ± 13.7	11.1	0.79	0.50	0.74
Hippocampus	14.9 ± 17.3	15.7	0.75	-5.9 ± 11.8	9.7	0.91	4.5 ± 17.9	12.7	0.58	0.78	0.83	-2.0 ± 15.2	12.3	0.57	0.23	0.56
Cerebellum	9.6 ± 9.4	10.2	0.94	-4.9 ± 10.0	8.2	0.96	2.3 ± 12.0	9.2	0.76	0.88	0.95	-1.5 ± 9.4	7.8	0.90	0.45	0.87
Neocortex	5.8 ± 12.6	10.2	0.92	-3.2 ± 12.8	10.5	0.92	1.3 ± 13.2	10.4	0.88	0.79	0.92	-2.8 ± 9.6	8.5	0.91	0.57	0.85

Note: PD: percentage difference; ICC: intraclass correlation coefficient; V_T: distribution volume.

Supplemental Material

Figure 1 Plasma to whole-blood ratio of HAB ($N=2 \times 3$) and MAB ($N=2 \times 5$) with immediate centrifugation

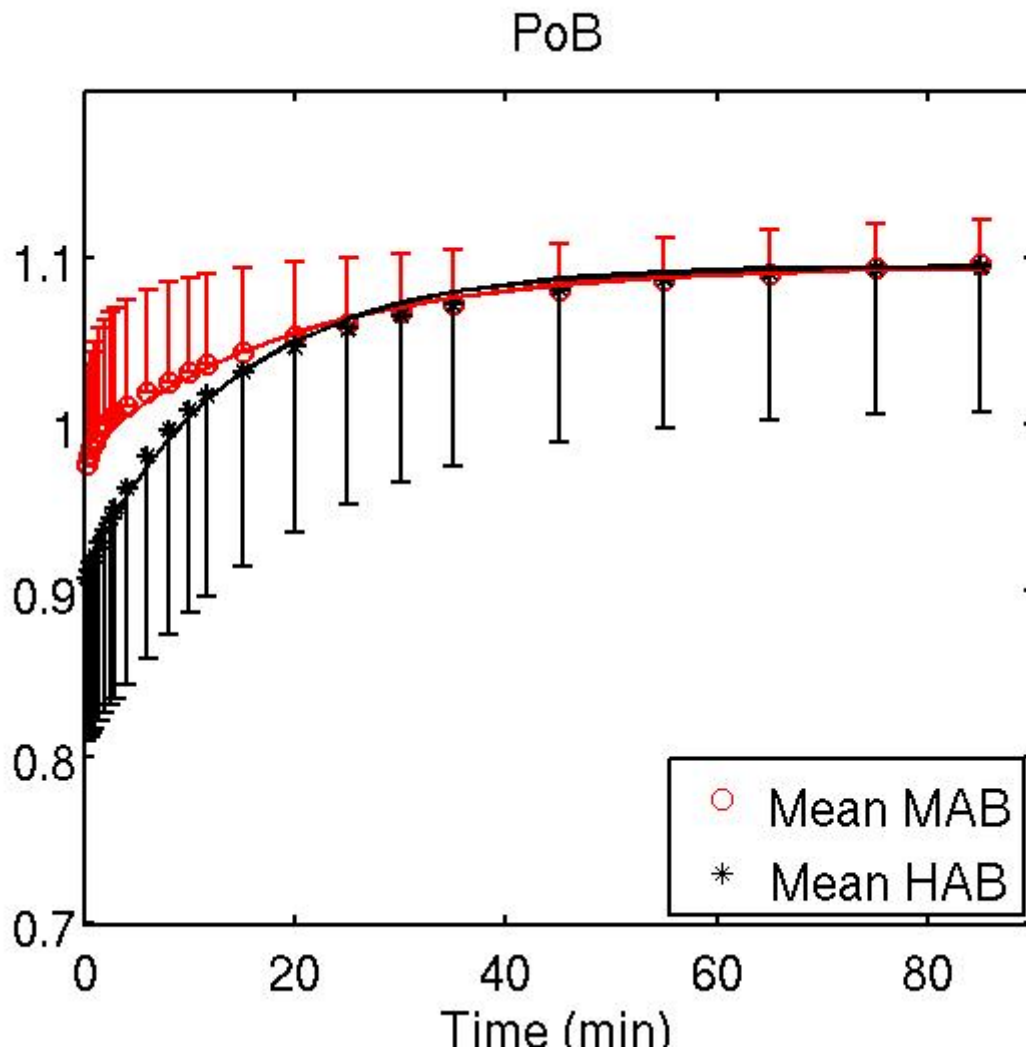


Figure 2 Test-retest absolute percentage difference of radioligand concentration in plasma and metabolite-corrected plasma input function before applying the population-adjusted method: Plasma C_p and Plasma input function C_{mcp} ; and after: Population-based C_p (PB- C_p) and PB- C_{mcp}

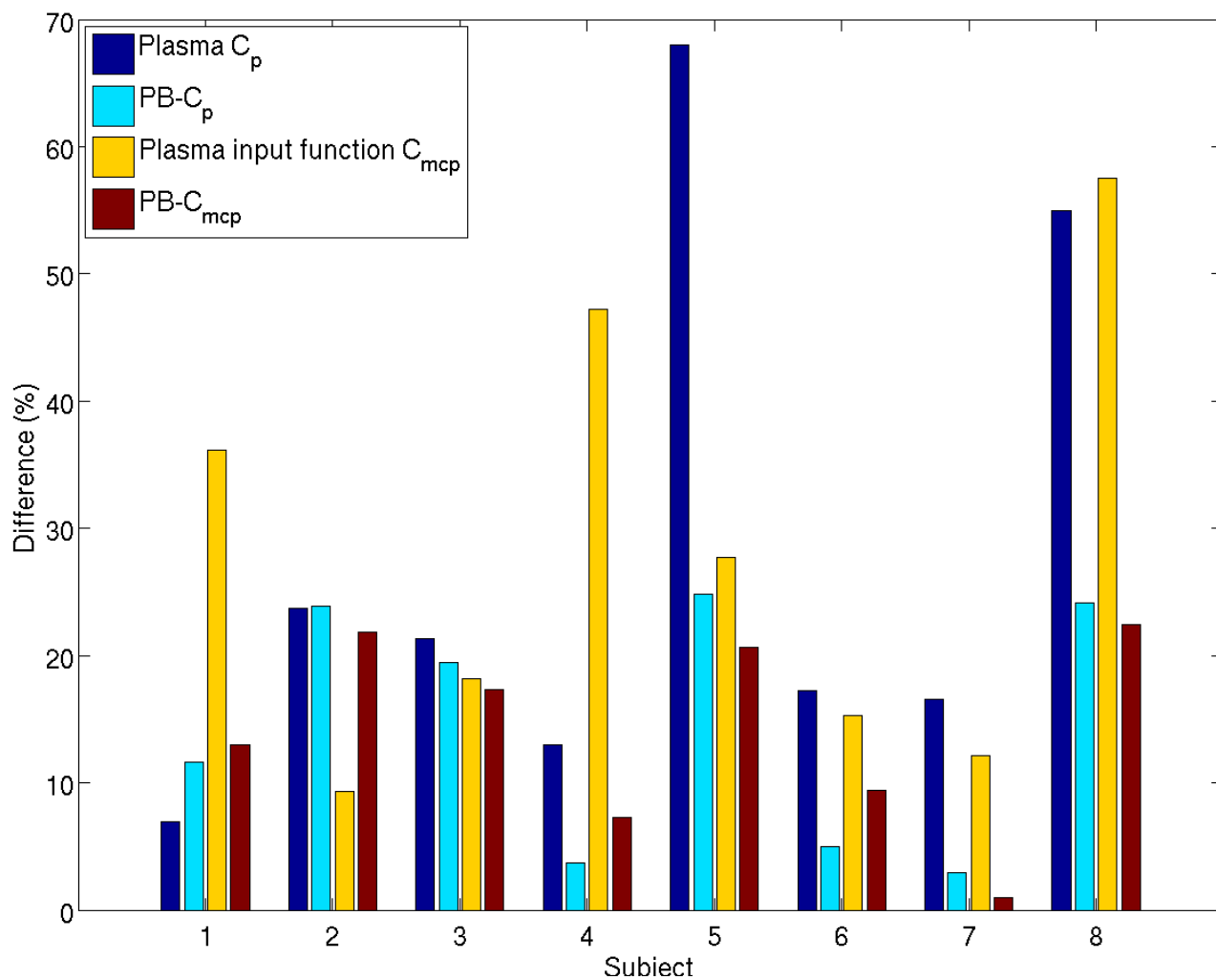


Table 1 Regional distribution volume V_T (mL/cm³) from 2TCM of the immediate centrifuged scans for high affinity binders

(HAB) and mixed affinity binders (MAB)

ID	HAB		HAB		HAB		MAB		MAB		MAB		MAB		MAB	
	Test	Retest	Test	Retest	Test	Retest	Test	Retest	Test	Retest	Test	Retest	Test	Retest	Test	Retest
Regions	11	11	15	15	16	16	9	9	10	10	12	12	13	13	14	14
Midbrain	7.5	9.1	7.1	6.5	10.2	13.4	6.3	5.2	5.1	5.1	6.1	5.3	5.0	5.0	4.1	4.3
Thalamus	8.3	9.5	7.4	7.3	8.2	11.7	3.1	4.2	3.5	3.5	4.4	4.7	4.6	4.9	5.0	5.5
Pons	8.5	6.4	8.8	8.1	8.2	12.0	3.3	4.1	5.3	5.8	4.7	4.4	4.5	6.8	4.6	4.6
Pallidostriatum	6.5	8.9	7.3	7.3	8.8	8.0	3.2	3.4	3.5	2.9	3.5	3.6	3.9	5.6	3.8	4.1
Hippocampus	5.6	7.4	6.0	5.8	7.1	7.5	3.1	3.1	2.9	3.5	3.7	4.0	6.2	5.7	4.1	4.4
Cerebellum	5.4	6.3	6.3	6.3	6.5	7.0	2.4	3.1	3.2	3.0	3.5	3.3	3.5	3.8	3.7	3.8
Neocortex	5.0	6.0	6.4	6.1	6.1	7.2	2.3	2.7	3.5	3.1	3.3	3.3	4.5	4.1	3.9	4.0

Table 2 Regional distribution volume V_T (mL/cm³) from 2TCM of the delayed centrifuged scans without population-based adjustment of the metabolite-corrected input function, but with parent fraction adjustment for high affinity binders (HAB) and mixed affinity binders (MAB)

ID	MAB		MAB		MAB		HAB		HAB		HAB		HAB		HAB	
	Test	Retest	Test	Retest	Test	Retest	Test	Retest	Test	Retest	Test	Retest	Test	Retest	Test	Retest
Regions	1	1	2	2	6	6	3	3	4	4	5	5	7	7	8	8
Midbrain	5.0	5.8	4.7	4.4	10.2	10.5	7.5	12.3	8.7	7.3	12.9	9.5	7.1	6.2	7.5	5.7
Thalamus	5.6	6.7	4.4	3.9	9.6	10.6	7.6	11.2	8.3	6.5	12.8	7.4	5.1	4.7	9.0	5.5
Pons	4.4	4.7	4.4	4.5	9.3	10.8	6.4	12.5	9.0	10.4	11.4	11.2	7.1	5.3	8.1	6.8
Pallidostriatum	3.5	4.6	4.3	3.9	7.5	8.6	6.1	11.6	7.3	5.2	9.4	8.2	4.8	4.1	5.3	4.9
Hippocampus	4.5	4.7	3.1	3.5	8.2	7.5	6.0	9.9	7.3	8.6	8.9	7.0	4.5	4.8	7.4	4.4
Cerebellum	3.6	3.8	2.9	2.9	6.7	7.1	5.7	9.5	6.9	5.0	8.3	6.0	4.7	4.0	5.3	3.9
Neocortex	3.3	3.8	3.0	2.7	6.5	7.1	5.0	8.0	6.5	4.6	8.1	5.8	4.6	4.0	5.4	3.6

Table 3 Regional distribution volume V_T (mL/cm³) from 2TCM of the delayed centrifuged scans with population-based adjustment of the metabolite-corrected input function for high affinity binders (HAB) and mixed affinity binders (MAB)

ID	MAB		MAB		MAB		HAB		HAB		HAB		HAB		HAB	
	Test	Retest	Test	Retest	Test	Retest	Test	Retest	Test	Retest	Test	Retest	Test	Retest	Test	Retest
Regions	1	1	2	2	6	6	3	3	4	4	5	5	7	7	8	8
Midbrain	4.7	5.4	5.4	4.9	6.9	5.4	15.4	17.6	7.8	8.8	11.1	10.7	5.7	4.8	6.3	5.8
Thalamus	4.5	4.7	5.1	4.6	6.6	5.3	9.5	8.7	7.7	6.0	13.9	12.5	4.1	4.2	7.2	6.0
Pons	3.7	3.2	5.0	5.1	5.8	5.4	8.8	12.2	7.8	7.6	11.2	12.4	5.8	5.6	7.4	7.6
Pallidostriatum	5.0	3.1	4.4	4.4	4.9	4.4	7.4	9.4	6.8	5.5	8.6	10.0	3.9	3.3	4.6	5.1
Hippocampus	5.0	3.2	4.2	4.4	5.1	3.6	7.4	7.1	5.8	5.6	7.3	6.8	4.4	4.2	5.3	4.2
Cerebellum	2.9	2.6	3.2	3.1	4.4	3.8	7.2	7.4	6.2	4.7	7.1	7.0	3.7	3.4	4.7	4.2
Neocortex	2.3	2.6	3.2	3.1	4.2	3.7	6.1	6.4	5.8	4.2	7.1	6.6	3.8	3.4	4.5	4.4

Study 4

Expression, evolution and prognostic value of translocator protein in middle cerebral artery stroke patients - A longitudinal ¹²³I-CLINDE-SPECT imaging study.

Jensen P^{1,2}, Feng L¹, Meden P³, Thomsen G¹, Knudsen LV¹, Steglich-Arnholm H⁴, Dyssegaard A¹, Møller K⁵, Thomsen C⁶, Svarer C¹, Beliveau V¹, Ozenne B^{1,7}, Mikkelsen JD^{1,2}, Knudsen GM^{1,2} and Pinborg LH^{1,8}.

1 Neurobiology Research Unit, Rigshospitalet, University of Copenhagen, Denmark

2 Faculty of Health and Medicine, University of Copenhagen, Denmark

3 Department of Neurology, Bispebjerg Hospital, University of Copenhagen, Denmark

4 Department of Neurology, Rigshospitalet, University of Copenhagen, Denmark

5 Department of Neuroanaesthesiology, Rigshospitalet, University of Copenhagen, Denmark

6 Department of Radiology, Rigshospitalet, University of Copenhagen, Denmark

7 Department of Public Health, Section of Biostatistics, University of Copenhagen, Denmark

8 Epilepsy Clinic, Rigshospitalet, University of Copenhagen, Denmark

Corresponding Author

Lars H Pinborg, Ass. Professor, MD, DMSc

Neurobiology Research Unit, Rigshospitalet, Copenhagen Denmark

Email: pinborg@nru.dk, Phone: +45 3545 6712, Fax: +45 3545 6713

Running title: TSPO in stroke

Reprints are not available

Word count: 5490

Abstract

Introduction

Molecular imaging of the translocator protein (TSPO) may provide insight into regional neuroinflammation following ischemic stroke. In this study, we measured the regional cerebral TSPO expression over time after ischemic stroke using ^{123}I -CLINDE single photon emission computed tomography (SPECT) imaging.

Methods

Twelve patients (ten high affinity (HAB) and two mixed affinity binders (MAB)) who suffered a first-ever ischemic middle cerebral artery stroke and ten healthy volunteers (all HAB) were recruited for the study. Patients underwent concomitant ^{123}I -CLINDE SPECT, structural magnetic resonance imaging (MRI) and were clinically tested between week 1-2 (scan 1), week 5-6 (scan 2), and week 15-18 weeks (scan 3). Patients were additionally clinically tested at 25-26 weeks. The healthy volunteers were scanned once with ^{123}I -CLINDE SPECT and structural MRI. TSPO expression was measured in lesional and perilesional regions of interest (ROIs) as well as in ROIs connected to the lesion and ROIs unrelated to the lesion. Furthermore, The necrotized volume was determined from the structural MRI at scan 3.

Results

Lesional TSPO expression was high at scan 1 (median $V_T = 10.5 \text{ mL/cm}^3$) and decreased by 35.6% from scan 1 to 3 ($p=0.004$). In contrast, TSPO expression in brain regions unrelated to the stroke lesion was significantly lower in stroke patients at scan 1 compared to similar ROIs in healthy volunteers ($p=0.001$), but increased over time to values similar to those of healthy volunteers. No significant correlations between initial ^{123}I -CLINDE binding and clinical test scores found. However, the initial overlap percentage of the T2-weighted lesion ROI and the ^{123}I -CLINDE lesion ROI correlated negatively with the volume of lesion necrosis on structural MRI at scan 3 ($p=0.030$).

Conclusions

This study shows a remarkable intersubject variation in the spatial and temporal pattern of neuroinflammation in patients after a MCA stroke with cortical involvement. TSPO expression in periinfarct or remote areas to the stroke did not correlate with clinical test scores. This implies

that TSPO expression after stroke is multifaceted and cannot be attributed to either neuroprotective or detrimental effects of neuroinflammation.

Initial TSPO levels were lower in regions unrelated to the stroke when compared to healthy subjects and normalized after 4 months, which may be an effect of anti-inflammatory cytokine release or stroke induced immunomodulation.

Introduction

Ischaemic stroke remains a leading cause of acquired disability and a source of increasing disease burden worldwide despite thrombolytic therapy and novel treatment strategies, such as acute mechanical thrombectomy of occluded cerebral vessels ('WHO | The Atlas of Heart Disease and Stroke'; Berkhemer *et al.*, 2015). In the weeks and months following an ischemic stroke, rehabilitation treatment focus solely on stroke care, physio- and occupational therapy in order to improve outcome. No medical treatment has proved effective to enhance functional recovery of cerebral stroke patients during the rehabilitation period. Additional research in the cellular and functional changes of the recovering brain is warranted.

Upon brain damage, such as after stroke, microglia in the brain may transform from a 'resting' ramified phenotype into a 'reactive' state and move to the site of the lesion (Davalos *et al.*, 2005). Reactive microglia together with invading blood borne macrophages may have detrimental effects on patient recovery because of excessive collateral damage to healthy tissue (Huang *et al.*, 2013), but also has the potential to augment functional recovery by suppressing inflammation and facilitate neurogenesis (Cherry *et al.*, 2014). Glial reactivity after brain injury may be investigated by molecular imaging of the 18 kDa translocator protein (TSPO), which has been applied in both experimental stroke models and, to a limited extent, in human stroke patients (Boutin and Pinborg, 2015). The largest previous study in human stroke by Thiel *et al.* (2010) included 16 patients with subcortical stroke scanned longitudinally within the first 3 weeks and at 6 months follow-up with ^{11}C -PK11195 positron emission tomography (PET) and diffusion tensor MRI (DTI). The study established a correlation between pyramidal tract damage quantified with DTI and increased ^{11}C -PK11195 uptake in the brainstem at 6 months follow up (Thiel *et al.*, 2010). A study by Gerhard *et al.* (2005) found increased expression of TSPO in connected ipsilesional areas and the contralesional thalamus at 150 days after stroke onset. Furthermore, when controlling for pyramidal tract damage a negative partial correlation was discovered between initial ^{11}C -PK11195 uptake in the brainstem and follow-up motor function

as evaluated by the Rivermead Motor Function Test. It has been hypothesised that TSPO upregulation in areas connected to the lesion can show effects of Wallerian degeneration but also in reactive microglia with beneficial properties for stroke rehabilitation (Boutin and Pinborg, 2015).

^{123}I -CLINDE is a second generation TSPO tracer for single photon computed tomography (SPECT) imaging and has previously been used in human studies with stroke, glioblastoma multiforme and anti N-methyl-D-aspartate receptor encephalitis (Feng *et al.*, 2014; Jensen *et al.*, 2015; 2015b). Recently, the ^{123}I -CLINDE SPECT modality has been validated in a test-retest study showing similar test-retest variability as the two second-generation TSPO PET tracers ^{11}C -PBR28 and ^{11}C -DPA713 (Feng *et al.*, 2016). ^{123}I -CLINDE is a second generation TSPO tracer and therefore susceptible to the rs6971 polymorphism which affects the affinity of tracer to TSPO (Owen *et al.*, 2012).

The aim of the current study was to accurately describe the temporal and spatial development in TSPO expression from 2 to 18 weeks in MCA stroke patients with cortical involvement and relate finding to clinical test scores.

We hypothesize:

- Increased perilesional binding of ^{123}I -CLINDE to TSPO at 1-2 weeks is a biomarker of poor recovery at 25-26 weeks.
- Increased binding of ^{123}I -CLINDE to TSPO in the ipsilesional thalamus and pons at 1-2 weeks is a biomarker of poor recovery at 25-26 weeks.
- Increased binding of ^{123}I -CLINDE to TSPO in the contralesional thalamus at 5-6 weeks is a biomarker of good recovery at 25-26 weeks.

Materials and methods

Patients, healthy volunteers and genotyping

This study was conducted in accordance with the Declaration of Helsinki at the Copenhagen University Hospital, Rigshospitalet, Denmark. The ethical committee of the Copenhagen Capital Region (H-2-2010-086 amendment 39319) approved the study protocol. All subjects provided written informed consent. Patients were recruited from Bispebjerg hospital and Rigshospitalet, Copenhagen University hospital, Denmark. Twelve stroke patients with first-ever infarction in the MCA territory, a lesion involving cortical brain tissue and impairment of the contralesional

upper extremity were included within the first week after onset. Patients were scanned longitudinally three times at 1-2, 5-6 and 15-18 weeks after stroke onset with concomitant ^{123}I -CLINDE SPECT and structural MRI. Table 1 shows the patient data and Figure 1 shows the study design. All subjects were genotyped for the rs6971 polymorphism to determine TSPO binder-status as described previously (Feng *et al.*, 2014) revealing 10 HABs and 2 mixed MAB. Accordingly, a cohort of healthy volunteers was genotyped and 10 healthy volunteers with the HAB genotype were included in the study and ^{123}I -CLINDE SPECT and structural MRI scanned once. All healthy volunteers had normal physical and neurological examinations, and blood tests. Table 2 shows the healthy volunteer data.

Image acquisition and arterial blood sampling

^{123}I CLINDE-SPECT scanning

To block thyroidal uptake of free radioiodine, 200 mg of potassium perchlorate was administered intravenously 20 min before injection of ^{123}I -CLINDE. A headband was applied to minimize head movements during scanning. Dynamic SPECT scanning with a triple-head IRIX camera (Philips Medical) was started simultaneously with a bolus injection of ^{123}I -CLINDE (MAP Medical Technologies), and lasted for 90 minutes. The acquisition protocol consisted of 10 x 2-minute frames, followed by 7 x 10-minute frames.

Blood sampling

Blood samples were drawn manually from a cannula inserted into the radial artery arterial at 0.25, 0.5, 0.75, 1, 1.5, 2, 2.5, 3, 4, 6, 8, 10, 12, 15, 20, 25, 30, 35, 45, 65 and 85 min for measuring radioactivity in plasma and whole-blood. Additionally, 8 blood samples were drawn at 0.5, 4, 10, 20, 30, 45, 65 and 85 min for metabolite analysis by radio-high performance liquid chromatography (radio-HPLC). Fractions of HPLC eluent were collected using a fraction collector device (Foxy Jr FC144, Teledyne Isco) and counted off-line in a well-counter (2480 Wizard2 Gamma Counter, Perkin Elmer) for accurate measurements of parent tracer. During the study we discovered that the handling of blood-samples affects the test-retest variance (Feng *et al.*, 2016) and due to this, the time between sampling and centrifugation was changed from within 90 minutes to 5 minutes. Subject specific details on the centrifugation can be found in Table 1 for patients, all blood samples from healthy volunteers were centrifuged immediately. Total radioactivity in plasma and whole-blood was measured in a well-counter (Cobra 5003; Packard Instruments) and data were decay-corrected to the time of injection. Furthermore, the radioligand *purity* was measured for each batch of ^{123}I -CLINDE, and trapping efficiency of the

HPLC column (*plasma control*) was determined twice for each blood sample batch by spiking water and blank plasma with ^{123}I -CLINDE. All equipment was cross-calibrated to the SPECT scanner. Blood screening including white blood cell differential count was performed at each scan session.

Structural MRI

Three-dimensional T1- and T2-weighted magnetic resonance images (MRI) were acquired within 24 hours of the corresponding [^{123}I]CLINDE-SPECT for patients and healthy volunteers. Voxel-size was 1x1x1 mm for both T1 and T2 images. MRI was performed using a 3-T Prisma scanner (Siemens, Erlangen). A trained neurologist interpreted the structural MRI scans from all healthy volunteers to be normal.

Image analysis

Image pre-processing and regions of interest

For each subject, the T1- and T2-weighted MRIs were co-registered to the time-weighted mean SPECT image by interactive image overlay (Willendrup *et al.*, 2004). Regions of interest (ROIs) were delineated both automatically and manually. Automatic ROI delineation was performed on both patients and HC's using probability maps using a data processing pipeline as described previously (Svarer *et al.*, 2005). Automatically delineated ROIs were defined according to the side of the lesion for the individual patients and labelled as either ipsi- or peri-lesional. Five automatically delineated ROIs were investigated in this study: Ipsilesional cerebellum, contralesional occipital cortex, ipsilesional thalamus, contralesional thalamus and pons. Regions connected to the lesion was defined as: Ipsi- and contralesional thalamus and pons. Regions unrelated to the lesion was defined as: Ipsilesional cerebellum and contralesional occipital cortex. Stroke lesion ROIs were manually delineated on the MRI and SPECT images acquired at the first time point. Structural T2-weighted lesion ROIs were delineated around the area of the stroke, shown as the high intensity voxels on T2-weighted structural MRIs. Further, a SPECT lesion ROI was delineated on the SPECT image by automatically selecting voxels in the vicinity of the stroke with a value above 1.5 times the mean cerebellar ^{123}I -CLINDE uptake. Finally, a perilesional SPECT ROI was defined by subtracting the manually delineated T2-weighted lesion ROIs from the SPECT lesion ROI. Regions of lesion necrosis were manually delineated at the boundary of the region which shows loss of T1-weighted MRI signal at scan 3. Volume sizes of manually delineated ROIs and the overlap between SPECT and MRI regions were estimated.

The ipsilesional cerebellum ROI for patient no. 10 and the cerebellum ROI for healthy volunteer no. 3 were excluded due to the SPECT recording not encompassing total cerebellum.

See Figure 2 for examples of the T2-weighted and SPECT lesion ROIs. Due to the limited spatial resolution of SPECT images, no segmentation of grey matter, white matter and cerebrospinal fluid was attempted. All pre-processing was performed using Matlab R2013a (Mathworks Inc.).

Kinetic modelling

Parent fraction (PF) curves were adjusted to account for the tracer trapped in the HPLC as:

$$PF_{\text{adj}} = PF \times (1 + \text{purity} - \text{plasma control}).$$

PF measurements were lost due to failure of the HPLC apparatus at scan 3 of patient 11 and scan 2 of patient 12. In these two occasions, The $PF_{\text{adj_mean}}$ was estimates as the mean of the two remaining PF_{adj} curves.

^{123}I -CLINDE binding was quantified as distribution volume (V_T) by a two-tissue compartment model (rate constants: K_1 , k_2 , k_3 and k_4 , with a fixed blood volume in brain tissue of 5%) as described in (Feng *et al.*, 2016). Kinetic modelling was done using PMOD 3.0 (PMOD Technologies Inc., Switzerland).

Clinical evaluation

At each scan and clinical follow-up, patients were evaluated under supervision by a trained neurologist performing a battery of rehabilitation measures (Figure 1). Stroke severity and functional status were assessed by National Institute of Health Stroke Scale (NIHSS), Scandinavian Stroke Scale (SSS), Fugl-Meyer Assessment of the Upper Extremity (FMA-UE), Motricity Index (MI), Action Research Arm Test (ARAT), Nine-Hole Peg Test (NHPT), Grip strength (GS), Modified Ranking Scale (MRS) and Barthel Index (BI). NHPT and GP was measured for both affected and non-affected extremity three times and the mean fraction of the affected vs. non-affected extremity was calculated. Recovery was calculated for each measure as the PD between scan 1 and 25 week follow-up.

Statistical analysis

Data are presented as medians [1st quartile; 3rd quartile] for continuous variables and percentage for categorical variables.

To investigate whether TSPO expression in stroke patients changed over time, we compared regional V_T at the three time points. However, due to the disparity in affinity of ^{123}I -CLINDE to TSPO between HAB and MAB, two separate analyses were performed. In the first analysis, we disregarded the two MAB patients and performed repeated measures ANOVAs on the group of the remaining ten HAB patients, with separate models for each ROI. The magnitude of the change over time was additionally quantified by estimating the relative percentage differences (PD) between scan 1 and scan 3, computed as:

$$PD_{V_T} = \frac{\text{mean } V_{T \text{ scan } 3} - \text{mean } V_{T \text{ scan } 1}}{\text{mean } V_{T \text{ scan } 1}} \times 100\%$$

Where the mean V_T is mean value for all subjects.

In the second analysis, to include the total patient cohort of HABs and MABs, we computed the PD between scan 1 and 3 as above, for all twelve patients, and performed a two-sided one-sample t-test.

To explore the association between TSPO and other experimental variables, we performed Pearson correlations for the following experimental variables:

- To compare TSPO expression to clinical outcome, the regional V_T at scan 1 (lesion, perilesional, ipsi- and contralesional thalamus, and pons) was correlated to PD of rehabilitation measures between scan 1 and the 25-26 week follow-up.
- The same correlation was done for the regional V_T at scan 2 and the PD of rehabilitation measures between scan 2 and the 25-26 week follow-up.
- To explore the finding from experimental studies that TSPO is expressed predominantly perilesionally in permanent ischemia in our data, the percentage overlap between the ^{123}I -CLINDE lesion and the T2-lesion at scan 1 was correlated to the percentage atrophy of the T2-lesion at scan 3 and also correlated to the PD of rehabilitation measures between scan 1 and follow-up.

To investigate the impact of stroke on brain regions that was unrelated to the stroke lesion, V_T of ipsilesional cerebellum and contralesional occipital cortex for stroke patients at scan 1,2 and 3 were compared to the V_{TS} of cerebellum and occipital cortex in healthy volunteers using Mann-Whitney U tests.

Repeated measure ANOVA, t-test, pearson correlation, and Mann-Whitney U tests were performed using Prism 6.0c (Graphpad Software Inc.). Percentage difference was calculated using Matlab (Mathworks inc).

RESULTS

The clinical characteristics of the stroke patients and healthy volunteers are summarized in Table 1 and 2. Descriptive statistics are given in table 3.

In general, the TSPO expression showed massive variance. This was evident for the initial scans where the size and intensity of the CLINDE uptake was very different for the patients.

Furthermore, the heterogeneity in change in expression between scan 1, 2 and 3 was generally sizeable. See figure 3 for a visual comparison of all patients.

Lesional and perilesional TSPO expression in stroke patients

The repeated measures ANOVA showed a significant decrease in lesional V_T for the HAB patients over the three scans ($p=0.004$) and a trend towards a perilesional decrease ($p=0.07$). Distribution volumes for HAB stroke patients at scan 1,2 and 3 were 10.5 ± 2.3 , 8.16 ± 2.0 and 6.9 ± 1.2 mL/cm³, respectively. This corresponds to a relative decrease between scans 1 and 3 of 34.7%. Performing a two tailed t-test on the PD from scan 1 to 3 of lesional and perilesional V_T on all 12 patients revealed a significant mean decrease of 22.6 % lesionally ($p=0.04$) and 21.3 % perilesionally ($p=0.001$). The temporal evolution of lesional and perilesional ¹²³I-CLINDE uptake is visualised on ¹²³I-CLINDE SPECT images in Figure 2 and 3.

Correlations between TSPO expression, atrophy and clinical outcome measures

We did not find any correlations between V_T of ¹²³I-CLINDE lesionally, perilesionally, pons or ipsi- and contralesional thalamus at scan 1 or 2 and the recovery in rehabilitation measures. See figure 5 for a Pearson correlation plot between V_{TS} of ¹²³I-CLINDE and recovery.

A negative correlation was found between the percentage overlap of SPECT and T2-weighted structural lesion at scan 1 and the volume of lesion necrosis at scan 3 ($p=0.001$).

TSPO expression in ROIs unrelated to the lesion

Comparing ^{123}I -CLINDE binding in ipsilesional cerebellum and the perilesional occipital cortex of 10 HAB stroke patients to the occipital cortex of 10 HAB healthy volunteers by Mann-Whitney U test revealed that stroke patients had significantly lower TSPO expression at scan 1 ($p=0.001$ and $p=0.002$). However, no significant differences were found for scan 2 ($p=0.11$ and $p=0.52$) and scan 3 ($p=0.45$ and $p=0.31$). Between scan 1 and 3, the mean V_T in the ipsilesional cerebellum and the perilesional occipital cortex significantly increased by 72.3% and 51.4% ($p=0.01$ and $p=0.002$) for the HAB patients, respectively. Results are presented graphically in Figure 4 C and D.

DISCUSSION

TSPO evolution after stroke and TSPO as a biomarker of recovery

This study shows that the TSPO expression after stroke is a particularly dynamical and heterogeneous process. In human stroke, eleven previous publications have reported on TSPO expression after stroke (Ramsay *et al.*, 1992; Gerhard *et al.*, 2000, 2005; Pappata *et al.*, 2000; Price, 2006; Radlinska *et al.*, 2009; Thiel *et al.*, 2010; Gulyas *et al.*, 2012; Gulyás *et al.*, 2012; Feng *et al.*, 2014; Ribeiro *et al.*, 2014). Five of these studies have included longitudinal TSPO imaging in a total of 25 stroke patients (Boutin and Pinborg, 2015), reporting negligible TSPO upregulation in the first 72 hours after stroke in the lesional and perilesional areas, followed by a significant increase at day 5 (Price, 2006). A further increase was observed in the lesioned hemisphere at day 13-20 and at later time points, between 3-4 weeks and 6-8 months, TSPO levels have been demonstrated to decrease at the lesion site (Ramsay *et al.*, 1992). The current is in agreement with previous findings as it shows initial high TSPO expression lesionally and perilesionally between 1-2 weeks after stroke and a gradual decrease at 3-4 weeks and 15-18 weeks. However, it is also very apparent that the initial increase in TSPO expression is very heterogeneous in both intensity and size and that the heterogeneity of the TSPO expression prevails throughout the entire study period (Figure 2 and 3).

Prior to the initiation of this study, we hypothesized that the initial perilesional TSPO expression would be a biomarker of poor recovery and that the initial TSPO expression in ROIs connected to the lesion would be a biomarker of good recovery. In our study we found no correlation between the binding of ^{123}I -CLINDE to TSPO in the examined ROIs at scan 1 and recovery in

the follow-up clinical test scales. An explanation for this negative finding may be that the TSPO expression after human stroke is complex and cannot be directly associated to functional recovery because that it reflects a combination of pro- and anti-inflammatory properties in the glia and macrophages with upregulated TSPO. A tracer with selectivity to the pro-inflammatory or anti-inflammatory properties of glia would be advantageous in this case, however, such tracer does not currently exist.

Another explanation may be ceiling and floor effects of rehabilitation measures which are commonly known issues when studying stroke recovery, especially for minor to moderate strokes (Lindemann *et al.*, 2012). These effects can potentially hamper the measurement of clinical progress and thus bias the results.

TSPO expression in MCA stroke compared to healthy volunteers

To our knowledge, this is the first study to show low TSPO expression in non-stroke related areas in the subacute phase after stroke in man, followed by a longitudinal TSPO normalization of TSPO expression as compared to healthy volunteers.

Several possible biological hypotheses can be made for this finding.

Reactive microglia and macrophages release pro-inflammatory and anti-inflammatory cytokines like IL-10, TGF β and IGF (Patel *et al.*, 2013), however, the spatial distribution in the brain of these cytokines in relation to stroke are not well known. It may be that anti-inflammatory cytokines are expressed more predominantly than pro-inflammatory cytokines in regions remote to the lesion. Post stroke immunomodulation is a known phenomenon occurring after stroke and is increase susceptibility to infections (Samary *et al.*, 2016).

Another explanation for initial low TSPO expression in ROIs unrelated to the lesion compared to healthy volunteers, is that the microglial cells could have redistributed within the brain and migrated to the site of the lesion (Kettenmann *et al.*, 2011). However, TSPO is not expressed to a large extent in resting microglia cells, and would not contribute markedly to the background TSPO signal in healthy brain (Chen and Guilarte, 2008).

This finding infers that one should be very careful with using a supposedly non-affected brain region (eg. cerebellum or unaffected hemisphere) as a reference for quantification of the TSPO expression. Nearly 30% of stroke patients develop depression in the initial weeks after stroke onset (Paolucci, 2008). An interesting biological mechanism for future study may be the link between decreased TSPO expression after stroke and post stroke depression.

TSPO expression and lesion necrosis

A negative correlation between percentage overlap of SPECT and structural lesion delineated on T2 weighted MRI at scan 1 and the volume of lesion necrosis at scan 3 was discovered. This corresponds to previous findings in animal studies where TSPO is expressed primarily lesionally in transient ischemia whereas in cases of permanent ischemia, TSPO expression occurs predominantly in the outer infarct margins and peri-lesional areas and to a lesser extent in the infarct core (Boutin and Pinborg, 2015).

Limitations

The groups of healthy volunteers and stroke patients are not matched by age with a median patient age of 61 and a median healthy volunteer age of 34. Previously, TSPO imaging with ^{11}C -PK11195 has demonstrated increasing TSPO expression with age in a cohort of 25 healthy subjects including 10 children (Kumar *et al.*, 2012). An age-related increase in TSPO expression would cause a smaller difference between stroke patients and healthy volunteers in the case of the current study where the volunteer group is younger than the patient group. Two of the patients had delayed centrifugation of blood samples. This will possibly cause an overestimation of V_T due to an under-estimation of the plasma parent compound as previously described (Feng *et al.*, 2016). However, this issue would not accentuate the difference between patients and healthy volunteers as all blood samples for healthy volunteers were centrifuged immediately. Hence, the actual decrease in non-affected brain regions of stroke patients is likely lower than what the current results show.

CONCLUSION

In conclusion, the current study shows that the TSPO expression is an remarkably temporally and spatially dynamic and complex process but not a useable biomarker for functional recovery after stroke. TSPO expression in regions unrelated to the stroke are reduced two weeks after stroke compared to similar regions in healthy volunteers and normalizes within the first 4 months. This may be a proxy to the peripheral immunomodulation known to occur after ischemic stroke or the release of anti-inflammatory cytokines from glial cells in the lesional region.

DISCLOSURES

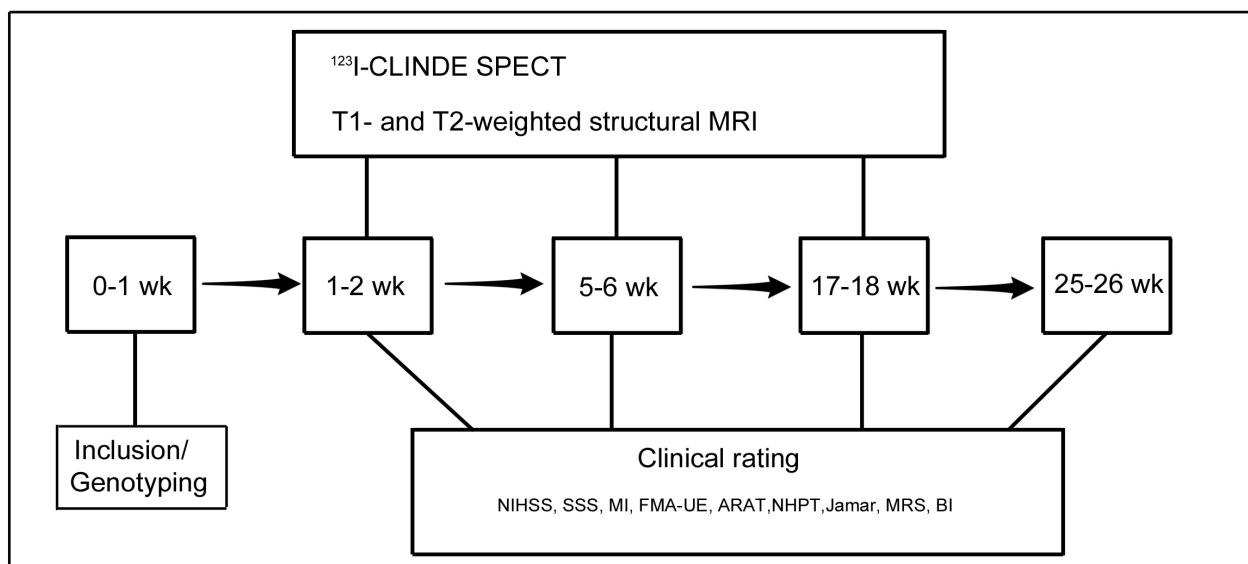
This work was financially supported by the European Union's Seventh Framework Programme (FP7/2007-2013) under grant agreement n° HEALTH-F2-2011-278850 (INMiND), the Danish Council for independent Research, the Research Committee of Rigshospitalet, and Savværksejer Jeppe Juhl og hustru Ovita Juhls Mindelegat.

ACKNOWLEDGEMENTS

We acknowledge Svitlana Olsen and Glenna Skouboe for technical assistance.

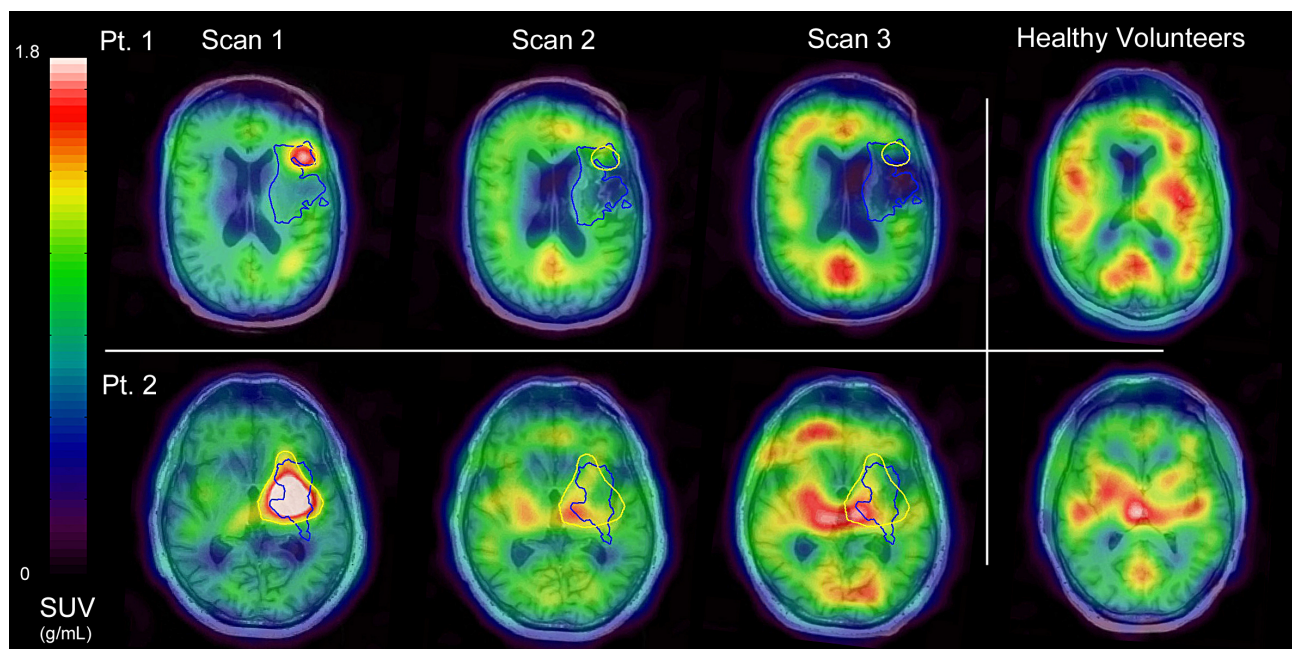
Figures and Tables

Figure 1. Study design



Patients were recruited and genotyped for the rs6971 polymorphism in the first days after stroke. Scanning with ¹²³I-CLINDE SPECT was performed at 1-2, 5-6, and 17-18 weeks after stroke. Clinical rating was performed at scan days and at follow-up 25-26 weeks after stroke. The scanning of healthy volunteers is not included in this figure. Abbreviations: Wk: Week NIHSS: National Institute of health stroke scale, MI: Motricity index, FMA-UE: Fughl-Meyer assessment

Figure 2. ^{123}I -CLINDE SPECT and structural MRI in stroke patients



T1-weighted MRI overlaid by ^{123}I -CLINDE SPECT in patient no. 1 (HAB) and 2 (HAB) scanned longitudinally three times after left MCA stroke and compared to two healthy HAB volunteers. For each row, scan 2, 3 and the healthy volunteer scan were coregistered to scan 1. All SPECT images were normalised by bodyweight and injected ^{123}I -CLINDE dose. Yellow ROIs depict the lesional SPECT upregulation and blue ROIs depict the structural lesion delineated on T2-weighted MRI (not shown) on scan 1.

Both patients demonstrated low TSPO expression in cortical regions not related to the stroke at scan 1, gradually increasing towards healthy control intensities at scan 3.

Pt. 1 demonstrated a small volume of TSPO upregulation in the infarct margin at scan 1 and the predominant part of the lesion was necrotized at scan 3, probably as a result of permanent ischemia. Pt. 2 demonstrated high lesional and perilesional TSPO expression at scan 1, and only a small part of the lesion was necrotized at scan 3, possibly as a result of better perfusion of the lesional area.

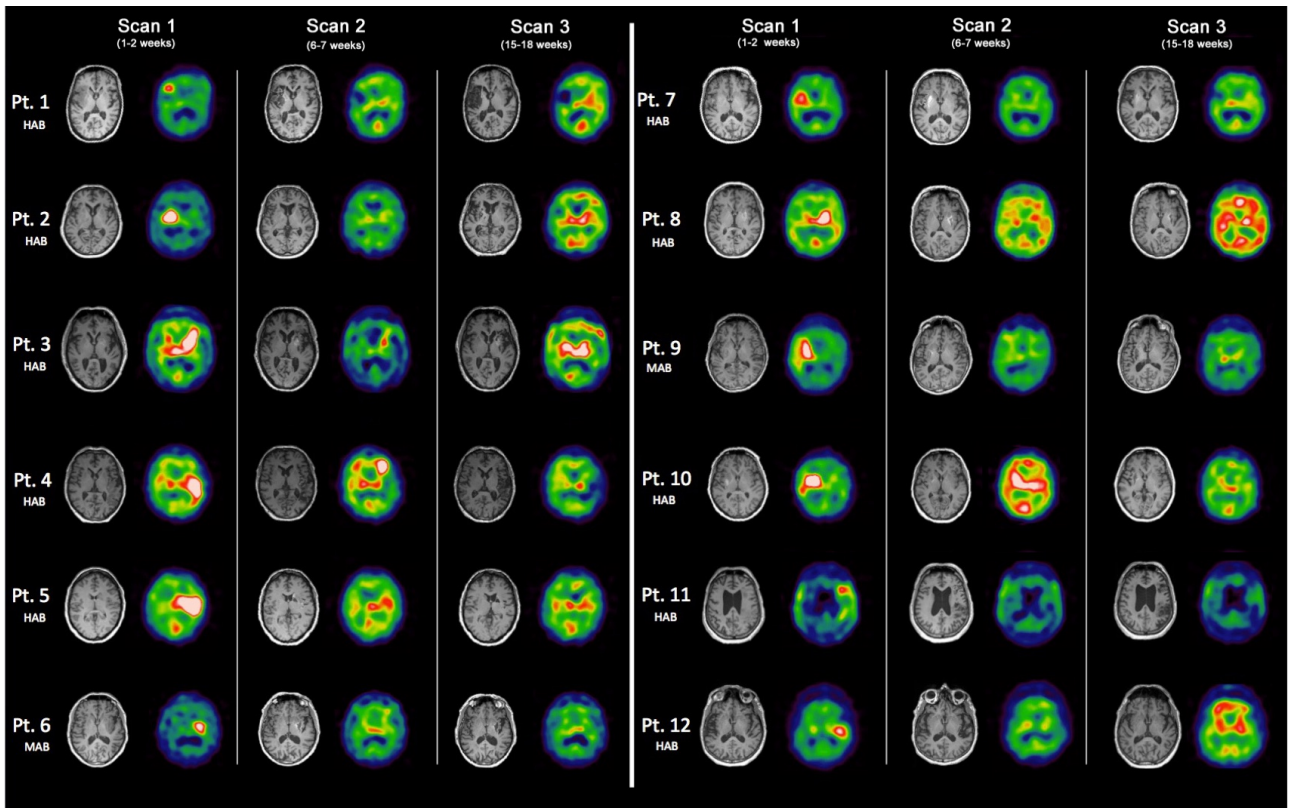
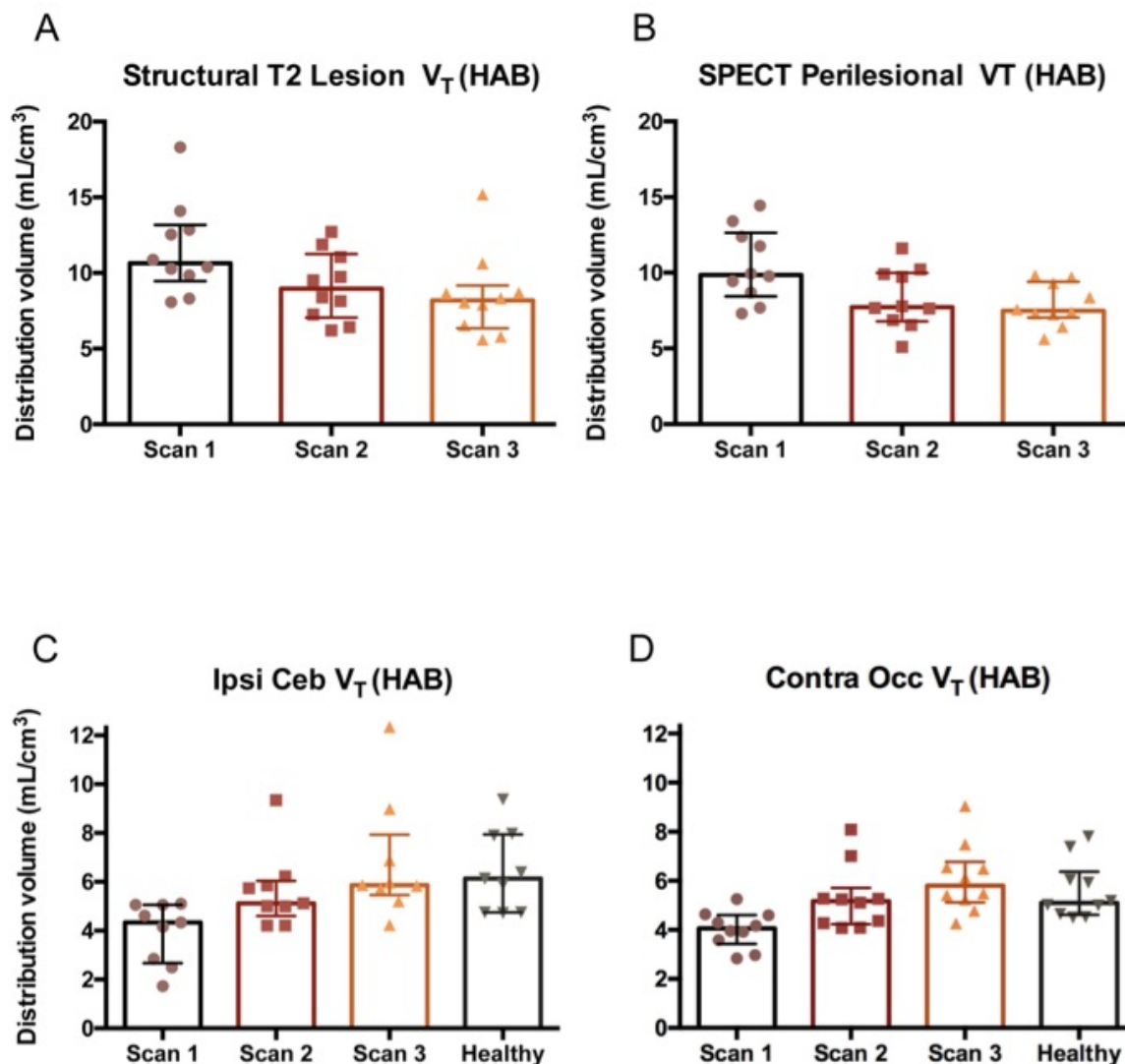


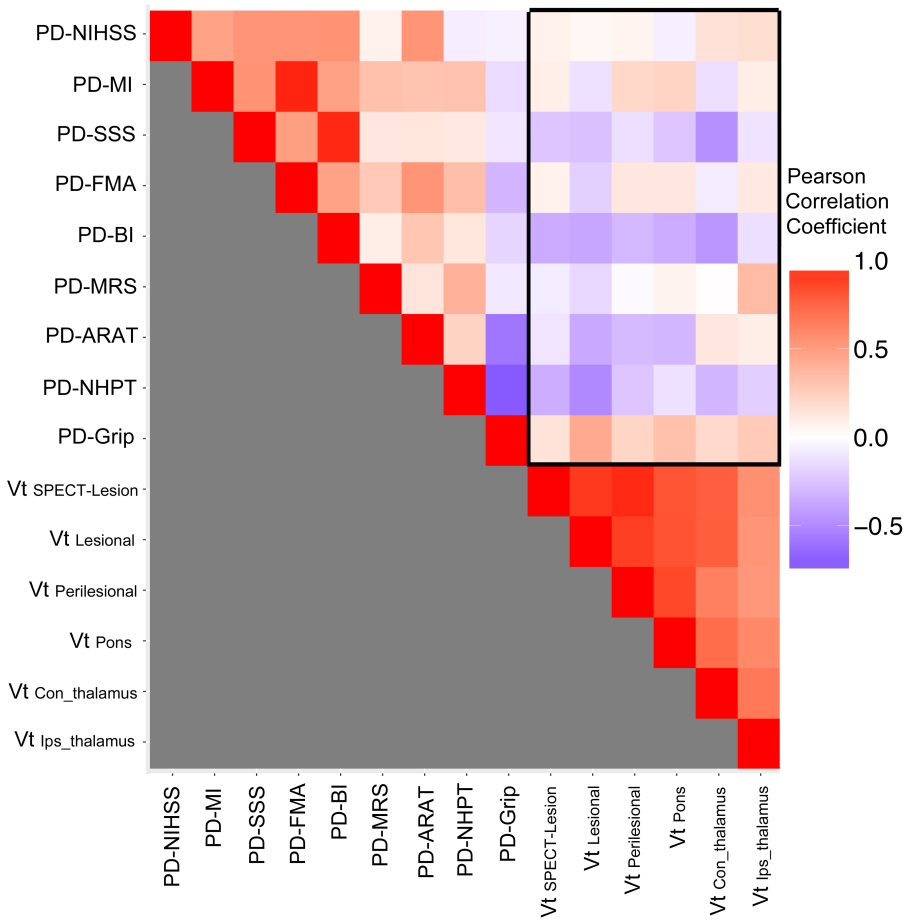
Figure 3. T1-Weighted MRI and ^{123}I -CLINDE SPECT comparison of all patients. For each patient, the ^{123}I -CLINDE SPECT is normalised by weight and injected ^{123}I -CLINDE dose.

Figure 4. Evolution of TSPO expression and comparison to healthy volunteers



An illustration of V_T 's in ten HAB patients and ten HAB healthy volunteers. Columns represent median values and brackets span the interquartile range. Longitudinally, V_T 's decreased in the structural lesion delineated on T2-weighted MRI (A) and in the perilesional SPECT ROI (B). In brain regions unrelated to the stroke V_T 's in patients were lower than for healthy volunteers at scan 1 and increased towards normal values at scan 3 for the ipsilesional cerebellum (C) and contralesional occipital cortex (D).

Figure 5. Pearson correlation coefficient plot



Pearson correlation coefficient plot between the ROI V_T 's at 1-2 weeks after stroke and the PD of rehabilitation measures between 1-2 weeks and 24-25 weeks. No correlation was significant. Abbreviations: Percentage difference (PD), National Institutes of Health Stroke Scale (NIHSS), Scandinavian Stroke Scale (SSS), Fugl-Meyer Assessment of the Upper Extremity (FMA-UE), Motricity Index (MI), Action Research Arm Test (ARAT), Nine-Hole Peg Test (NHPT), Grip strength (Grip), Modified Ranking Scale (MRS) and Barthel Index (BI).

Table 1. Patients

Patient no.	Days after stroke	Gender	Age at inclusion (Years)	lesion side / Artery	Etiology	TSPO Genotype	Injected activity (MBq)	Centrifugation
Pt. 1	10 38 101	F	52	Left MCA	ICA dissection (Trauma)	HAB	108.9 113.4 103.1	Delayed Delayed Delayed
Pt. 2	10 46 157	M	63	Left MCA	ICA dissection - (HT)	HAB	112.3 102.5 117.5	Delayed Delayed Immediate
Pt. 3	12 40 130	M	57	Left MCA	Thrombo-embolism (HC)	HAB	135.7 114.8 126.8	Immediate Immediate Immediate
Pt. 4	15 43 139	M	60	Left MCA	Thrombo-embolism (HT+HC)	HAB	110.9 115.9 128.3	Immediate Immediate Immediate
Pt. 5	11 39 131	F	42	Right MCA	Thrombo-embolism (Contraception)	HAB	127.3 114.7 108.9	Immediate Immediate Immediate
Pt. 6	9 35 135	M	68	Right MCA	ICA dissection - (HC)	MAB	121.5 123.2 113.0	Immediate Immediate Immediate
Pt. 7	7 41 126	F	72	Right MCA	Thrombo-embolism (AF)	HAB	118.9 117.7 108.3	Immediate Immediate Immediate
Pt. 8	13 41 125	F	68	Right MCA	Thrombo-embolism - (HC+HT)	HAB	117.8 122.1 103.2	Immediate Immediate Immediate
Pt. 9	10 37 121	F	59	Left MCA	Thrombo-embolism (HC)	MAB	137.0 117.4 122.1	Immediate Immediate Immediate
Pt. 10	13 41 132	F	55	Right MCA	ICA dissection - (HT)	HAB	123.7 130.5 111.3	Immediate Immediate Immediate
Pt. 11	10 38 122	M	61	Left MCA	Thrombo-embolism (HT)	HAB	113.6 112.8 114.4	Immediate Immediate Immediate
Pt. 12	10 44 122	M	62	Right MCA	Thrombo-embolism (AF)	HAB	117.6 124.9 109.9	Immediate Immediate Immediate

Demographic data for the stroke patients. Abbreviations Pt: Patient, MCA: Middle cerebral artery, HT: Hypertension, HC: Hypercholesterolemia, AF: Atrial fibrillation, HAB: High affinity binder, MAB: Mixed affinity binder.

Table 2. Healthy volunteers

Volunteer no.	Gender	Age at inclusion (Years)	Injected activity (MBq)
HV 1	M	49	124.9
HV 2	M	36	119.9
HV 3	F	48	104.5
HV 4	M	25	112.5
HV 5	F	34	115.3
HV 6	F	44	116.2
HV 7	F	30	105.8
HV 8	F	34	118.4
HV 9	F	24	128.2
HV 10	F	21	120.9

Healthy volunteer data: Gender, age and injected activity for the healthy volunteers.

Table 3. Descriptive data

Descriptive statistics	Unit	Median	Quartiles [1st;3rd]	Range
Patient age	Years	60.7	[55.9;66.7]	[41.7;71.7]
Healthy volunteer age	Years	33.6	[24.3;45.5]	[21.4;49.0]
NIHSS at stroke onset	Points	17.5	[13.3;19.8]	[8;22]
NIHSS at scan 1	Points	6.5	[4.3;10.0]	[1;12]
NIHSS at follow-up	Points	1.5	[1.0;4.5]	[0;5]
T2 lesion volume at scan 1	mL	40.5	[25.1;63.8]	[17.5;76.1]
T1 necrosis volume at scan 3	mL	4.7	[3.1;15.9]	[2.0;50.8]
Overlap: SPECT Lesion/ T2 Lesion	%	68.8	[51.6;80.0]	[6.4;90.4]
V _T lesional scan 1 (HAB)	mL/cm ³	10.2	[8.6;12.6]	[7.5;15.0]
V _T lesional scan 2 (HAB)	mL/cm ³	8.0	[6.3;10.5]	[5.4;11.0]
V _T Lesional scan 3 (HAB)	mL/cm ³	7.1	[6.2;7.8]	[4.6;8.5]
V _T Con Occ cortex scan 1 (HAB)	mL/cm ³	4.1	[3.4;4.6]	[2.8;5.3]
V _T Con Occ cortex scan 2 (HAB)	mL/cm ³	5.2	[4.2;5.7]	[4.1;8.1]
V _T Con Occ cortex scan 3 (HAB)	mL/cm ³	5.8	[5.1;6.8]	[4.3;9.1]
V _T Occ cortex (healthy volunteers) (HAB)	mL/cm ³	5.1	[4.6;6.4]	[4.5;7.8]

Descriptive data for stroke patients and the healthy volunteers.

References

- Berkhemer OA, Fransen PSS, Beumer D, van den Berg LA, Lingsma HF, Yoo AJ, et al. A randomized trial of intraarterial treatment for acute ischemic stroke. *N. Engl. J. Med.* 2015; 372: 11–20.
- Boutin H, Pinborg LH. TSPO imaging in stroke: from animal models to human subjects. *Clin. Transl. Imaging* 2015: 1–13.
- Chen M-K, Guilarte TR. Translocator protein 18 kDa (TSPO): Molecular sensor of brain injury and repair. *Pharmacol. Ther.* 2008; 118: 1–17.
- Cherry JD, Olschowka JA, O'Banion MK. Neuroinflammation and M2 microglia: the good, the bad, and the inflamed. *J Neuroinflammation* 2014; 11: 98.
- Davalos D, Grutzendler J, Yang G, Kim JV, Zuo Y, Jung S, et al. ATP mediates rapid microglial response to local brain injury in vivo. *Nat. Neurosci.* 2005; 8: 752–758.
- Feng L, Jensen P, Thomsen G, Dyssegaard A, Svarer C, Knudsen LV, et al. The variability of translocator protein signal in brain and blood of genotyped healthy humans using in vivo 123I-CLINDE SPECT imaging – a test-retest study. *J. Nucl. Med.* 2016: jnumed.116.183202.
- Feng L, Svarer C, Thomsen G, de Nijs R, Larsen VA, Jensen P, et al. In Vivo Quantification of Cerebral Translocator Protein Binding in Humans Using 6-Chloro-2-(4'-123I-Iodophenyl)-3-(N,N-Diethyl)-Imidazo[1,2-a]Pyridine-3-Acetamide SPECT [Internet]. *J. Nucl. Med.* 2014[cited 2014 Nov 21] Available from: <http://jnm.snmjournals.org/cgi/doi/10.2967/jnumed.114.143727>
- Gerhard A, Neumaier B, Elitok E, Glatting G, Ries V, Tomczak R, et al. In vivo imaging of activated microglia using [11C]PK11195 and positron emission tomography in patients after ischemic stroke. *Neuroreport* 2000; 11: 2957–2960.
- Gerhard A, Schwarz J, Myers R, Wise R, Banati RB. Evolution of microglial activation in patients after ischemic stroke: a [11C](R)-PK11195 PET study. *NeuroImage* 2005; 24: 591–595.
- Gulyás B, Tóth M, Schain M, Airaksinen A, Vas Á, Kostulas K, et al. Evolution of microglial activation in ischaemic core and peri-infarct regions after stroke: A PET study with the TSPO molecular imaging biomarker [11C]vinpocetine. *J. Neurol. Sci.* 2012; 320: 110–117.
- Gulyas B, Toth M, Vas A, Shchukin E, Hillert J, Halldin C. Visualising Neuroinflammation in Post-Stroke Patients: A Comparative PET Study with the TSPO Molecular Imaging Biomarkers [11C]PK11195 and [11C]vinpocetine. *Curr. Radiopharm.* 2012; 5: 19–28.
- Huang Y, Feng Z. The good and bad of microglia/macrophages: new hope in stroke therapeutics. *Acta Pharmacol. Sin.* 2013; 34: 6.
- Jensen P, Feng L, Law I, Svarer C, Knudsen GM, Mikkelsen JD, et al. TSPO imaging in glioblastoma multiforme: A direct comparison between 123ICLINDE-SPECT, 18F-FET PET and gadolinium-enhanced MRI. [Internet]. *J. Nucl. Med.* 2015[cited 2015 Sep 10] Available from: <http://jnm.snmjournals.org/cgi/doi/10.2967/jnumed.115.158998>

Jensen P, Kondziella D, Thomsen G, Dyssegaard A, Svarer C, Pinborg LH. Anti-NMDAR encephalitis: demonstration of neuroinflammation and the effect of immunotherapy. *Neurology* 2015b; 84: 859.

Kettenmann H, Hanisch U-K, Noda M, Verkhratsky A. Physiology of microglia. *Physiol. Rev.* 2011; 91: 461–553.

Kumar A, Muzik O, Shandal V, Chugani D, Chakraborty P, Chugani HT. Evaluation of age-related changes in translocator protein (TSPO) in human brain using ¹¹C-[R]-PK11195 PET. *J. Neuroinflammation* 2012; 9: 232.

Lindemann U, Jamour M, Nicolai SE, Benzinger P, Klenk J, Aminian K, et al. Physical activity of moderately impaired elderly stroke patients during rehabilitation. *Physiol. Meas.* 2012; 33: 1923–1930.

Owen DR, Yeo AJ, Gunn RN, Song K, Wadsworth G, Lewis A, et al. An 18-kDa Translocator Protein (TSPO) polymorphism explains differences in binding affinity of the PET radioligand PBR28. *J. Cereb. Blood Flow Metab.* 2012; 32: 1–5.

Paolucci S. Epidemiology and treatment of post-stroke depression. *Neuropsychiatr. Dis. Treat.* 2008; 4: 145–154.

Pappata S, Levasseur M, Gunn RN, Myers R, Crouzel C, Syrota A, et al. Thalamic microglial activation in ischemic stroke detected in vivo by PET and [¹¹C]PK1195. *Neurology* 2000; 55: 1052–1054.

Patel AR, Ritzel R, McCullough LD, Liu F. Microglia and ischemic stroke: a double-edged sword. *Int. J. Physiol. Pathophysiol. Pharmacol.* 2013; 5: 73–90.

Price CJS. Intrinsic Activated Microglia Map to the Peri-infarct Zone in the Subacute Phase of Ischemic Stroke. *Stroke* 2006; 37: 1749–1753.

Radlinska BA, Ghinani SA, Lyon P, Jolly D, Soucy J-P, Minuk J, et al. Multimodal microglia imaging of fiber tracts in acute subcortical stroke. *Ann. Neurol.* 2009; 66: 825–832.

Ramsay SC, Weiller C, Myers R, Cremer JE, Luthra SK, Lammertsma AA, et al. Monitoring by PET of macrophage accumulation in brain after ischaemic stroke. *The Lancet* 1992; 339: 1054–1055.

Ribeiro M-J, Vercouillie J, Debiais S, Cottier J-P, Bonnaud I, Camus V, et al. Could ¹⁸F-DPA-714 PET imaging be interesting to use in the early post-stroke period? *EJNMMI Res.* 2014; 4: 28.

Santos Samary C, Pelosi P, Leme Silva P, Rieken Macedo Rocco P. Immunomodulation after ischemic stroke: potential mechanisms and implications for therapy [Internet]. *Crit. Care* 2016; 20[cited 2017 Feb 12] Available from: <http://ccforum.biomedcentral.com/articles/10.1186/s13054-016-1573-1>

Svarer C, Madsen K, Hasselbalch SG, Pinborg LH, Haugbøl S, Frøkjær VG, et al. MR-based automatic delineation of volumes of interest in human brain PET images using probability maps. *NeuroImage* 2005; 24: 969–979.

Thiel A, Radlinska BA, Paquette C, Sidel M, Soucy J-P, Schirmacher R, et al. The Temporal Dynamics of Poststroke Neuroinflammation: A Longitudinal Diffusion Tensor Imaging-Guided PET Study with ¹¹C-PK11195 in Acute Subcortical Stroke. *J. Nucl. Med.* 2010; 51: 1404–1412.

Willendrup P, Pinborg LH, Hasselbalch SG, Adams KH, Stahr K, Knudsen GM, et al. Assessment of the precision in co-registration of structural MR images and PET images with localized binding. *Int. Congr. Ser.* 2004; 1265: 275–280.

WHO | The Atlas of Heart Disease and Stroke [Internet]. WHO Available from: http://www.who.int/cardiovascular_diseases/resources/atlas/en/

Declarations of co-authorship

GRADUATE SCHOOL OF HEALTH AND MEDICAL SCIENCES
UNIVERSITY OF COPENHAGEN



DECLARATION OF CO-AUTHORSHIP

Information on PhD student:	
Name of PhD student	Per Jensen
E-mail	per.jensen@nru.dk
Date of birth	08-10-1981
Work place	Neurobiology Research Unit
Principal supervisor	Lars Hageman Pinborg


Title of PhD thesis:
Translocator protein imaging with 123I-CLINDE SPECT - Method development and clinical research

This declaration concerns the following article:
Anti-NMDAR encephalitis: demonstration of neuroinflammation and the effect of immunotherapy

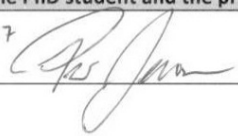
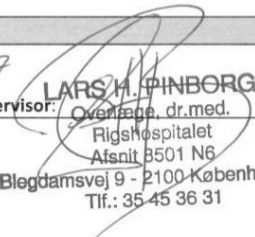
The PhD student's contribution to the article: <i>(please use the scale (A,B,C) below as benchmark*)</i>	(A,B,C)
1. Formulation/identification of the scientific problem that from theoretical questions need to be clarified. This includes a condensation of the problem to specific scientific questions that is judged to be answerable by experiments	A
2. Planning of the experiments and methodology design, including selection of methods and method development	B
3. Involvement in the experimental work	C
4. Presentation, interpretation and discussion in a journal article format of obtained data	B

*Benchmark scale of the PhD student's contribution to the article		
A. refers to:	Has contributed to the co-operation	0-33 %
B. refers to:	Has contributed considerably to the co-operation	34-66 %
C. refers to:	Has predominantly executed the work independently	67-100 %

Signature of the co-authors:			
Date:	Name:	Title:	Signature:
22/2-17	Daniel Kondziella	MD, DMSc	
15/2-2017	Gerda Thomsen	Researcher	
15/2-2017	Agnete Dyssegaard	MSc	

	Claus Svarer	Senior reseacher	
	Lars Hageman Pinborg	MD	

Signature of the PhD student and the principal supervisor:

Date: 15/2/17	Date: 15/2/17
PhD student: 	Principal supervisor: 

LARS H. PINBORG
 Overlege, dr.med.
 Rigshospitalet
 Afsnit 8501 N6
 Blegdamsvej 9 - 2100 København Ø
 Tlf.: 35 45 36 31



DECLARATION OF CO-AUTHORSHIP

Information on PhD student:	
Name of PhD student	Per Jensen
E-mail	per.jensen@nru.dk
Date of birth	08-10-1981
Work place	Neurobiology Research Unit
Principal supervisor	Lars Hageman Pinborg


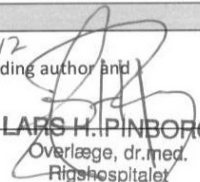
Title of PhD thesis:
Translocator protein imaging with 123I-CLINDE SPECT - Method development and clinical research

This declaration concerns the following article:
TSPO imaging in glioblastoma multiforme: A direct comparison between 123I-CLINDE-SPECT, 18F-FET PET and gadolinium-enhanced MRI (13 authors)

The PhD student's contribution to the article: <i>(please use the scale (A,B,C) below as benchmark*)</i>	(A,B,C)
1. Formulation/identification of the scientific problem that from theoretical questions need to be clarified. This includes a condensation of the problem to specific scientific questions that is judged to be answerable by experiments	C
2. Planning of the experiments and methodology design, including selection of methods and method development	B
3. Involvement in the experimental work	A
4. Presentation, interpretation and discussion in a journal article format of obtained data	C

*Benchmark scale of the PhD student's contribution to the article		
A. refers to:	Has contributed to the co-operation	0-33 %
B. refers to:	Has contributed considerably to the co-operation	34-66 %
C. refers to:	Has predominantly executed the work independently	67-100 %

Signature of the co-authors:			
Date:	Name:	Title:	Signature:

Signature of the PhD student and the principal supervisor:	
Date: 15/2-17 PhD student: 	Date: 15/2/17 Senior author, Corresponding author and Principal supervisor: 

LARS H. PINBORG
 Overlæge, dr.med.
 Rigshospitalet
 Afsnit 8501 M6
 Blegdamsvej 9 - 2100 København Ø
 Tlf.: 35 45 36 31



DECLARATION OF CO-AUTHORSHIP

Information on PhD student:	
Name of PhD student	Per Jensen
E-mail	per.jensen@nru.dk
Date of birth	08-10-1981
Work place	Neurobiology Research Unit
Principal supervisor	Lars Hageman Pinborg



Title of PhD thesis:
Translocator protein imaging with 123I-CLINDE SPECT - Method development and clinical research

This declaration concerns the following article:
The variability of translocator protein signal in brain and blood of genotyped healthy humans using in vivo 123I-CLINDE SPECT imaging – a test-retest study.

The PhD student's contribution to the article: <i>(please use the scale (A,B,C) below as benchmark*)</i>	(A,B,C)
1. Formulation/identification of the scientific problem that from theoretical questions need to be clarified. This includes a condensation of the problem to specific scientific questions that is judged to be answerable by experiments	B
2. Planning of the experiments and methodology design, including selection of methods and method development	B
3. Involvement in the experimental work	C
4. Presentation, interpretation and discussion in a journal article format of obtained data	B

*Benchmark scale of the PhD student's contribution to the article		
A. refers to:	Has contributed to the co-operation	0-33 %
B. refers to:	Has contributed considerably to the co-operation	34-66 %
C. refers to:	Has predominantly executed the work independently	67-100 %

Signature of the co-authors:			
Date:	Name:	Title:	Signature:
15/2 - 12	Ling Feng (1 st and corresponding author)	phd	

Signature of the PhD student and the principal supervisor:	
Date: 15/2 - 17	Date: 15/2/17
PhD student: 	Principal supervisor: 

LARS H. PINBORG
 Overlæge, dr.med.
 Rigshospitalet
 Afsnit 8501 N6
 Blegdamsvej 9 - 2100 København Ø
 Tlf.: 35 45 36 31



DECLARATION OF CO-AUTHORSHIP

Information on PhD student:	
Name of PhD student	Per Jensen
E-mail	per.jensen@nru.dk
Date of birth	08-10-1981
Work place	Neurobiology Research Unit
Principal supervisor	Lars Hageman Pinborg

Title of PhD thesis:
Translocator protein imaging with 123I-CLINDE SPECT - Method development and clinical research


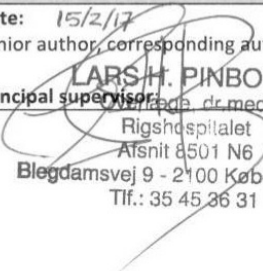
This declaration concerns the following article:
Expression, evolution and prognostic value of Translocator protein in middle cerebral artery stroke patients - A longitudinal [123I]CLINDE-SPECT imaging study (15 authors)

The PhD student's contribution to the article: <i>(please use the scale (A,B,C) below as benchmark*)</i>	(A,B,C)
1. Formulation/identification of the scientific problem that from theoretical questions need to be clarified. This includes a condensation of the problem to specific scientific questions that is judged to be answerable by experiments	B
2. Planning of the experiments and methodology design, including selection of methods and method development	B
3. Involvement in the experimental work	C
4. Presentation, interpretation and discussion in a journal article format of obtained data	C

*Benchmark scale of the PhD student's contribution to the article		
A. refers to:	Has contributed to the co-operation	0-33 %
B. refers to:	Has contributed considerably to the co-operation	34-66 %
C. refers to:	Has predominantly executed the work independently	67-100 %

Signature of the co-authors:			
Date:	Name:	Title:	Signature:

Signature of the PhD student and the principal supervisor:

<p>Date: 15/2/17</p> <p>PhD student: </p>	<p>Date: 15/2/17</p> <p>Senior author, corresponding author and Principal supervisor:  LARS H. PINBORG Rigshospitalet Afsnit 8501 N6 Blegdamsvej 9 - 2100 København Ø Tlf.: 35 45 36 31</p>
--	--